OSMOTIC DEHYDRATION IN PLANT TISSUES

Bai-sen HE, BEng, MEng

Doctor of Philosophy

ASTON UNIVERSITY
BIRMINGHAM, UK
2005

Aston University

OSMOTIC DEHYDRATION IN PLANT TISSUES

Bai-sen He, BEng, MEng

Doctor of Philosophy

2005

SUMMARY

Osmotic dehydration is an important technology that enables both the removal of water from the product and the modification of its functional properties by the impregnation of desired solutes. It has been the subject of numerous theoretical and experimental investigations over the last two decades. The mechanism of mass transfer in osmotic dehydration is complicated and still at the investigative stage. It is a relatively new process applied to food dewatering and as a pre-treatment technology to reduce energy consumption and to improve the fruits or vegetable products. Hitherto, there has been no widely used model that can be employed to analyze the osmotic dehydration process.

The primary aim of the thesis is to provide a comprehensive investigation of the osmotic dehydration processes in plant tissue. Effort has been concentrated on the modelling for simulating the processes.

Two mathematical models for simulating the mass transfer during osmotic dehydration processes in plant tissues are developed and verified using existing experimental data. Both models are based on the mechanism of diffusion and convection of any mobile material that can transport in plant tissues.

The mass balance equation for the transport of each constituent is established separately for intracellular and extra-cellular volumes with taking into account the mass transfer across the cell membrane between the intracellular and extra-cellular volumes and the shrinkage of the whole tissue. The contribution from turgor pressure is considered in

both models. Model two uses Darcy's law to build the relation between shrinkage velocity and hydrostatic pressure in each volume because the plant tissue can be considered as the porous medium. Moreover, it has been extended to solve the multi-dimensional problems.

A lot of efforts have been made to the parameter study and the sensitivity analyses. The parameters investigated including the concentration of the osmotic solution, diffusion coefficient, permeability of the cell membrane, elastic modulus of the cell wall, critical cell volume etc. The models allow us to quantitatively simulate the time evolution of intracellular and extra-cellular volumes as well as the time evolution of concentrations in each cross-section.

Keywords: osmotic dehydration, plant tissue, mass transfer, porous media, cell.

ACKNOWLEDGEMENTS

Foremost, I am truly indebted to my supervisor, Dr. Long-yuan Li, who has provided me an excellent study and working environment. I would like to appreciate his consistent patience, encouragements and affections under whose discussions, guidance and supervisions of the thesis were carried out. Without him, this work would have never been completed.

I would like to acknowledge the financial support provided partly by the Committee of Vice-Chancellors and Principals of the universities of U.K. through the Overseas Research Studentship (ORS) awards and by research scheme of Dr. Long-yuan Li.

Great thanks to Dr. J. Purkiss, for my first year report and some important suggestions.

I am most grateful to Rob Poole, who helped me with numerous computer and network problems, and particularly for maintaining the UNIX computer system. I also gave my thanks to secretaries, Mrs Joy Atkins, Mrs Hellen Mallinson and Mrs Diane Markley, for their kind assistance.

Thanks to my postgraduate colleagues and dear friends, Mr Brendon Donnellan, Mrs Xiao-ting Chu, Mr Zhi-zhou Zhong, Mr Kevin Yin, Mrs Ya-nan Yang, Miss Mei Yang, Mr Dinh-tuan Tran and Miss Hui Jin who gave me generous support at various times. I enjoyed the days being with them.

Sincerely thank my girl-friend, Vicky Deng and her mother, Mrs Ai-min Wang. They provided great support and encouragement, especially when I was sick in the third year of the PhD study.

Finally, my most sincerely appreciation attributes to my family. My dearest mother and father provided great support and encouragement and understanding throughout the whole period of my study. I would like to give my best acknowledgement and honour to my parents for their affections. It is to them that this thesis is dedicated.

CONTENTS

LIST OF FIGURES

LIST OF TABLES

NOMENCLATURE

Roman Characters

a	absorption coefficient
a_j	activity of solute j
A^c, A^f, A^w	cross sectional areas of the intracellular volume, free volume and cell wall fibre volume
A_0^c, A_0^f	initial cross sectional areas of the intracellular and extra-cellular volumes
A_{cp}^i, A_{cs}^i	transfer areas of plasmodesma and symplasma transfer ways
$\dot{A}_j$	cross sectional area of cell j cut by the g-plane
A_m	total area of membranes
A_m^1	area of the plasmalemma
A^t	total cross sectional area
c	diffusion coefficient
C	molar concentration (kmol/m^3)
C_i	molar concentration of component i (kmol/m^3)
C_A, C_B	molar concentration of component A and B (kmol/m^3)
C_{A1}, C_{A2}	molar concentration of A in the fluid and solid phase (kmol/m^3)
C^f	molar concentration of the free space (kmol/m^3)
C_s^c, C_s^f	concentrations of species s in the intracellular and extra-cellular volumes (kmol/m^3)
$C_{s,0}^c$, $C_{s,0}^f$	initial concentration in the intracellular volume and extra-cellular volumes (kmol/m^3)
C_s^l	molar concentration in the osmotic solution (kmol/m^3)

$\overline{C}_s$	average concentration (solute s) of intracellular and extra-cellular volumes (kmol/m^3)
$C_s^c\big\|_{Surface}$	concentration on the surfaces of the intracellular volume (kmol/m^3)
$C_s^f\big\|_{Surface}$	concentration on the surfaces of the extra-cellular volume (kmol/m^3)
d	diameter of the average cell (m)
d_a	mass coefficient
d^l	diameter of the average unit cell (m)
d^c	diameter of the sphere representing the intracellular volume of the average cell (m)
D_{AB}	diffusion coefficient of A through B (m^2/s)
D_{apj}	apparent diffusion coefficient of the i^{th} species (m^2/s)
D_s^c, D_s^f	diffusion coefficients of species s in the intracellular and extra-cellular volumes (m^2/s)
D_{im}	diffusion coefficient of i with respect to the mixture M (m^2/s)
D_i^∞	diffusivity at infinite dilution (m^2/s)
E	dimension in y-direction (m)
E_0	initial dimension in y-direction (m)
E^c	empirical modulus (N/m^2)
E^f	elastic modulus of the extra-cellular volume (N/m^2)
E^w	elastic modulus of cell wall (N/m^2)
f	source term
g	gravitational acceleration (N/s^2)
G	Gibbs free energy
h	a vertical height (m)
H	height of the sample (m)
j_i	average bulk velocity for mass flux (kg/m^2 s)
J_i	average bulk velocity for molar flux (kmol/m^2 s)
J_A, J_B	molar diffusion flux of component A and B (kmol/m^2 s)

J_D	exchange flow (kmol/m^2 s)
J_{i_m}, J_{i_p}	plasmalemma and symplastic molar fluxes of species I (kmol/m^2 s)
J_w	Net water flux (kmol/m^2 s)
J_s	Net solute(s) flux (kmol/m^2 s)
J_s^c, J_s^f	molar flux of species s in the intracellular and extra-cellular volumes (kmol/m^2 s)
J_0^{fc}	apoplastic transport flux of the water (kmol/m^2 s)
J_s^{fc}	apoplastic transport flux of species s from the extra-cellular volume into the intracellular volume through cell membrane (kmol/m^2 s)
J_v^{fc}	volume flux from the extra-cellular volume into the intracellular volume through cell membrane (m/s)
J_v	net volume flux (m/s)
k	the compliance factor
k_c, k_ρ	mass transfer coefficient (m^2/s)
k_{mG}, k_{mL}	mass transfer coefficients in the gas and liquid phases (m^2/s)
K_{mG}, K_{mL}	overall mass transfer coefficients in the gas and liquid phases (m^2/s)
kj_p, kj_s	plasmalemmatic and simplastic transmembrane mass transfer coefficients (m^2/s)
K	peameability
K^c, K^f	medium permeabilities for the solution in the intracellular and extra-cellular volumes
l	length of the sample (m)
L_{ki_m}, L_{ki_p}	macroscopic phenomenological coefficient
L_p	Hydraulic conductivity of membrane (m/Pa s)
m	mass of the mixture (kg)

m_i	mass of the component i (kg)
M_i	molecular weight of component i (kg/kmol)
n	mole number of the mixture
n_i	mole number of the component i
n_s, n_w	molar fractions of solute and water
$\overline{n}$	mass bulk flux of a mixture relative to fixed coordinates (kg/m^2 s)
N	total number of cells
$\overline{N}$	molar bulk flux of a mixture relative to fixed coordinates (kmol/m^2 s)
N_A, N_B	molar flux of component A and B (kmol/m^2 s)
N_{cv}	cell shape constant
N_w	mole number of the solvent in the solution
P_0^c, P_0^f	initial hydrostatic pressures in the intracellular and extra-cellular volumes (MPa)
P^c, P^f	hydrostatic pressures in the intracellular and extra-cellular volumes (MPa)
P_T	turgor pressure (MPa)
P_0^t	initial turgor pressure (MPa)
R	universal gas constant (J/kmol K)
R_b	radius of the buffer cylinder
R_C	radius of the cellular cylinder
R_I	radius of the interstitium cylinder
S	surface area of the average cell
S^c	surface area of the sphere
t	time (s)
T	absolute temperature (K)
u_i	mass diffusion velocity (m/s)
U_i	molar diffusion velocity (m/s)
v	mass bulk velocity of the mixture (m/s)
v^f, v^c, v^w	bulk velocity of free volume, intracellular volume and cell wall fibre

	volume (m/s)
v_i	mass bulk velocity of the component i (m/s)
V	volume of the mixture (m^3)
V^c, V^f	bulk velocities of solutions in the intracellular and extra-cellular volumes (m/s)
V_C, V_f	cellular and free space volumes
V_d	a correction factor
$\overline{V}$	molar bulk velocity of the mixture (m/s)
$\overline{V}_i$	molar bulk velocity of the component i (m/s)
$\overline{V}_j$	partial molar volume of the species (m^3/mole)
V_C^1	cellular volume of the average unit cell
V_c^i, V_0^i	intracellular and extra-cellular volumes
w_i	mass fraction of component i
x	position (m)
x_i	molar fraction of component i
x_1, x_2	film thickness
X_s, X_w	conjugate forces
z_j	charge number of the species

Greek Characters

α	the conservative flux convection coefficient
α_p	proportion of the total cell membrane occupied by plasmodesmata
β	convection coefficient
γ	conservative flux source term
γ_j	activity coefficient of solute j

ρ	mass concentration (kg/m^3)
ρ_i	mass concentration of component i (kg/m^3)
ρ_{A1}, ρ_{A2}	mass concentration of the fluid and solid (kg/m^3)
ρj_c^i, ρj_0^i	mass concentrations of the j^{th} species in intracellular volume and extra-cellular volume (kg/m^3)
ϕ	porosity
μ	dynamic viscosity (kg/m s)
μ^c, μ^f	dynamic viscosities in the intracellular and extra-cellular volumes
μ_i	partial molar free energy of i
μ_j	total chemical potential of the species s (J/mole)
μ_j^*	chemical potential at reference level
ν	kinematic viscosity (m^2/s)
υ^*	local value of the volume average velocity
τ_l	geometrical tortuosity
ε^i	fraction of the geometric area
ε^c, ε^f	intracellular and extra-cellular volumes in the referenced unit volume
ε_0^c, ε_0^f	initial intracellular and extra-cellular volumes in the referenced unit volume
ε_b^c, ε_b^f	intracellular and extra-cellular volumes on the boundary
Ψ_w	water potential
Δp	hydrostatic pressure difference (MPa)
$\Delta\pi_i$	osmotic pressure difference due to i (MPa)
$\Delta\pi_s$	osmotic pressure difference due to s (Mpa)
ω_s	solute permeability of membrane

σ_s	reflexion coefficient of membrane
δ	local shrinkage rate
Ω	volume of the average cell
Ω_0	initial value of the average cell
Ω^c, Ω^f	intracellular and extra-cellular volumes of the average cell
Ω_0^c, Ω_0^f	initial intracellular and extra-cellular volumes of the average cell

Chapter 1 INTRODUCTION

1.1 General Background

Osmotic dehydration is a water removal process in which cellular structure of a tissue consisting of individual cells (such as fruits and vegetables) is immersed in a concentrated osmotic solution containing one or more solutes. During the process, the solute diffuses into the cellular structure. The penetration of the solute creates a chemical potential difference across the cell membrane and draws the water out from the cellular structure. Therefore, there are at least two simultaneous, counter-current flows during the osmotic process: the solute flow from the concentrated solution into the tissue and the water flow out from the tissue into the solution. In addition, the tissue shrinks because the amount of water flowing out, in general, is more than that of solute diffusing in.

In food industry, osmotic dehydration is an important technology that enables both the removal of water from the product and the modification of its functional properties by impregnation of desired solutes. Osmotic dehydration is often applied as a pre-treatment process for fruit and vegetables, which reduces the physical, chemical and biological changes during drying at high temperature. As an example, drying is a good way of preserving food. Food can be dried in many ways, such as, by the sun if the air is hot and dry enough, or in an oven or dryer if the climate is humid. Although solar drying is a popular and very inexpensive method, dependable solar dehydration of foods requires 3 to 5 consecutive days when the temperature is over than 30°C and the humidity is very low. Drying in the oven of a kitchen range, on the other hand, can be very expensive. Osmotic dehydration would be a good method for drying food. Removal of water by osmotic dehydration from biological materials has drawn increasing attention as a potential alternative or supplementary operation to conventional drying, freezing and dehydro-freezing processes in recent years. This is because the process is carried out at a low temperature and does not involve the phase change that would be present in the

processes of drying and freezing, resulting in high quality products and low operating cost.

The second major application of the osmotic dehydration is to reduce the water activity of many food materials so that microbial growth will be inhibited. Since most foods contain large amounts of water, they are costly intensive to ship, pack and store. Osmotic dehydration is acknowledged to be an energy-efficient method of partial dehydration, since there is no need for a phase change.

It is also a useful technique in the food industry for partial concentration of cellular material, like fruits and vegetables, because it offers minimized heat damage, increased retention of volatile and pigments, and improved textural quality of dehydrated products.

The mechanism of mass transfer in osmotic dehydration is very complicated and is still at the investigative stage (Yao *et al.*, 1994). When a cellular material is immersed in an osmotic solution, the solute penetrates into the tissue along the extra-cellular volume first. The selective properties of the cell membrane restrict the solute partially or fully from entering the intracellular volume (depending on the solute characteristics), but allows water to pass through easily. The trans-membrane flux tries to bring the cell to a new equilibrium state by concentrating the solution in the intracellular volume and diluting the solution in the extra-cellular volume. Since the water coming out from the intracellular volume has to flow out along the extra-cellular volume, the water forms an out flowing bulk flow starting from the centre and accumulating along the way towards the surface. The bulk flow opposes the solute penetration and sharpens the concentration gradient. Yao and Le Maguer (1996a) demonstrated that the bulk flow could transport up to 90% of the water removed during osmotic dehydration of potatoes with mannitol solution, and wash back about 60% of the mannitol diffused in. In addition, the shrinkage of the whole tissue and the internal rearrangement of the cellular structure make the analysis of the osmotic dehydration process more complex. The time scale of the osmotic dehydration is strictly affected by the characteristics of the tissue samples, such as the thickness of the tissue, the pre-treatment etc.

The solute concentration in the extra-cellular volume is a net result of solute diffusion from the osmotic solution into the tissue, dilution by trans-membrane water flux, and washout by bulk flow. The concentration, therefore, varies with time and position. Unfortunately, there is no information in the literature concerning how bulk flow and trans-membrane flux vary with time and position in the extra-cellular volume, this lack of information makes accurate modelling of mass transfer in osmotic dehydration difficult. Hitherto, there is no widely used model can be adopted to analyze all the osmotic dehydration phenomena. The lack of knowledge greatly limits the application of the osmotic dehydration processes in the food industry.

1.2 Objectives of the Project

As mentioned before, osmotic dehydration is very important technology in so many fields, the mechanism of mass transfer in osmotic dehydration is complicated and still at the investigative stage; the current models are constrained in abstract one-dimensional simulation, which limits the understanding and application of the osmotic dehydration processes in food industry. Therefore, it is necessary to study the mechanism of osmotic dehydration processes.

The purpose of this study is to provide a comprehensive investigation of the osmotic dehydration processes in plant tissue. In this study, attention will be concentrated on the modelling of the mass transfer during osmotic dehydration processes. The models to be developed will be based on the mechanism of diffusion and convection of any mobile material that can transport in plant tissues. The mass balance equation for the transport of each constituent is established separately for intracellular and extra-cellular volumes but with taking into account the mass exchange across the cell membrane between the intracellular and extra-cellular volumes. The mass transfer results in not only the change of intracellular and extra-cellular volumes but also the shrinkage of whole tissue.

The models allow us to quantitatively simulate the time evolution of intracellular and extra-cellular volumes and hydrostatic pressures as well as the concentrations. The models can also be extended to multi-dimensional simulation which can obtain more effective and intuitionistic results.

1.3 Order of Presentation

A detailed review of previous research on osmotic dehydration processes in plant tissue, especially the recent modelling for simulating these processes, is presented in chapter 2. For the better understanding of osmotic dehydration process, the plant cell structure, some basic parameters and concepts are also introduced in this chapter.

The introductory chapter 3 contains the bare theoretical bones that are necessary to understand the work described in later chapters. Essentially we are concerned with the flows of water and uncharged solutes across a membrane. In this chapter, the concept of chemical potential is also introduced which is very important to the later modelling analysis.

Two mathematical models based on previous research are developed and described in details in chapter 4 and chapter 6, respectively. They take into account the diffusion and convection of each constituent within the tissue. By establishing the mass balance and volume balance equations for the transport of each constituent separately with taking into account the mass exchange across the cell membrane between the intracellular and extra-cellular volumes, the models describe the variations of concentrations in each volume as well as the changes of individual volume. Different from other models, the plant tissue in one of these two models is considered as porous medium and the shrinkage velocities are analyzed by Darcy's law.

Chapter 5 and chapter 7 are the numerical analyses chapters. The results of comparative studies will be performed to validate the models. A sensitivity analysis and parametric study of the models will be presented in these two chapters.

The mathematical model two is extended to two-dimensional analyses in chapter 8. Some two-dimensional results and shrinkage phenomena are discussed in this chapter.

Chapter 9 provides the conclusions drawn from the present studies. It summarizes the developed work and orientates the future work in this area.

Chapter 2 LITERATURE REVIEW

2.1 Introduction

Osmotic dehydration, a subject first proposed by Ponting *et al.* (1966), is a technique that, when applied to horticultural products, allows the water content to be reduced (up to a final value of 50-60% weight basis) while increasing soluble solids content (Spiazzi & Mascheroni, 1997). It is a water removal process, which is based on placing foods, such as fruits and vegetables, into concentrated solutions of soluble solids having higher osmotic pressure and lower water activity. The diffusion of water is accompanied by the simultaneous counter diffusion of solutes from the osmotic solution into the tissue. Since the membrane responsible for osmotic transport is not perfectly selective, other solutes present in the cells can also be leached into osmotic solution (Ponting, Walters, Forrey, Jackson & Stanley, 1966; Dixon & Jen, 1977; Lerici, Pinnavaia, Dalla Rosa & Bartolucci, 1985; Giangiacomo, Torreggiani & Abbo, 1987; Rastogi, Raghavarao, Niranjan & Knor, 2002; Agnelli, Marani & Mascheroni, 2004).

The influence of the main process variables, such as concentration and composition of the osmotic solution, temperature, immersion time, pre-treatments, agitation, nature of food and its geometry, solution/sample ratio, on the mass transfer mechanism and the product quality have been studied extensively (Magee *et al.*, 1983; Toupin & Le Maguer, 1989; Beristain *et al.*, 1990; Lenart & Lewicki, 1990; Yao & Le Maguer, 1996; Mavroudis *et al.*, 1998). A number of recent publications have described the influence of these variables on mass transfer rates during osmotic dehydration (Torreggiani, 1993; Rastogi & Raghavarao, 1995, 1997a, 1997b; Rastogi, Raghavarao & Niranjan, 1997). It is worth noting that these variables can only be manipulated over a limited range, outside of which they adversely affect the food quality even though mass transfer rates may be enhanced. Hence, there is a need to identify methods that increase mass transfer rates without affecting quality significantly.

The methods to increase the rate of mass transport have been explored in recent years. A number of technologies have been tried to improve mass transfer rate. These technologies include: ultra high hydrostatic pressure (Farr, 1990; Dornenburg & Knorr, 1993; Rastogi, Subramanian & Raghavarao, 1994; Rastogi, Angersbach & Knorr, 2000); high intensity electrical field pulses (Rastogi, Eshtiaghi & Knorr, 1999; Ade-Omowaye, Rastogi, Angersbach and Knorr, 2001); ultrasound (Simal, Benedito, Sanchez & Rossello, 1998); partial vacuum (Fito, 1994; Rastogi & Raghavarao, 1996; Mujica-Paz, Valdez-Fragoso, Lopez-Malo, Palou & Welti-Chanes, 2003); centrifugal force (Azuara, Garcia & Beristain, 1996).

In the last two decades, numerous studies have been carried out to better understand the internal mass transfer occurring during osmotic dehydration of foods and to model the process (Islam & Flink, 1982; Magee *et al.*, 1983; Lenart *et al.*, 1988; Toupin & Maguer, 1989; Marcotte *et al.*, 1991; Azuara *et al.*, 1992; Raoult-Wack, 1994; Wijmans & Baker, 1995; Yao & Le Maguer, 1997; Spiazzi & Mascheroni, 1997; Rastogi *et al.*, 1997; Kaymak-Ertekin & Sultanoglu, 2000; Mizrahi, 2001; Barat *et al.*, 2001; Mauro *et al.*, 2002; Li, 2005). Moreover, a number of experiments have been carried out to verify these models. In most cases, the water loss (WL) and solid gain (SG) were measured and compared with the results obtained by these models (Mavroudis *et al.*, 1998; Sereno *et al.*, 2001; Sacchetti *et al.*, 2001; Kowalska & Lenart, 2001; Moreira & Sereno, 2003; Telis *et al.*, 2004).

Let us recall some basic knowledge about the cell structure and osmotic phenomena before the present mathematical models are introduced.

2.2 The Cellular Structure of Plant Tissues

2.2.1 Generalized Plant Cell

Fig. 2.1 depicts a representative plant cell. Surrounding the protoplast is the cell wall, composed mainly of cellulose and other polysaccharides; these polymers help provide rigidity to individual cells as well as to the whole plant. Since the cell wall contains numerous relatively large interstices, it does not serve as the main permeability barrier

to water or solute movement into plant cells. The main barrier, a cell membrane known as the plasma membrane or plasmalemma, occurs inside the cell wall and surrounds the cytoplasm. The permeability of this membrane varies with the particular solute so the plasmalemma can regulate what enters and leaves a plant cell. The cytoplasm contains organelles like chloroplasts and mitochondria, distinct membrane-surrounded compartments in which energy can be converted from one form to another. Also in the cytoplasm are micro-bodies such as peroxisomes, numerous ribosomes, proteins, as well as many other macromolecules and structures that influence the thermodynamic properties of water. The term cytoplasm includes the organelles (but often not the nucleus), while the increasingly used term cytosol refers to the cytoplasmic solution delimited by the plasmalemma and the tonoplast (to be discussed next) but exterior to all the organelles (Lüttge *et al.*, 1976).

In mature cells, there is a large central aqueous phase referred to as the vacuole. This vacuole is surrounded by a membrane known as the tonoplast. The tonoplast is usually quite large in area, since the central vacuole can occupy up to 90% of the volume of a mature cell. The relatively simple aqueous solution in the central vacuole contains mainly inorganic ions or organic acids as solutes, although considerable amounts of sugars and amino acids may be present in some species. Water uptake into this vacuole occurs during cell growth.

One immediate impression of plant cells is the great prevalence of membranes. In addition to surrounding the cytoplasm, membranes also separate various compartments in the cytoplasm. Diffusion of substances across these membranes is much more difficult than diffusion within the compartments. Thus organelle and vacuolar membranes can effectively control the contents and consequently the reactions occurring in the particular compartments which they surround. Diffusion can also impose limitations on the overall size of a cell, since the time for diffusion increases with the square of the distance as it is shown in the classical diffusion equation (Lüttge *et al.*, 1976).

Although many plant cells share most of the features indicated in Fig. 2.1, they are remarkably diverse in size.

2.2.2 Plant Cell Structure

It is estimated that there are at least 260,000 species of plants in the world today. They range in size and complexity from small, nonvascular mosses to giant sequoia trees, the largest living organisms as tall as 100 meters (Lüttge *et al.*, 1976). Only a tiny percentage of those species are directly used by people for food, shelter, fiber, and medicine. Fig. 2.2 shows the cross-section of a plant cell. A plant cell is mainly composed of the following components:

- Cell Wall - Like their prokaryotic ancestors, plant cells have a rigid wall surrounding the plasma membrane. It is a far more complex structure, however, and serves a variety of functions, from protecting the cell to regulating the life cycle of the plant organism.

- Cell Membrane - All living cells have a plasma membrane that encloses their contents. In prokaryotes and plants, the membrane is the inner layer of protection surrounded by a rigid cell wall. These membranes also regulate the passage of molecules in and out of the cells.

- Chloroplast - Chloroplast is a specialized organelle where the plants make their own food by converting light energy into chemical energy.

- Endoplasmic Reticulum (ER) - The endoplasmic reticulum, including the rough ER and smooth ER, is a network of sacs that manufactures, processes, and transports chemical compounds for use inside and outside of the cell. It is attached to the double-layered nuclear envelope, providing a connection between the nucleus and the cytoplasm.

- Golgi Body - The Golgi body is the distribution and shipping department for the cell's chemical products. It modifies proteins and fats built in the endoplasmic reticulum and prepares them for export as outside of the cell.

- Mitochondrion - Mitochondria are oblong shaped organelles found in the cytoplasm of all eukaryotic cells. In plant cells, they break down

carbohydrate and sugar molecules to provide energy, particularly when light isn't available for the chloroplasts to produce energy.

- Nucleus - The nucleus, which contains nucleolus and nuclear membrane, is a highly specialized organelle that serves as the information and administrative centre of the cell.

- Ribosomes - All living cells contain ribosomes, tiny organelles composed of approximately 60 percent RNA and 40 percent protein. In eukaryotes, ribosomes are made of four strands of RNA. In prokaryotes, they consist of three strands of RNA.

- Vacuole - Each plant cell has a large, single vacuole that stores compounds, helps in plant growth, and plays an important structural role for the plant. (enchantedlearing.com)

2.2.3 Cell Wall

The cell walls of plants are made of fibrils of cellulose embedded in a matrix of several other kinds of polymers such as pectin and lignin (See Fig. 2.3). These walls can withstand quite high hydrostatic pressures, but are permeable to water and solutes. The presence of the cell wall means that the cell can survive, without bursting, in very dilute solutions.

Cell walls play many roles in plants. Their rigidity helps determine the size and shape of a cell and ultimately that of a plant. This supportive role is performed in conjunction with the internal hydrostatic pressure, which causes a distension of the cell walls. The cell wall is also intrinsically involved in many aspects of the ion and water relations of a plant. Since it surrounds the plasmalemma of each cell, all fluxes of water and solutes into or out of a plant cell protoplast must cross the cell wall, usually by diffusion. Cell walls vary from about 0.1 to 10um in thickness (Lüttge *et al.*, 1976).

2.2.4 Cell Membrane

The cell membrane composed of lipids and proteins as shown in Fig. 2.4 is that area of the cell immediately surrounding the cytoplasm and is perhaps the most conserved structure in plant cells. It is the major barrier in the cell, separating the inside of the cell from the outside. It is this structure which allows cells to selectively interact with their environment. Membranes are highly organized and asymmetric having two faces with different topologies and different functions. They are also dynamic, constantly adapting to changing environmental conditions. In most cases, the cell membrane is considered as a 'semi-permeable' membrane, which is permeable only to the solvent and impermeable to solutes.

Cell membrane also plays a very important role in plants, which include:

- Retains the cytoplasm

The concentration of solutes, sugars, ions etc. are much higher within the cell than outside. A fundamental principle of nature, however, is that solute concentrations will tend to equilibrate. In this case, the water will flow into the cell (a process known as osmosis) and the solutes will flow out. The cell membrane prevents free flow of material and thus serves as an osmotic barrier.

- Selective barrier

Since the cell is separated from its environment and needs to get nutrients in and waste out, the membrane must be able to accommodate this. It acts as a selective barrier. Some molecules can cross the membrane without assistance, most cannot. Water, non-polar molecules and some small polar molecules can cross. Non-polar molecules penetrate by actually dissolving into the lipid bilayer. Most polar compounds such as amino acids, organic acids and inorganic salts are not allowed entry, but instead must be specifically transported across the membrane by proteins (Lüttge *et al.*, 1976).

2.2.5 Vacuoles

Fig. 2.5 is the diagram of vacuole structure. Vacuoles are membranous sacs consisting mostly of water containing various dissolved sugars, salts, proteins, and other nutrients. Each plant cell has a large, single vacuole that typically takes up most of the room in the cell.

Some contain pigments that give certain flowers their colours. The central vacuole also contains plant wastes that taste bitter to certain insects and animals, thus discouraging them from consuming the plant.

The plant vacuole stores compounds, helps in plant growth, and plays an important structural role for the plant. Under optimal conditions, the vacuoles are filled with water to the point that they exert a turgor pressure against the cell wall. This helps maintain the structural integrity of the plant, along with the support from the cell wall. When plant cells can not obtain the water they need, pressure in the vacuole is reduced and the plant wilts (Lüttge *et al.*, 1976).

2.2.6 Cytoplasm

The cytoplasm or protoplasm is the portion of the cell that lies within the cytoplasmic membrane. The cytoplasm holds many cellular constituents, such as proteins, vitamins, ions, nucleic acids and their precursors etc. It is within the cytoplasm that many of the functions for cell growth, metabolism and replication are carried out.

Cytoplasm is basically the substance that fills the cell. It is a jelly-like material that is eighty percent water and usually clear in colour. It is more like a viscous (thick) gel than a watery substance, but it liquefies when shaken or stirred. Cytoplasm, which can also be referred to as cytosol, means cell substance. This name is very fitting because cytoplasm is the substance of life that serves as a molecular soup in which all of the cell's organelles are suspended and held together by a fatty membrane. The cytoplasm is found inside the cell membrane, surrounding the nuclear envelope and the cytoplasmic organelles.

The cytoplasm, as seen through an electron microscope, appears as a three-dimensional lattice of thin protein-rich strands. These lattices are known as microtrabecular lattice (MTL) and serves to interconnect and support the other "solid" structures in the cytoplasm. In other words, the cytoplasm is like a fence that is made up of lattes that are connected together. This fence's main purpose is to hold together the organelles within the cytoplasm.

Cytoplasm is the home of the cytoskeleton, a network of cytoplasmic filaments that are responsible for the movement of the cell and give the cell its shape. The cytoplasm contains dissolved nutrients and helps dissolve waste products. The cytoplasm helps materials move around the cell by moving and churning through a process called cytoplasmic streaming. The nucleus often flows with the cytoplasm changing the shape as it moves. The cytoplasm contains many salts and is an excellent conductor of electricity, which therefore creates a medium for the vesicles, or mechanics of the cell. The function of the cytoplasm and the organelles which sit in it, are critical the cell's survival (Lüttge *et al.*, 1976).

2.3 Osmotic Phenomena

In the system illustrated in Fig. 2.6, compartment 1 contains a pure solvent, A, and compartment 2 contains a solution of solute, B, and solvent, A. The two liquids are separated by a membrane, M. Here, we assume that the membrane M is permeable to A but impermeable to B.

When such a system is set up, with the surfaces of the liquids in the two side-arms at the same level, it is found that solvent, A, flows across the membrane from compartment 1 to compartment 2, that is, from the pure solvent to the solution. This flow is called osmosis. A membrane, such as M, which is permeable only to the solvent is said to be semi-permeable.

The flow of solvent from side 1 to side 2 causes the level of the liquid in the side-arm attached to compartment 1 to drop, while the level in the side-arm attached to compartment 2 rises. The hydrostatic pressure in the solution thus becomes greater than

that in the pure solvent. This pressure difference tends to drive solvent through the membrane from compartment 2 to compartment 1. Eventually a point is reached where the osmotic force driving solvent from 1 to 2 is exactly balanced by the pressure difference acting in the opposite direction, so that no net flow of solvent occurs. The pressure difference required to produce zero flow of solvent is called the osmotic pressure of the solution in compartment 2. In general, the osmotic pressure of a solution increases with its concentration.

It should be noted that this definition of the osmotic pressure of a solution is an operational one. The state of osmotic equilibrium described above is really one of zero flow of volume across the membrane. If the membrane is truly semi-permeable, this state is also one of zero flow of solvent. However, if the membrane is also permeable slightly to the solute, solute will flow from compartment 2 to compartment 1. This flow partly balances the volume flow due to osmosis. Consequently the pressure head required to produce zero volume flow across the membrane is less than it would be if the membrane were truly semi-permeable. The apparent osmotic pressure of the solution, measured with a solute-leaky membrane, is thus lower than the true osmotic pressure.

A better definition of the osmotic pressure of a solution is based on a thermodynamic function, the chemical potential of the solvent. The osmotic pressure of a solution is that pressure which must be applied to the solution to make the chemical potential of the solvent in the solution equal to that of the pure solvent at the same temperature.

2.4 Mass Transfer Process in Plant Tissue

Mass transfer in plant tissue can be caused by three processes: diffusion, convection and trans-membrane flux. Before each process is introduced, the mass transfer pathways and the definition of variables need to be described first.

2.4.1 Transfer Pathways

Mass transfer in a plant tissue during osmotic dehydration can be interpreted from the scheme shown in Fig. 2.7. Water is transferred through the cellular membrane from the cell inside towards the extra-cellular space (which is called as apoplastic transport) and via small channels from one cell to another (which is called as symplastic transport). Once the water reaches the extra-cellular space, it will be quickly transferred into the osmotic solution. The solutes in osmotic solution are transferred in the same manner as the water but in an opposite direction. The extra-cellular space is composed of the space between cell wall and cell membrane plus the intercellular spaces themselves. Although the channel permeability of the plasmodesmata for the symplastic transport can be up to 100 times as high as that of the membrane, the number of channels does not exceed 1% of the cellular surface (Spiazzi *et al.*, 1997). Therefore, as far as the mass transfer is concerned the two transports are equally important.

Because of the transfer of water and solutes during the process, the volume and shape of each individual cell change. In addition, because of the change of pressures in the cell and in the extra-cellular space, the volume and shape of the whole plant tissue structure will change. Thus, the problem is a coupled mass transfer and structure deformation problem.

2.4.2 Mass Transfer Variables

Mass transfer processes involve concentration, velocity, and flux variables, which are defined and governed by a set of differential equations.

2.4.2.1 Concentration

The concentration of a mixture and its components may be expressed in terms of mass or molar. If it is in terms of mass, we have the mass concentration of the mixture (ρ, kg/m^3), the mass concentration of a component i (ρ_i, kg/m^3), and the mass fraction of component i (w_i), which are given by:

$$\rho = m/V \tag{2.1}$$

$$\rho_i = m_i/V \tag{2.2}$$

$$w_i = m_i/m = \rho_i/\rho \tag{2.3}$$

where m and m_i are the mass of the mixture and component i, respectively; V is the volume of the mixture.

The bulk molar concentration (C, kmol/m^3), the molar concentration of component i, (C_i, kmol/m^3), and the mole fraction of component i (x_i) are defined by:

$$C = n/V \tag{2.4}$$

$$C_i = n_i/V \tag{2.5}$$

$$x_i = n_i/n = C_i/C \tag{2.6}$$

where n and n_i are the mole number of the mixture and component i, respectively.

According to the definitions given in Eqs. (2.1) - (2.6), it can be easily seen that:

$$m = \sum_{i=1}^{n} m_i \text{ and } \rho = \sum_{i=1}^{n} \rho_i \tag{2.7}$$

$$n = \sum_{i=1}^{n} n_i \text{ and } C = \sum_{i=1}^{n} C_i \tag{2.8}$$

$$w = \sum_{i=1}^{n} w_i = 1 \text{ and } x = \sum_{i=1}^{n} x_i = 1 \tag{2.9}$$

where x_i is the mole fraction of component i, and ρ_i and C_i are related to each other through the molecular weight of constituent i (M_i, kg/kmol); that is,

$$\rho_i = M_i C_i \tag{2.10}$$

2.4.2.2 Velocity

In mass transfer, the velocity of a bulk mixture and of its components can be measured with respect to fixed coordinates. In addition, the velocity of the components can also

be measured relative to the bulk velocity. Fig. 2.8 illustrates these velocities in a binary system of components A and B in the x-direction.

The mass bulk velocity of the mixture (v, m/s) relative to fixed coordinates is defined as:

$$v = \sum_{i=1}^{n} w_i v_i = \sum_{i=1}^{n} \frac{m_i}{m} v_i = \sum_{i=1}^{n} \frac{\rho_i}{\rho} v_i \tag{2.11}$$

where v_i is the velocity of components with respect to stationary coordinates.

In a similar manner, a molar bulk velocity ($\overline{V}$, m/s) measured relative to stationary coordinates can be defined as:

$$\overline{V} = \sum_{i=1}^{n} x_i \overline{V}_i = \sum_{i=1}^{n} \frac{n_i}{n} \overline{V}_i = \sum_{i=1}^{n} \frac{C_i}{C} \overline{V}_i \tag{2.12}$$

The velocity of the constituent i relative to the bulk velocity of the mixture is:

$$u_i = v_i - v \tag{2.13}$$

$$U_i = \overline{V}_i - \overline{V} \tag{2.14}$$

where u_i (m/s) and U_i (m/s) are the mass and molar diffusion velocities, respectively.

2.4.2.3 Flux

The mass bulk flux ($\overline{n}$, kg/m^2 s) and the molar bulk flux ($\overline{N}$, kmol/m^2 s) of a mixture relative to fixed coordinates are:

$$\overline{n} = \rho v = \sum_{i=1}^{n} \rho_i v_i \tag{2.15}$$

$$\overline{N} = CV = \sum_{i=1}^{n} C_i V_i \tag{2.16}$$

The flux of the components of a mixture can also be expressed relative either to fixed coordinates or to the bulk average velocity. The flux of the component i relative to stationary coordinates is:

$$\overline{n}_i = \rho_i v_i \tag{2.17}$$

$$\overline{N}_i = C_i V_i \tag{2.18}$$

The diffusion flux of the constituent i of the mixture with respect to the average bulk velocity is j_i (kg/m^2 s) for the mass flux and J_i (kmol/m^2 s) for the molar flux.

$$j_i = \rho_i u_i = \rho_i (v_i - v) \tag{2.19}$$

$$J_i = C_i U_i = C_i (\overline{V}_i - \overline{V}) \tag{2.20}$$

The use of concentration, velocities, and fluxes in mass or molar terms is subject to preferences and convenience. Nevertheless, in most case, the concentration and flux expressed in molar units and average molar velocity are preferred.

2.4.2.4 Flux relations for binary system

For a binary mixture of components A and B, Eqs. (2.18) and (2.20) become:

$$N_A = C_A \overline{V}_A \tag{2.21}$$

$$J_A = C_A U_A = C_A (\overline{V}_A - \overline{V}) \tag{2.22}$$

Substituting V from Eq. (2.12) into Eq. (2.22),

$$J_A = C_A \overline{V}_A - C_A \overline{V} = C_A \overline{V}_A - \frac{C_A}{C}(C_A \overline{V}_A + C_B \overline{V}_B) \tag{2.23}$$

Since $N_A = C_A \overline{V}_A$ and $N_B = C_B \overline{V}_B$, for component A, Eq. (2.23) becomes:

$$N_A = J_A + \frac{C_A}{C}(N_A + N_B) \tag{2.24}$$

A similar mathematical derivation gives for component B:

$$N_B = J_B + \frac{C_B}{C}(N_A + N_B) \tag{2.25}$$

Eqs. (2.24) and (2.25) show that the absolute molar flux (N_A and N_B) results from a concentration gradient contribution or a molar diffusion flux (J_A and J_B) and a convective contribution ($C_A\overline{V}$ or $C_B\overline{V}$). The molar diffusion flux is described by using Fick's law, which, for component A, is written as:

$$J_A = -D_{AB}\frac{dC_A}{dx} \tag{2.26}$$

where D_{AB} is the diffusion coefficient of A through B and dC_A/dx is the change of the concentration A with respect to the position x.

In terms of mass, the mass fluxes for components A and B are expressed by:

$$\overline{n}_A = j_A + \frac{\rho_A}{\widetilde{\rho}}(\overline{n}_A + \overline{n}_B) \tag{2.27}$$

$$\overline{n}_B = j_B + \frac{\rho_B}{\widetilde{\rho}}(\overline{n}_A + \overline{n}_B) \tag{2.28}$$

2.4.3 Mass Transfer by Diffusion

2.4.3.1 Diffusion

The process of diffusion is the random movement of substances from a region of high concentration to a region of low concentration until no more concentration differences remain. It is the random movement of particles, such as atoms or molecules, toward a state of equal distribution. It is important to realize that in diffusion each individual particle moves at random. When a lot of individual particles move at random in a solution over a long enough period of time, they will end up evenly distributed throughout the solution. So, where there used to be a higher concentration will now be lower, and where there used to be a lower concentration will now be higher.

Before we introduce the diffusion of substance across a cell membrane, let us review the definition of Permeable.

Definition of Permeable

A membrane is said to be permeable to a given substance if it allows that substance to pass through it.

Cell membranes are selectively permeable or semi-permeable, meaning they are permeable to some substances but not to others.

Definition of ideal solution

By definition, an ideal solution is one in which the intermolecular forces between all types of molecules are the same, whether they are forces between solute and solvent molecules, or forces between solute molecules, or forces between solvent molecules. Also the sizes of the solute and solvent molecules are the same.

Diffusion of Substance across a Cell Membrane

If there is a greater concentration of a substance on one side of a membrane that is permeable to that substance, the substance will move from the region of high concentration to the region of low concentration. This process will not stop until:

- the membrane is no longer permeable to that substance. Or,
- the substance is evenly distributed across the membrane.

There are two kinds of diffusion across a cell membrane:

- Materials may move passively through the membrane itself by simple diffusion.
- Materials may move passively through special protein channels in the membrane, by facilitated diffusion. Most biochemical molecules are hydrophilic ("water-loving") and cannot therefore cross directly through the cell membrane. These molecules and ions require special tunnels in the membrane that shield them from the hydrophilic lipids. These channels are made of proteins embedded in the membrane, like a concrete train tunnel stretching through a

rock cliff. In other words, the diffusion of these hydrophilic substances is helped or facilitated by proteins.

Mass transfer by diffusion is the transport of molecules caused by the random molecular motion in a region in which a composition gradient exists.

2.4.3.2 Steady state diffusion

Steady state diffusion, in which the concentration does not change with time at any position, is described by:

$$\frac{dC_i}{dt} = 0 \tag{2.29}$$

where C_i is the concentration of component i (kmol/m^3), t is the time (s).

The corresponding mass concentration (ρ_i) of the component i is expressed as:

$$\frac{d\rho_i}{dt} = 0 \tag{2.30}$$

2.4.3.3 Unsteady state diffusion

The unsteady state diffusion, in which the local concentration change with time is described in one dimension for slab shape and for constant D_{AB}, is shown by Fick's second law:

$$\frac{\partial C_A}{\partial t} = D_{AB} \frac{d^2 C_A}{dx^2} \tag{2.31}$$

Analogous equations can be written for diffusion in spherical or cylindrical shapes and in two or three dimensions. These equations are used to find the concentration of a solute as a function of time and position and are mainly applicable to diffusion in solids and to limited situations in fluids. The analysis of unsteady state system, however, is frequently simplified to a one-directional flow in most fields of industrial applications.

2.4.4 Mass Transfer by Convection

2.4.4.1 Convection

Convective mass transport, which occurs in liquids and gases, results from bulk motion of the fluid imposed by external forces (forced convection) or occurring mutually, due to the concentration difference or density variations (free convection). The free or forced character is determined by the nature of the motion of the fluid, which may be either laminar or turbulent. In laminar flow, the mechanism is the same as in a stationary medium, and the transfer occurs by diffusion. In turbulent flow, mass transfer is affected by the irregular motion of small volumes of the fluid (Welti-Chanes *et al.*, 2003).

2.4.4.2 Film theory and mass transfer coefficient

Convective mass transfer problems in turbulent flow are not always amenable to analytical methods of solution. Consequently, they are usually approached with the aid of coefficients and empirical relationships. Among several models proposed for a better understanding of mass transfer under turbulent regime, we find the model built around the film theory. In this theory the interfacial region is treated as a hypothetical stagnant film of thickness x, called the boundary layer, and it is assumed that all the concentration changes occur in this layer (Fig. 2.9) (Welty *et al.*, 1984).

Thus, the molar flux and the concentration profile of species A (J_A) are found from

$$J_A = \frac{D_{AB}}{x}(C_{A1} - C_{A2}) = -k_m(C_{A1} - C_{A2}) \tag{2.32}$$

where D_{AB} and k_m, are the mass transfer coefficients; C_{A1} and C_{A2} are the bulk concentrations in the fluid and solid phase, respectively, and

$$C_A = C_{A1} - \frac{z(C_{A1} - C_{A2})}{x} \tag{2.33}$$

Similarly, the corresponding expression for mass flux is:

$$j_A = k_\rho(\rho_{A1} - \rho_{A2}) \tag{2.34}$$

where C_A is the concentration of the components A, and ρ_{A1} and ρ_{A2} are the mass concentration of the fluid and solid, respectively.

The mass transfer coefficient k_ρ has units of velocity (m^2/s), which can be determined either from experimental data and empirical formulas. A rough estimation of k_m can be attained by assuming $k_m=D/x$, provided the effective film thickness and the diffusion coefficient are known (Sherwood, 1974).

2.4.4.3 Two-film theory and mass transfer coefficient

Mass transfer from a gas and/or a liquid to another fluid is a common engineering problem. For interface transfer, it is convenient to use an overall mass transfer coefficient, the interpretation of which is achieved with the aid of the two-film theory. Fig. 2.10 schematically shows the transfer of component A from the gas phase to the liquid phase. The two-film theory assumes that the resistance to mass transfer lies in each adjacent phase to the interphase and that no resistance is offered to the transfer of the solute across the interphase (Welty *et al.*, 1984).

At steady state, the fluxes in gas and liquid (J_1) phases must be equal:

$$J_1 = k_{mG}(C_{A1} - C_{A1i}) = K_{mL}(C_{A2i} - C_{A2}) \tag{2.35}$$

where k_{mG} and k_{mL} are the mass transfer coefficients in the gas and liquid phases, respectively, C_{A1i} and C_{A2i} are the concentrations of component A at the interface, and C_{A1} and C_{A2} are the bulk concentrations in the gas and liquid phases, respectively.

Since the concentrations at the inter-phase are not easily measurable, it is convenient to calculate an overall mass transfer coefficient based on an overall potential gradient between the bulk compositions. The over all driving force is not, however, C_{A1}-C_{A2}, since at the interface discontinuity of the concentrations exists, and the solubility in the liquid is not necessarily the same as in the gas. Moreover, the film thickness x_1 and x_2 and the diffusivity of the solute may be different in the two phases (Welti-Chanes *et al.*, 2003).

The solubility relationship that governs the equilibrium concentration between different phases is of the form:

$$C_G = mC_L \tag{2.36}$$

where m is the solubility constant between the gas and liquid phases, and C_G and C_L are the concentrations of the gas and liquid, respectively.

Thus, the flux in terms of the total potential gradient in the gas phase is:

$$J = K_{mG}\left(C_{A1} - C_{A1}^{*}\right) = K_{mG}\left(C_{A1} - \frac{C_{A2}}{m}\right) \tag{2.37}$$

where $C_{A2}/m = C_{A1}^{*}$, which is the concentration in the gas phase that would exist in equilibrium with C_{A2}, the concentration of species A in the liquid.

A similar equation can be obtained for the overall coefficient if the driving force is based on the concentration in the liquid phase:

$$J = K_{mL}\left(C_{A1}^{*} - C_{A2}\right) = K_{mL}\left(mC_{A1} - C_{A2}\right) \tag{2.38}$$

where mC_{A1} is the concentration in the liquid that would exist in equilibrium with C_{A1}^{*}. K_{mG} and K_{mL} represent the overall mass transfer coefficient based on the gas phase and the liquid concentration driving force.

Coefficient K_{mG} and K_{mL} are related to the individual mass transfer coefficients and the equilibrium constant m of a gas-liquid (k_{mG}) or vapour-liquid (k_{mL}) system as follows:

$$\frac{1}{K_{mG}} = \frac{1}{k_{mG}} + \frac{m}{k_{mL}} \tag{2.39}$$

$$\frac{1}{K_{mL}} = \frac{1}{mk_{mG}} + \frac{1}{k_{mL}} \tag{2.40}$$

These last two equations show the relationship among the coefficients for the individual phases and the overall transfer coefficients, expressed as a global resistance ($1/K_{mG}$ or $1/K_{mL}$) to the transfer of the diffusing component. In studying performance separation processes, it is important to determine which individual resistance is the limiting factor.

2.5 Porous Media

2.5.1 Definition of Porous Medium

A porous medium is a solid with small holes in it. In the broadest sense an open pipe is a limit case of a porous medium. Usually the number of holes or pores is sufficiently large that a volume average is needed to calculate pertinent properties. The matrix of a porous medium is the material in which the holes or pores are imbedded, and the description of their location, size, shape, and interconnection characterize the porous medium (Dullien, 1979).

There is an extremely large array of materials that can be classified as porous media. Broadly we classify media as unconsolidated and consolidated; as ordered and random. Examples of unconsolidated media are beach sand, glass beads, catalyst pellets, column packings, soil, gravel, and packing, such as charcoal. Examples of consolidated media are most of the naturally occurring rocks such as sandstones and limestone. In addition, concrete, cement, bricks, paper, cloth, etc., are manmade consolidated media. Wood can be considered as a consolidated medium, as can be human lung. Ordered media are regular packing of various types of media such as spheres, column packings, woods, etc. Random media are media that are without any particular correlating factor. They are hard to find, since if one looks carefully at almost any media one can correlate some factor. Perhaps media that come the closest to being random are beach or river sands that were not sorted when they were laid down. Bread seems to be random since the pores result from random expansion of gases inside (Scheidegger, 1974). Plant tissues can be considered as unconsolidated or ordered media.

2.5.2 Macroscopic Pore Structure Parameters

There are two important quantities describing the properties of a porous medium: the porosity ϕ and the permeability K. The porosity of a porous medium is defined as:

$$\phi = \frac{pore\ volume}{matrix\ volume} \tag{2.41}$$

where the pore volume denotes the total volume of the pore space in the matrix and the matrix volume is the total volume of the matrix including the pore space. Thus, $0 \leq \phi \leq 1$. The porosity has to be averaged over many pores and the considered matrix volume must be larger than the pore size. Often the porosity can be chosen as constant for the whole medium.

The permeability K describes the ability of the fluid to flow through the porous medium. K is often called the absolute permeability and is a quantity depending on the geometry of the medium only. Below the concept of relative permeability which also depends on the fluids flowing in the porous network will be introduced. There has been much effort to establish relations between the permeability and the porosity. The permeability of the porous media depends not only on the porosity, but also on the pore size and geometrical tortuosity.

The fluid flowing in the pore space is characterized by the dynamical viscosity μ. The viscosity indicates the resistance in the fluid due to shear and tangular deformations. At microscopic level there are friction forces in the fluid caused by the interchange of momentum in collisions between the molecules. The strength of the friction forces sets the viscosity of the fluid. Another expression for the viscosity which is often used, is the kinematic viscosity ν defined as $\nu = \mu / \rho$, where ρ is the density of the fluid. Moreover, the viscosity of incompressible Newtonian fluids is assumed to be isotropic, thus, such fluids are characterized by only one viscosity coefficient μ.

Fluid flow through a porous medium is often given by the phenomenological Darcy's equation. Consider a porous medium of absolute permeability K in a homogeneous gravitation field where the fluid of the dynamic viscosity being μ, is injected through the medium by applying a pressure gradient ∇P across the matrix. The Darcy's equation gives the flow rate V of the fluid through the medium, which is expressed as:

$$V = -\frac{K}{\mu} \cdot (\nabla P - \rho g) \tag{2.42}$$

where g denotes the acceleration due to the gravitational forces and ρ is the density of the fluid. For fluid flow in a horizontal layer g can be neglected (Scheidegger, 1974).

2.6 Turgor Pressure and Plasmolysis

2.6.1 Turgor Pressure

A plant cell consists of a membrane 'bag' or protoplast, contained in a 'rigid' box, the cell wall. Accumulation of solutes (sugars and salts) inside the protoplast (Fig. 2.11a) causes water to move into the cell across the membrane by a process called osmosis (Fig. 2.11b). This is because the presence of solutes inside the cell leaves less room for water, thus lowering the concentration of water. Since only water can cross a semi-permeable membrane, water diffuses into the cell thus lower its concentration gradient. The solutes can not cross the membrane and so remain in the cell.

As water enters the protoplast it swells (Fig. 2.11c), but its continuous expansion is restricted by the cell wall. Further entry of water into the cell generates hydrostatic pressure as the cell wall resists the swelling. The hydrostatic pressure generated is called the turgor pressure (Fig. 2.11d). When the osmotic force, pulling the water into the cell, is balanced by the turgor pressure, squeezing water out then turgor is constant.

A major factor determining the magnitude of the turgor pressure is the total number of solutes accumulated inside the protoplast; the osmotic pressure of the cell contents (π) provides a measure of this. The osmotic pressure (π) and turgor pressure (P_T) of a cell are conveniently combined in the term water potential (Ψ_w), which is a measure of the energy state of the water at any point.

$$\Psi_w = P_T - \pi \tag{2.43}$$

It must be emphasized that the chemical potential of the water in a plant cell not only depend on the osmotic term, but also on the turgor pressure. In a plant, the direction in which water moves from one cell to another depends on their relative water potentials, not merely on their relative osmotic pressures. Water moves from cells with higher water potentials to cells with lower water potentials (Thain, 1967; Sajnin *et al.*, 1999).

2.6.2 Plasmolysis

When the cell completely fills the space inside the cell wall and distends it slightly, so that the wall exerts a turgor pressure, the cell is said to be turgid. The concentration of the external solution can be so chosen that its osmotic pressure is equal to that of the cell. The turgor pressure is then equal to zero, and the cell just fills the space inside the cell wall, without distending it. Such a cell is said to be in a state of incipient plasmolysis. If it is placed in a solution with a still greater osmotic pressure, more water leaves the cell. The cell shrinks and the plasmalemma withdraws from the cell wall. The spaces between the plasmalemma and the wall become injected with the external solution. In this state, the cell is said to be plasmolysed. As the osmotic pressure of the external solution is increased, the cell shrinks further. When plasmolysis takes place, the cell does not always separate completely from the cell wall. Points of adhesion may remain, as in Fig. 2.12.

Plasmolysis is generally reversible. If a plasmolysed cell is returned to a solution with a low osmotic pressure, the cell swells and distends the cell wall slightly so that it regains its turgidity (Thain, 1967).

2.7 Mathematical Modelling of Osmotic Dehydration

2.7.1 Introduction

There are two resistances opposing mass transfer during osmotic dehydration of horticultural products, internal resistance and external resistance. The fluid dynamics of the solid-fluid interface governs the external resistance whereas the internal resistance, much more complex, is influenced by cell tissue structure, cellular membrane permeability, deformation of vegetable/fruit pieces and the interaction between the different mass fluxes. Under the usual treatment conditions, the external resistance is negligible compared to the internal one.

While solute transfer is assumed to be of the diffusional type, the fact that water loss is greater than solid gain is attributed to an osmotic transport phenomenon across the

semi-permeable cellular membranes (Ponting *et al.*, 1966; Ponting, 1973; Bolin *et al.*, 1983; Lenart & Flink, 1984; Djelveh *et al.*, 2001; Medina-Vivanco *et al.*, 2002). Thus, the process is termed 'osmotic dehydration', though perhaps the most appropriate term would be 'dehydration driven by concentration differences', or as proposed by Raoult-Wack and Guilbert (1990) 'dehydration and impregnation by immersion'. These authors observed that the above-mentioned behavior is not confined only to vegetables or fruits. Immersion of pieces of agar - where no membranes are present - in concentrated sucrose solutions leads to a water loss several times higher than the solute gain. The same thing happened when placing the tilapia fillets in the limited volumes of ternary solutions (salt-sugar-water) (Medina-Vivanco *et al.*, 2002) and placing fresh refrigerated bovine semi-tendinosus muscles slices in salt and sugar solutions (Djelveh *et al.*, 2001).

According to some authors, solute penetration is confined to extra-cellular spaces (Hawkes & Flink, 1978; Bolin *et al.*, 1983). Isse and Schubert (1991) and Saurel (1995) showed by microscope observations that, sucrose passes through the cell wall and accumulates between the cell wall and the cellular membrane, where it forms a hypertonic solution leading to a water outflow through the cellular membrane. Other authors (Hawkes & Flink, 1978; Bolin *et al.*, 1983; Giangiacomo *et al.*, 1987; Biswal & Bozorgmehr, 1992) have suggested that water loss is greater than solute gain only because of differences between the diffusion coefficient of water and solute in the product.

The existence of two simultaneous and opposite mass fluxes is one of the main difficulties arising when modelling mass transfer in osmotic dehydration. Moreover, these fluxes take place in strong non-equilibrium conditions, accompanied by significant shrinkage and deformation of the vegetable/fruit piece (Lenart & Flink, 1984; Barat *et al.*, 2001; Maura *et al.*, 2002) and, possibly, by interactions between the different fluxes (Biswal & Le Maguer, 1989; Toupin & Maguer, 1989; Sereno *et al.*, 2001; Sacchetti *et al.*, 2001).

As everything seems to indicate that several transfer mechanisms coexist during the osmotic dehydration of horticultural products, the development of a mathematical model able to include all these mechanisms is very difficult. After a bibliographical

review of the subject, we identified a number of simple mathematical models that are capable of representing the experimental data but the use of them is limited to certain cases because they did not take into account the mechanisms on which the results depend. On the other hand, some models, which are much more elaborate, allow the above-mentioned complexity to be described but their experimental validation becomes extremely difficult owing to the number of parameters that have to be known in order to solve the equations.

All osmotic dehydration models attempt to interpret or predict the usual results of an osmotic dehydration of a horticultural product. In general, the time evolution of osmotic dehydration is quantified by measuring weight reduction (WR) and total solids content (TS). In literature, the parameters or variables used to quantify the osmotic dehydration process include: water loss (WL), defined as grams of water removed per 100 g of initial product mass; solid gain (SG), expressed as the grams of solute incorporated into 100 g of initial product; concentrations of soluble solids (C_s) and the volume reduction (VR).

Based on Fick's unsteady state law of diffusion,

$$\frac{\partial C}{\partial t} = D\frac{\partial^2 C}{\partial x^2} \tag{2.44}$$

(where C is the concentration of solute, D is the diffusion coefficient of this solute and t is time of diffusion), numerous studies have been carried out to estimate the water or solute diffusivity, simulating the experiments with boundary conditions to overcome the assumptions involved in Fick's law (Crank, 1979; Conway *et al.*, 1983; Kaymak-Ertekin *et al.*, Rastogi *et al.*, 1994). Assumptions include constant concentrations of external solution and negligible surface resistance compared with the internal diffusion resistance (Lazarides *et al.*, 1995). The assumption of constant solution concentration can be satisfied by maintaining a high solution to food ratio. This assumption can be satisfied in laboratory scale. But, many problems can be faced when high volumes of concentrated solutions are to be circulated through the equipment in an industrial application (Matusek *et al.*, 2002). The solution/food ratio of 4 to 6 is optimum for the optimum osmotic effect (Lenart *et al.*, 1984). The assumption of negligible external resistance cannot always be satisfied at high viscosity, at low temperature and high

solute concentration (Matusek *et al.*, 2002). It was shown that the external resistance cannot be negligible for osmotic dehydration carried out at different agitation conditions (Mavroudis *et al.*, 1998).

The changes in the state of the cellular structure have not been considered in most of the earlier studies. Since the cellular volume can change with the time, it produces a large influence to the whole osmotic dehydration process. Moreover, the cell membrane properties also change due to osmotic stress. So, the models previously reported are not very appropriate.

Toupin *et al.* (1989) simplified a plant cell as a cylindrical equivalent consisting of two hollow coaxial cylinders and a membrane located between the two cylinders. The cylindrical equivalents are attached to each other to form a continuum. The conceptual model not only provides a means to permit concentration gradients to exist in the extra-cellular volume, but also considers the volume average flux and allows for mass exchange between the intracellular and extra-cellular volumes for one dimensional mass transfer analysis. Later the model was modified by Marcotte *et al.* (1991) to give a closer thermodynamic description of the forces involved in osmotic dehydration processes.

Yao *et al.* (1996) developed a conceptual model to represent the cellular structure of a tissue consisting of individual cells embedded in a continuous cell wall matrix incorporating diffusion, bulk-flow, trans-membrane flux and shrinkage of the matrix. And in the following year, the authors presented a detailed analysis of mass transfer mechanisms in osmotic dehydration by examining the profiles of several dependent variables as a function of time and position. The dependent variables investigated included: the concentration of solute in the extra-cellular volume, the cross-section area of the extra-cellular volume, trans-membrane water flux and bulk flow velocity (volume average velocity).

Spiazzi *et al.* (1997) developed a mathematical model, which takes into account the capacity of each constituent to diffuse within tissue by using a diffusion coefficient and a trans-membrane mass transfer coefficient. The model also depends on the mass ratio of osmotic solution to product, on the initial chemical composition of the product and

solution and on the product shape. The model allows the main variables of osmotic dehydration to be estimated using a low number of fitting parameters, and interprets, through a simple algorithm, the complex phenomena of the main mass transfer mechanisms in plant tissues.

In the following sections of this chapter, more details of the three models (Toupin *et al.*, 1989; Yao *et al.*, 1996; Spiazzi *et al.*, 1997) will be discussed.

2.7.2 The equivalent cylindrical unit cell model (ECUC) (Toupin *et al.*, 1989)

Toupin *et al.* (1989) developed a mathematical model incorporating cell membrane characteristics for the simulation of water and solute fluxes in a complex cellular structure. The concept of equivalent cylindrical unit cell (ECUC) was proposed in this model. The main advantage of this model is that it simulates the continuity of the interstitium and the discontinuity created by spatial arrangement of the cells in the tissue matrix.

Fig. 2.13 shows one of the average unit cells. The first dimension to be established is the length of the coaxial cylinders which comprise the ECUC, namely, the cellular cylinder representing the cellular volume, the interstitium cylinder representing the interstitial volume and the buffer cylinder which will be introduced below.

To simulate possible shrinkage of the structure and in according with the decision to restrict this study to the analysis of mass transport in an infinite slab, the length of the ECUC will be related to the total volume of the average unit cell, such that changes at that level for any unit comprising the column will be represented by an equivalent decrease or increase in the length of its corresponding cylindrical cell.

Here, l, the length of the ECUC, is defined as the diameter, d^l, of a sphere representing the total volume of the average unit cell, that is, the cellular plus the interstitium volume, times the square root of the interstitium geometrical tortuosity, τ_I , defined as the ratio of the actual distance that a migrating molecule has to travel on average in the

interstitium, as part of a macroscopic unidirectional flow, compared with the distance covered normal to the surface, that is, (Toupin *et al.*, 1989).

$$l = d^1\sqrt{\tau_I} \tag{2.45}$$

The radii of the coaxial cylinders representing the components of the average unit cell are calculated in accordance with the following specifications:

(1) Radius of the interstitium cylinder (R_I). As the average unit cell is spherical, the surface of exchange between interstitium and cellular volume, that is, the area of the plasmalemma, A_m^1 (excluding the proportion of the total cell membrane occupied by plasmodesmata, α_p) is given by

$$A_m^1 = (1-\alpha_p)\pi(d_c^1)^2 \tag{2.46}$$

where d_c^1 is the diameter of the sphere representing the unit cellular volume. As, at any time, all the ECUC dimensions are dependent on geometrical properties which change as osmosis progresses, the radius of the interstitium cylinder, R_I, must be found from

$$A_m^1 \equiv A_m = 2\pi R_I l \tag{2.47}$$

That is, R_I is calculated to make the area of the interface cellular-interstitium cylinders, A_m, identical to the area of the plasmalemma.

(2) Radius of the cellular cylinder (R_C). As the cellular cylinder represents the cellular volume of the average unit cell, V_C^1, its radius, R_C, must be, at any time,

$$V_C^1 \equiv V_C = \pi l(R_C^2 - R_I^2) \tag{2.48}$$

(3) Radius of the buffer cylinder (R_b). The buffer cylinder is introduced as a geometrical artifice to ensure that, as l, R_I and R_C are now known, the volume of the interstitium cylinder, V_I, is identical to its average unit cell equivalent, V_I^1, that is

$$V_I^1 \equiv V_I = \pi l(R_I^2 - R_b^2) \tag{2.49}$$

As can be seen, the above design not only transposes the spherical average unit cell into another geometry but also inverts the whole system. This arrangement has the main advantage of linearizing the interstitial diffusion path at the level of each cell.

In this model, the mass transport across membrane is considered and described using irreversible thermodynamics. For the transport of species i across the plasmalemma,

$$J_{i_m} = -\sum_k L_{ki_m} \Delta\mu_{k_m} \qquad i, k = 1, 2, \ldots, m \tag{2.50}$$

and, for symplastic transport,

$$J_{i_p} = -\sum_k L_{ki_p} \Delta\mu_{k_p} \qquad i, k = 1, 2, \ldots, m \tag{2.51}$$

where J_{i_m} and J_{i_p} are plasmalemma and symplastic molar fluxes of species i, L_{ki_m} and L_{ki_p} are macroscopic phenomenological coefficient describing the permeability characteristics of the membranes considered. $\Delta\mu_{k_m}$ and $\Delta\mu_{k_p}$ are differences in chemical potential of species k across those membranes, which will be discussed in the later chapter in more details.

Based on above models, the convective diffusion equations in the interstitium was developed as

$$\frac{\partial C_{i_I}}{\partial t} = \frac{\partial}{\partial z}\left[D_i \frac{\partial C_{i_I}}{\partial z}\right] - \left[\upsilon^* \frac{\partial C_{i_I}}{\partial z} + C_{i_I} \frac{\partial \upsilon^*}{\partial z}\right] - \left[\frac{C_{i_I}}{V_I}\frac{\partial V_I}{\partial t}\right] - \left[\frac{A_m}{V_I} J_{i_m}\right] \tag{2.52}$$

where C_{i_I} is the local concentration of species i in the interstitium, t is the time variable and z the macroscopic direction of transfer. υ^* is the local value of the volume average velocity, which can be expressed as:

$$\frac{\partial \upsilon^*}{\partial z} = -\left[\frac{A_m}{V_I}\sum_i \overline{\upsilon}_i J_{i_m} + \frac{1}{V_I}\frac{\partial V_I}{\partial t}\right] \quad i = 1, 2, \cdots, m \tag{2.53}$$

From Eq. (2.52), it can be seen that there are four processes: transport by diffusion (first term), transport by convection (second term), concentration or dilution due to interstitial volume changes (third term), and production or depletion due to exchanges across the plasmalemma (trans-membrane transport, last term).

Referring to Fig. 2.13, for the j^{th} cellular volume considered as a whole, the following is the variation with time of the intracellular concentration C_{i_c} of species *i*:

$$\frac{dC_{i_c}}{dt} = \left[\frac{2\pi R_1}{V_C - V_d}\int J_{i_m} dz\right] - \left[\frac{C_{i_c}}{V_C - V_d}\frac{dV_C}{dt}\right] + \left[\frac{A_p^-}{V_C - V_d} J^-_{i_p}\right] + \left[\frac{A_p^+}{V_C - V_d} J^+_{i_p}\right] \quad (2.54)$$

The first term describes the contribution of the trans-membrane flux (where the integral is carried out over the entire length of the cell); the second term describes the effect of the cellular volume change on the concentration; the last two terms are employed to take into account the contribution of symplastic transport from/to the neighbouring cells, which are restricted to the ends of 'downstream' and 'upstream' cells, that is, the $(j\text{-}1)^{th}$ cell (superscript -) and $(j+1)^{th}$ cell (superscript +) of the representative column. V_d is a correction factor, usually referred to as apparent cellular non-osmotically active volume, which is introduced to account for the intrinsic non-ideality and non-diluteness of the intracellular solution (Toupin *et al.*, 1989).

By the treatment similar to Eq. (2.54), the total volume change of the cellular compartment is given by

$$\frac{dV_C}{dt} = \left[2\pi R_1 \int \sum_i \overline{\upsilon}_i J_{i_m} dz\right] + \left[A_p^- \sum_i \overline{\upsilon}_i J^-_{i_p}\right] - \left[A_p^+ \sum_i \overline{\upsilon}_i J^+_{i_p}\right] \quad (2.55)$$

where again the contributions of the trans-membrane (first term) and symplastic fluxes (second and third terms) to the total volume change are included.

It was assumed that there are three stages (seen Fig. 2.14) in the osmotic dehydration. Each stage was assumed to be the functions of the extent of cellular volume losses, which are given by

$$\frac{dV_1}{dt} = k\frac{dV_c}{dt} \quad (2.56)$$

where the compliance factor, *k*, takes the values of 0, -1 and 0, for stage 1, 2 and 3, respectively. The limits of each stage are defined as follows:

Stage 1, from full turgor to incipient plasmolysis, that is, from the maximum volume a typical cell can achieve upon swelling to its volume at which the internal hydrostatic pressure vanishes ($P_c=0$). This period describes the loss of turgescence of the tissue. At this stage, cell wall is under pressure and any water loss results in a decrease of intracellular volume but the extra-cellular volume is constant at a minimum.

Stage 2, from incipient plasmolysis to the critical cell volume, that is, from the point where $P_c=0$ to the point where the loss of cellular volume is such that the structure starts to collapse. At this stage, the cell wall is under tension and any water loss from the intracellular volume is gained by the extra-cellular volume. The extra-cellular volume in stage 2 increases from its minimum to a maximum but the total volume is constant (See Fig. 2.14).

Stage 3, from the critical cell volume to the equilibrium volume. Following stage 2, the extra-cellular volume remains constant at its maximum. The decrease of intracellular volume is equal to the decrease of the total volume. This stage will be considered as a period during which the whole structure collapse due to extreme volume diminution.

The main advantage of this model is that it allows each cell to experience the presence of concentration gradients in the interstitial solution all along its surface of exchange.

2.7.3 One-Dimensional Sandwich Models (Yao, *et al.*, 1996)

Yao *et al.* developed a simplified 'sandwich' model to represent a thin slab of tissue (Fig. 2.15). Due to symmetric properties, only half of the slab was considered. The model consists of intracellular and extra-cellular volumes that are separated by a 'semi-permeable' membrane. The individual cell membranes in the tissue are combined into one single equivalent membrane in this model. The extra-cellular volume is continuous and in contact with the membrane to form one layer of the model. All individual cellular volumes are collected and combined into the intracellular volume, which forms the other layer (Fig. 2.15). The extra-cellular volume was partitioned into free volume (including tissue free volume and the void within the cell wall) and cell wall fiber volume.

The volumes and the membrane area were determined according to the average cellular properties of the tissue. The height of the model (H) is equal to one half the physical thickness of the slice. The surface areas exposed to the solution for the model and the physical slice are equal, even though their shapes may be different. The dimension of the model in the y-direction (E, Fig. 2.15) is calculated from the total membrane area and the height of the model. The total membrane area was calculated through the average diameter of spherical cells. Then the dimensions in the x-direction for each volume were determined from the relationship between the individual volumes and the dimensions in the y- and z-directions.

Since the cellular volume in the tissue is discontinuous, the equivalent 'lumped' intracellular volume has to be treated in such a way as to maintain some of the features of the real tissue. The cross sectional area of the intracellular volume was defined through the following equation:

$$A^c = \sum_{j=1}^{n} \dot{A}_j \tag{2.57}$$

where $\dot{A}_j$ is the cross sectional area of cell j cut by the xy-plane and n is the total number of cells cut by the plane (seen Yao *et al.*, 1996). In view of the fact that the absolute size of a cell is very small and transport across the cell membrane is slow, it is reasonable to assume that there are no gradients of concentration and hydrostatic pressure within a cell. Therefore, the profiles of concentrations and hydrostatic pressure within the tissue are step-wise from cell to cell. The concept of volume average concentration (C^c) and pressure (P^c) within cells was used to represent these discontinuous properties as continuous functions of position. The volume average concentration and pressure in the intracellular volume were expressed as:

$$P^c = \frac{\sum_{j=1}^{n} \dot{A}_j P_j^c}{\sum_{j=1}^{n} \dot{A}_j} \tag{2.58}$$

$$C_i^c = \frac{\sum_{j=1}^{n} \dot{A}_j \dot{c}_{i,j}^c}{\sum_{j=1}^{n} \dot{A}_j} \tag{2.59}$$

where P and $\dot{c}$ are the absolute pressure and concentration within a cell, respectively; subscript i refers to component and j to cell; n is the total number of cells cut by the xy-plane and A is the individual cross sectional area of the cells.

Since the symplastic transport (transport between two neighboring cells through small channels) is ignored, direct mass exchange between cells cannot take place. The mass transfer has then to be bridged through the extra-cellular volume. Consequently, there is no z-direction diffusive mass transfer in the intracellular column. As cells lose water in osmotic dehydration, the volume and the cross sectional area of the cells will change as well as their position. This is because cells are essentially tied to the continuous cell wall framework which behaves as an elastic body during water withdrawal. Upon the loss of water the cell's canter of gravity follows the movement of the cell wall. When averaging at a given position, the average velocity of the cell material in the intracellular volume will be the same as the cell wall shrinking velocity at that position. The solution was assumed incompressible and so dilute that the partial molar volumes of all components were constant. It was also assumed that there was no concentration gradient in the xy-plane and that the concentration gradient existed only in the z-direction. This is because the x-dimension is very small. By making a mass balance and a volume balance on a small segment of the conceptual model along the z-direction (Fig. 2.15), the following equations were obtained:

Free volume:

$$\frac{\partial(C_i^f A^f)}{\partial t} = \frac{\partial}{\partial z}[A^f D_i^f \frac{\partial C_i^f}{\partial z}] - \frac{\partial(C_i^f v^f A^f)}{\partial z} + J_i E \tag{2.60}$$

$$\frac{\partial(v^f A^f)}{\partial z} = \sum_{i=1}^{k}(J_i \bar{v}_i)E - \frac{\partial A^f}{\partial t} \tag{2.61}$$

Intracellular volume:

$$\frac{\partial(C_i^c A^c)}{\partial t} = -\frac{\partial(C_i^c v^c A^c)}{\partial z} - J_i E \tag{2.62}$$

$$\frac{\partial(v^c A^c)}{\partial z} = -\sum_{i=1}^{k}(J_i \bar{v}_i)E - \frac{\partial A^c}{\partial t} \tag{2.63}$$

Cell wall fibre volume:

$$\frac{\partial A^w}{\partial t} = -\frac{\partial (v^w A^w)}{\partial z} = -\frac{\partial (v^c A^w)}{\partial z} \tag{2.64}$$

where C is the concentration, A is the cross sectional area, t is the time, D is the apparent diffusivity, v is the volume average velocity or shrinkage velocity (net volume flux through a fixed cross section = bulk flow velocity), J is the trans-membrane flux and E is the dimension of the model in the y-direction. The superscripts c, f and w distinguish the intracellular volume, free volume and cell wall fibre volume, respectively. The subscript i identifies one of the k components present in the solution and the free volume.

Eqs. (2.60) and (2.62) represent the concentration changes at a fixed position in the free volume and intracellular volume, and Eqs. (2.61) and (2.63) represent the variations with distance at a fixed time of the bulk flow along one dimension, respectively. Eq. (2.64) describes the cross sectional area changes as a consequence of the shrinkage.

The descriptions of mass transfer across the membrane J_i will be considered using irreversible thermodynamics by which phenomenological equations can be used to describe such processes. This term functions as a sink or source in these equations.

A significant breakthrough of this model is in the development of the conceptual model by eliminating the cell-to-cell basis as employed exclusively by previous researchers. The model maintains the physical thickness and the cross sectional area. A volume average concept expresses the discontinuous natural of the concentration and the pressure in the cells as continuous functions. After the elimination of the cell-to-cell basis and the introduction of the volume average concept, the mathematical modeling and the numerical solution procedure become much simpler because the medium is treated as continuous. Also this model eliminates the assumption that tissue consists of individual average unit cells arranged in a three dimensional lattice.

2.7.4 Osmotic-Diffusional Model (ODM) (Spiazzi, *et al.*, 1997)

Inspired by the models of Toupin *et al.* (1989) and Marcotte *et al.* (1991), Spiazzi, *et al.* developed an osmotic-diffusional model (ODM). This is based on mass transfer through

cellular membranes and the diffusion of different species through intercellular spaces. At the same time, the model is designed to be applied under the more usual conditions of osmotic dehydration in fruits and vegetables. Such conditions include several different solutes and various concentration levels in the osmotic solution, products of finite dimensions, and finite mass ratios of solution to product.

Mass transfer in a plant tissue during osmotic dehydration can be interpreted from the scheme shown in Fig. 2.16. Water and permeable natural constituents such as mineral salts or fructose/glucose are transferred through the cellular membrane from the cell inside towards the extra-cellular space (plasmalemmatic trans-membrane transfer, PTT) or, else, towards a neighbouring cell (simplistic trans-membrane transfer, STT). Once the water and the above-mentioned natural constituents reach the extra-cellular spaces, they are transferred towards the osmotic solution while solutes are transferred to the product via the same process but in opposite direction (diffusional-convective transport, DCT). The extra-cellular space is composed of the space between cell wall and cell membrane plus the intercellular spaces themselves.

To describe the aforementioned hypothesis mathematically, they divided the vegetable piece into N concentric and equal volumes. As, in the mass transfer, the vegetable is considered isotropic and mass fluxes are one-dimensional, that is, from the centre to the outside and vice-versa. Thus, every cell in the V^i volume is at the same distance z^i from the product-osmotic solution interface, and so will behave similarly. From the mathematical point of view, such cells can be considered as only one cell, the transfer area and volume of which is calculated as the sum of transfer areas and volumes of each cell placed at a distance z^i from the surface.

By bearing in mind the above-mentioned hypothesis, fluxes and mass balances for the j^{th} species in the volume V^i as follows: Trans-membrane mass fluxes are:

(PTT) $$nj_{cp}^{i} = kj_{p}(\rho j_{c}^{i} - \rho j_{0}^{i}) \tag{2.65}$$

(STT) $$nj_{cs}^{i} = kj_{s}(\rho j_{c}^{i+1} - \rho j_{c}^{i}) \tag{2.66}$$

where kj_p and kj_s are plasmalemmatic and symplastic trans-membrane mass transfer coefficients, respectively, kj_s being considered to be 100 times higher than kj_p. Symbols ρj_c^i and ρj_0^i are the mass concentrations of the j^{th} species in the cell volume V_c^i and in the extra-cellular volume V_0^i, respectively:

$$\rho j_c^i = \frac{mj_c^i}{V_c^i} \tag{2.67a}$$

$$\rho j_0^i = \frac{mj_0^i}{V_0^i} \tag{2.67b}$$

In turn, the cellular and extra-cellular volumes are calculated by assuming an ideal behaviour for the solutions, using the following expressions

$$V_c^i = \sum_{j=1}^{N} mj_c^i v_j \tag{2.68a}$$

$$V_0^i = \sum_{j=1}^{N} mj_0^i v_j \tag{2.68b}$$

The mass balance for each j^{th} species present in the cellular volume is as follows:

$$\frac{dmj_c^i}{dt} = -nj_{cp} A_{cp}^i + nj_{cs}^{i+1} A_{cs}^{i+1} - nj_{cs}^i A_{cs}^i \tag{2.69}$$

where A_{cp}^i and A_{cs}^i are transfer areas of plasmodesma and symplasma transfer ways, respectively, A_{cs}^i being about 1% of A_{cp}^i.

The transfer area A_{cp}^i is calculated from cell shape and size by:

$$A_{cp}^i = N_{cv} (V_c^i)^{2/3} \tag{2.70}$$

where N_{cv} is a constant which depends on the cell shape and the number of cells per unit volume. The extra-cellular mass fluxes are:

$$nj_0^i = D_{ap} j(\rho j_0^{i+1} - \rho j_0^i) / \Delta z^i + \rho j_0^i u^i \tag{2.71}$$

where D_{apj} is the apparent diffusion coefficient of the i^{th} species, and Δz^i is the thickness of the V^i volume. The velocity u^i is associated with the backward movement of the transfer area (the vegetable/fruit shrinks), and is calculated by:

$$u^i = \frac{z^i_{t+dt} - z^i_t}{dt} \tag{2.72}$$

On the other hand, the mass balance for each species, j, in the extra-cellular volume yields:

$$\frac{dmj^i_0}{dt} = -nj^{i+1}_0 A^{i+1}_0 - nj^i_0 A^i_0 + nj^i_{cp} A^i_{cp} \tag{2.73}$$

In turn, the transfer area of the intercellular volume A^i_0 is calculated by the following expression:

$$A^i_0 = C_g (V^i_0)^{2/3} \varepsilon^i \tag{2.74}$$

The constant C_g depends on the shape of the product piece, while ε^i represents the fraction of the geometric area which belongs to the extra-cellular spaces, a value considered to be equal to the volumetric fraction of those spaces:

$$\varepsilon^i = \frac{V^i_0}{V^i_c + V^i_0} \tag{2.75}$$

The concentration of each species j in the osmotic solution is deduced from the overall mass balance

$$\sum_{i=1}^{N} \frac{dmj^i_0}{dt} = -\frac{dmj_{sol}}{dt} \tag{2.76}$$

The resistance to mass transfer through the product-osmotic solution interface can be considered negligible compared to that inside the product, particularly because the outside solution is stirred in most processes. Therefore, we considered that the concentration of the j^{th} species that faces the product (the surface concentration of the j^{th} species) is the same as the bulk value for the external osmotic solution.

This model allows the main variables of osmotic dehydration to be estimated using a low number of fitting parameters, and interprets, through a simple algorithm, the complex phenomena of the main mass transfer mechanisms in plant tissue.

2.7.5 Limitations of Previous Models

Although many models have been built up and are capable of representing the experimental data, there are the following limitations in previous models:

- Limited to certain cases and do not take into account the mechanism on which the results depend on a large number of biophysical properties, such as elastic modulus of the cell wall, cell wall void fraction, cell wall tortuosity and membrane permeability coefficient, which are very difficult to measure or to predict.

- Some assumptions, such as three stages of osmotic dehydration process, are hard to be verified.

- Impossible to be extended to multi-dimensional analyses.

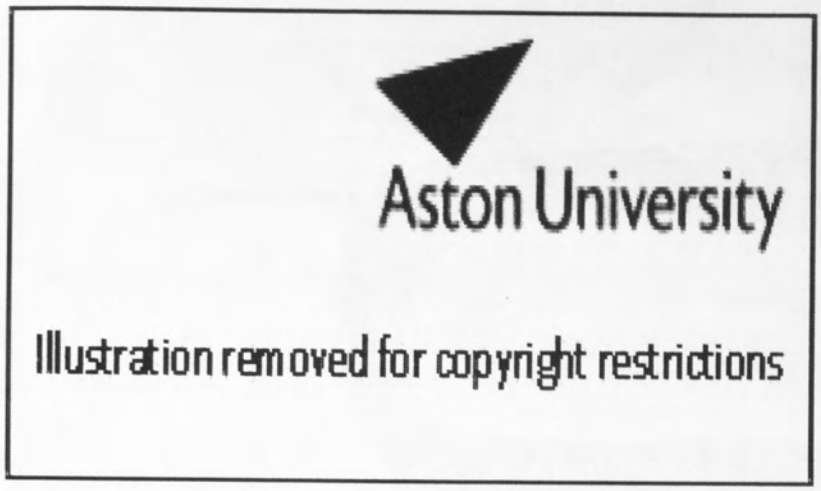

Figure 2.1 Schematic representation of a mature cell (Lüttge *et al.*, 1976)

Figure 2.2 Cross-section of a Plant Cell

Figure 2.3 Diagram of the layers structure of Cell Wall. (Terry Brown, 1998)

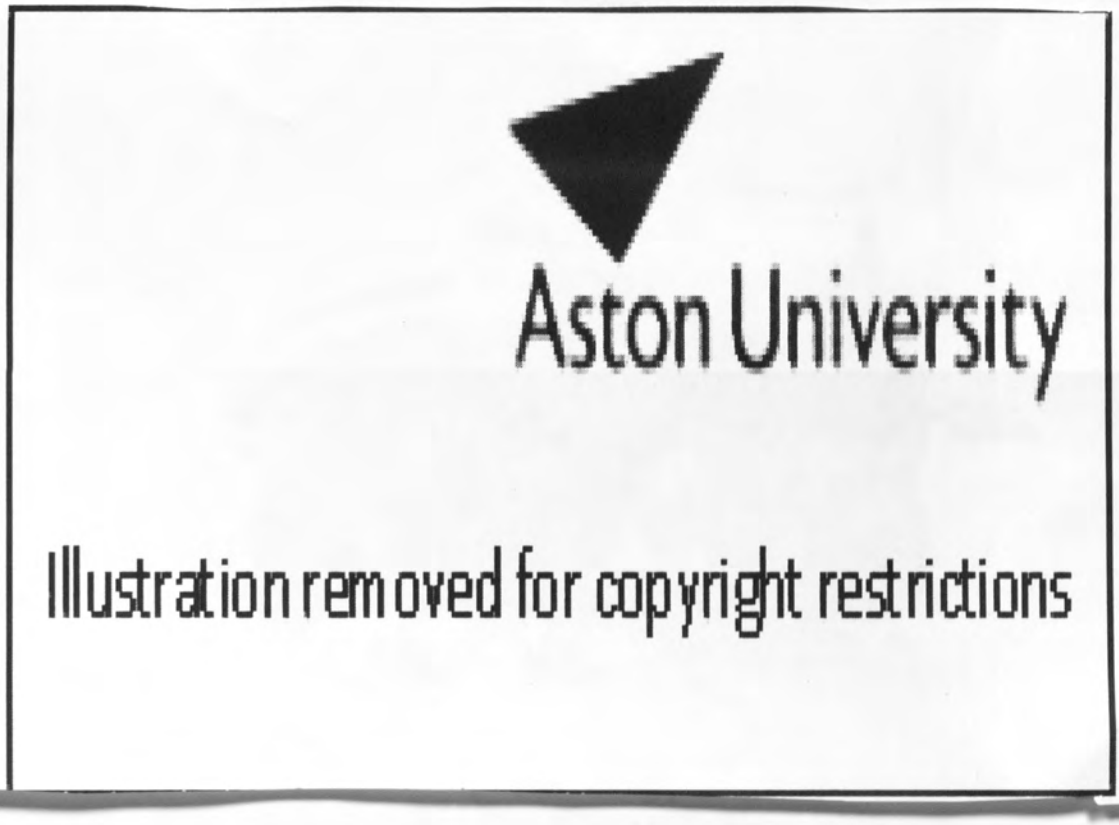

Figure 2.4 Diagram of the Cell Membrane. The proteins are embedded inside of the cell membrane. The lipid content of the membrane allows the cell membrane to automatically repair itself when it is torn. (http://library.thinkquest.org/C004535/cell_membranes.html)

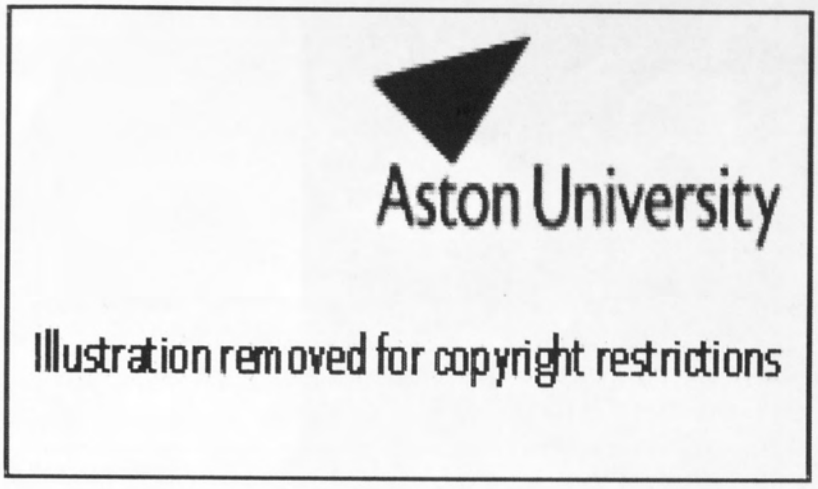

Figure 2.5 Diagram of the vacuole structure
(http://library.thinkquest.org/C004535/vacuole.html)

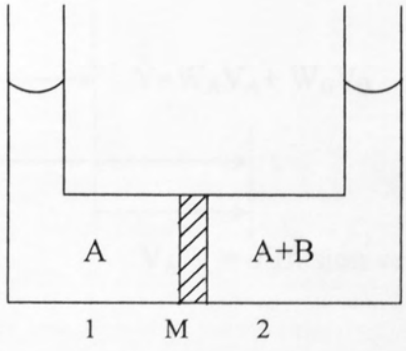

Figure 2.6 System for demonstration of osmosis and osmotic pressure

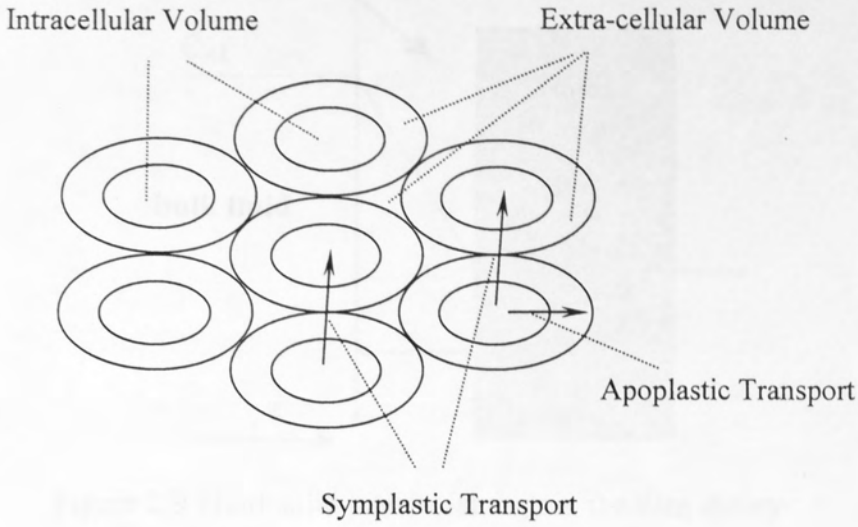

Figure 2.7 Mass Transport pathways in plant tissues

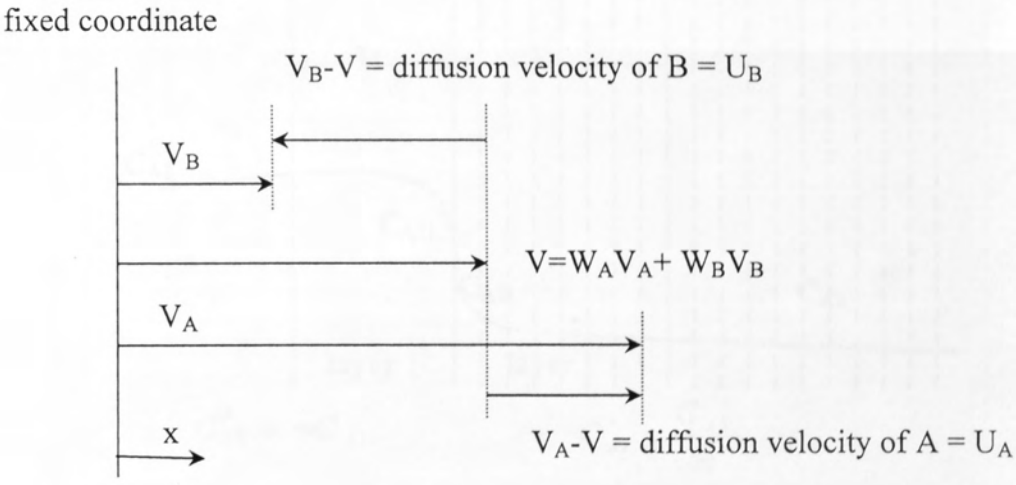

Figure 2.8 Scheme of individual and bulk velocities of a binary mixture

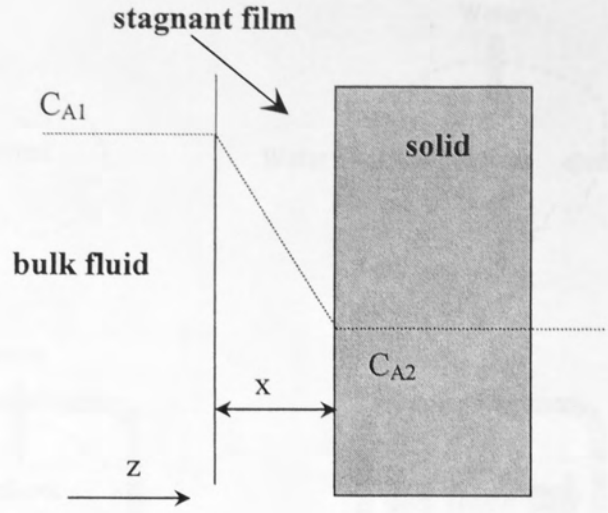

Figure 2.9 Fluid-solid interfacial region: the film theory

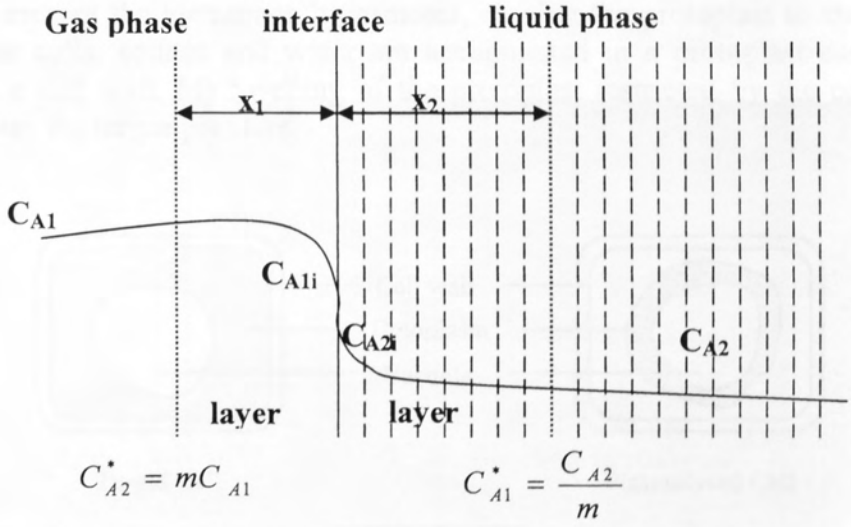

Figure 2.10 Mass transfer at a gas liquid interface: the two-film theory

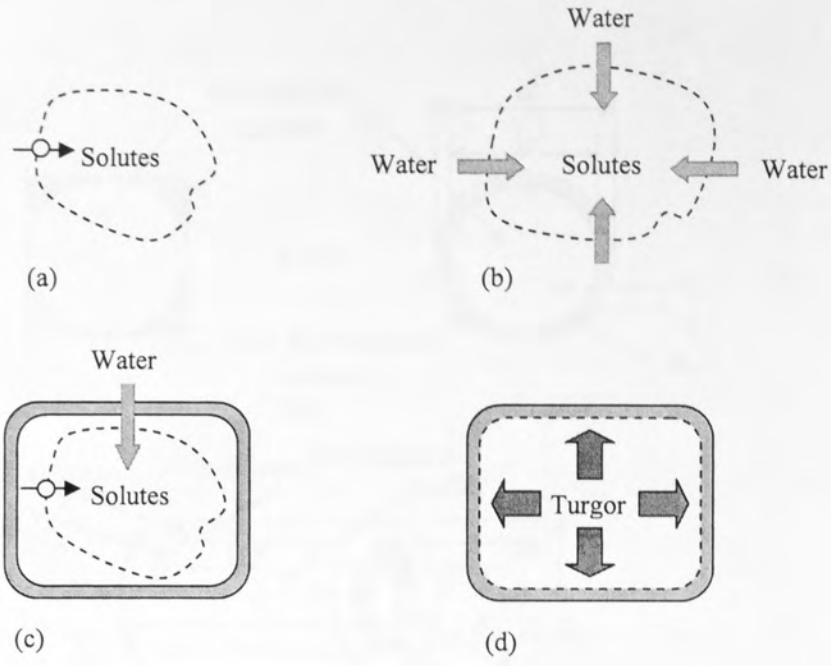

Figure 2.11 The generation of turgor pressure in plant cells. (a) Solutes are actively pumped across the semi-permeable membrane of the protoplast. (b) Water crosses the membrane by osmosis, causing the protoplast to swell. (c) In plant cells, solutes and water are accumulated in a protoplast contained within a cell wall. (d) Swelling of the protoplast restricted by the cell wall generates the turgor pressure.

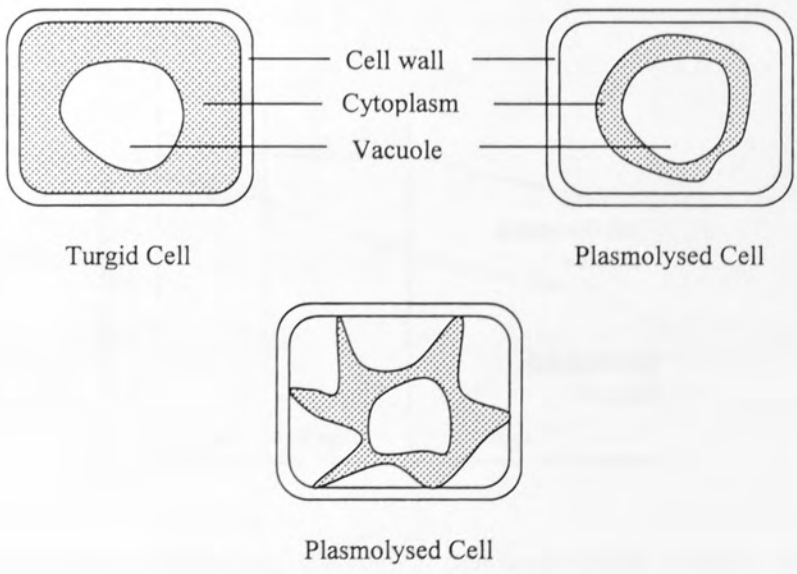

Figure 2.12 Plasmolysis

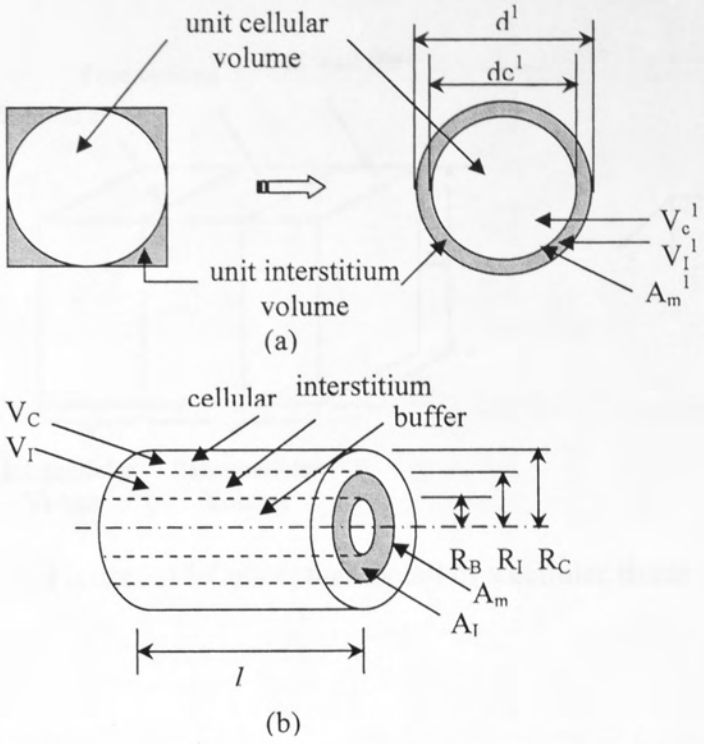

Figure 2.13 The average unit cell (a) and the equivalent cylindrical unit cell (b)

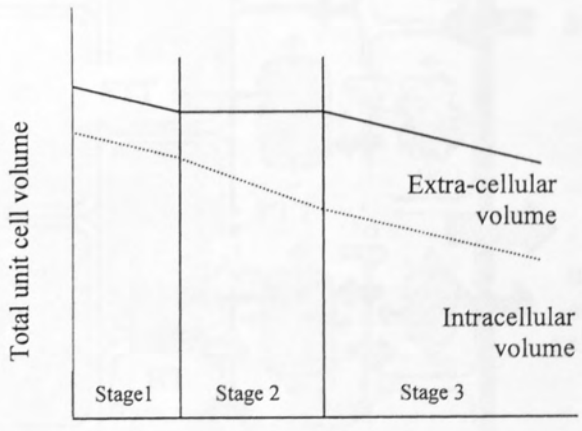

Figure 2.14 General behaviour of a typical cell undergoing osmotic dehydration

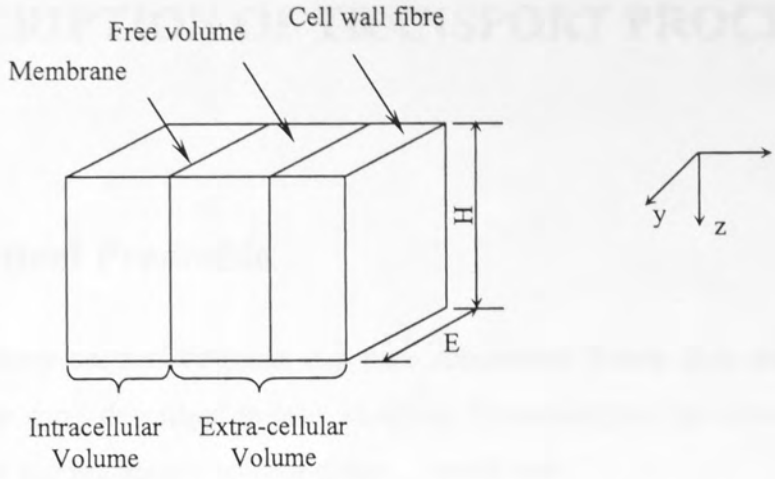

Figure 2.15 Conceptual model of a cellular tissue

Figure 2.16 Schema of the different mass transfer paths and mechanisms during osmotic dehydration of vegetable tissues. PTT: plasmalemmatic trans-membrane transfer, STT: Symplastic trans-membrane transfer, ET: extra-cellular transport. Δz^i: thickness of the transfer pathway, A_0: transfer area of intercellular volume, A_{cp}: plasmodesma transfer area, A_{cs}: symplasma transfer area. (Spiazzi, *et al.*, 1997)

Chapter 3 PHENOMENOLOGICAL DESCRIPTION OF TRANSPORT PROCESSES

3.1 Practical Preamble

This introductory section contains the bare theoretical bones that are necessary to understand the work described in later chapters. Essentially we are concerned with the flows of water and uncharged solutes across a membrane.

Consider a homogeneous membrane separating outer and inner (ideal) dilute solutions designated by superscripts *o* and *i*. Net fluxes of solute and water from outside to inside are taken as positive. The difference in solute concentration across the membrane is given by the outside concentration minus the inside one. Differences of hydrostatic and osmotic pressure are defined similarly.

The subscripts *v*, *s* and *i* refer to volume, permeable solute and impermeable solute respectively. The following symbols are used.

J_v	m/s	Net volume flux
J_s	kmol/m^2 s	Net solute(s) flux
R	J/kmol K	Gas constant
T	K	Absolute temperature
Δp	MPa	Hydrostatic pressure difference
$\Delta\pi_i$	MPa	Osmotic pressure difference due to *i*
$\Delta\pi_s$	MPa	Osmotic pressure difference due to *s*
$\bar{c}_s$	kmol/m^3	Average concentration of s across membrane
L_p	m/Pa s	Hydraulic conductivity of membrane
ω_s		Solute permeability of membrane
σ_s		Reflexion coefficient of membrane

The equations derived from irreversible thermodynamics to describe volume and solutes flows are (will be introduced later in details).

$$J_v = L_p(\Delta p - \sum \sigma_s \Delta \pi_s) \tag{3.1}$$

$$J_s = \omega_s \Delta \pi_s + J_v \bar{c}_s (1 - \sigma_s) \tag{3.2}$$

The derivations of Eqs (3.1) and (3.2) will be introduced in next section in details.

In order to use these equations L_p, ω_s and σ_s must be determined. The following description will outline briefly how these parameters are determined practically.

Hydraulic conductivity

The volume flow equation shows that when $\Delta \pi_i$ and $\Delta \pi_s$ are both zero

$$J_v = L_p \Delta p \tag{3.3}$$

L_p may be determined, therefore, by measuring J_v for a given Δp.

Alternatively when Δp and $\Delta \pi_s$ are both zero the volume flow is given by

$$J_v = -L_p \Delta \pi_i \tag{3.4}$$

where the negative sign indicates that volume moves in the opposite direction to that of $\Delta \pi_i$. This relation also yields L_p.

Solute permeability

The solute flux equation shows that when J_v is zero

$$J_s = \omega_s \Delta \pi_s = \omega_s RT \Delta c_s \tag{3.5}$$

or, more conveniently,

$$J_s = P_s \Delta c_s \tag{3.6}$$

In current practice $P_s = \omega_s RT$ is determined by measuring the unidirectional flux of labelled s for a given concentration difference of labelled s when there is no volume flow. This procedure can also be used to obtain the diffusional permeability of labelled water which is conventionally called P_d to distinguish it from L_p (House, 1973).

Reflection coefficient

This membrane coefficient can be determined in a number of ways that are indicated by inspection of the volume flow equation above.

Firstly, consider that $\Delta\pi_i$ is equal to zero. Then the volume flow will be halted, that is, $J_v = 0$, when

$$\Delta p = \sigma_s \Delta\pi_s \tag{3.7}$$

Knowing $\Delta\pi_s$ and appropriate value of Δp necessary to make J_v equal to zero one can obtain $\sigma_s = \Delta p / \Delta\pi_s$.

Secondly, consider that $\Delta p = 0$. Then the volume flow will be halted when

$$\Delta\pi_i = -\sigma_s \Delta\pi_s \tag{3.8}$$

In practice the appropriate value of $\Delta\pi_s$ for a known $\Delta\pi_i$ can be found by interpolation after a number of volume flow experiments have been performed at different values of Δc_s.

Thirdly, consider again that $\Delta p = 0$ and also that $\Delta\pi_i = 0$. Then the volume flow for a known $\Delta\pi_s$ is given by

$$J_v = -L_p \sigma_s \Delta\pi_s \tag{3.9}$$

By meaning J_v and L_p (in previous experiment) one can obtain σ_s.

Finally, consider again that $\Delta p = 0$. Suppose that two different volume fluxes, J_v' and J_v'' , are obtained for experiments where first $\Delta\pi_i$ only is set up across the membrane and subsequently an identical value of $\Delta\pi_s$ only is established. Then the separate experiments are described by

$$J_v' = -L_p \Delta\pi_i \tag{3.10}$$

$$J_v'' = -L_p \sigma_s \Delta\pi_s \text{ (where } \Delta\pi_s = \Delta\pi_i) \tag{3.11}$$

Thus, the reflexion coefficient is obtained from

$$\sigma_s = \frac{J_v''}{J_v'} \tag{3.12}$$

3.2 Chemical Potential

The chemical potential of species *j* thermodynamically indicates the free energy associated with it and available for performing work. Since there are many concepts to be mastered before understanding such a statement, we will first briefly explore the concept of free energy.

3.2.1 Free Energy and Chemical Potential

The Gibbs free energy, *G*, of a system is a thermodynamic quantity which is a measure of the system's capacity for doing work. The total free energy of a system can be considered to be composed of separate contributions from the various molecular or ionic species present, so that

$$G = \sum_i G_i = \sum_i n_i \mu_i \tag{3.13}$$

where G_i is the total contribution of species *i* to the free energy, and n_i is the number of moles of *i* in the system; μ_i is then the partial molar free energy of *i*. That is, if the system is so large that the addition of one mole of *i* does not appreciably alter the

composition, then μ_i is the change in the total free energy produced by the addition of one mole of i to the system. Alternatively

$$\mu_i = \left(\frac{\partial G}{\partial n_i}\right)_{T,P,n_j} \tag{3.14}$$

where the subscripts indicate that the temperature, pressure, and amounts of all other species in the system are kept constant during the infinitesimal change in n_i.

The partial molar free energy, μ_i, is usually called 'the chemical potential' of i, and is dependent on the pressure, temperature and composition of the system. A substance tends to move from a region where its chemical potential is high to one where its chemical potential is low. At equilibrium, the chemical potential of the component is the same throughout the system.

3.2.2 Analysis of Chemical Potential

For convenience - and also because it has proved experimentally valid – we will represent the chemical potential of any species j by the following sum of the various components into which it can be analyzed:

$$\mu_j = \mu_j^* + RT \ln a_j + \upsilon_j P + z_j FE + m_j gh \tag{3.15}$$

Chemical potential, like electrical or gravitational potential, is a relative quantity. By this we mean that it must be expressed relative to some arbitrary level. Thus, an unknown additive constant, or reference level, μ_j^*, is included in the equation above. Since it contains an unknown constant, the actual value of the chemical potential is not determinable. But for most applications of chemical potential, we are interested in the difference in the chemical potential between particular locations, so only relative values of the chemical potential are important anyway. Therefore, μ_j^* is cancelled out when the chemical potential in one location is subtracted from that in another to obtain the chemical potential difference between the two locations.

In the term of $RT \ln a_j$, a_j is called activity of solute j, which is usually related to its mole fraction or its relative concentration in the solution by means of an activity coefficient, γ_j, that is:

$$a_j = \frac{\gamma_j N_j}{N_w + \sum N_k} = \frac{\gamma_j C_j}{C_w + \sum C_k} \quad (j=1, 2, \ldots, m) \tag{3.16}$$

where γ_j is the activity coefficient of species j, N_j in mole is the mole number of species j in the solution, N_w in mole is the mole number of the solvent in the solution, C_j in mole/m^3 is the concentration of species j, C_w in mole/m^3 is the concentration of the solvent. The summation is applied to all the solute species involved in the solution (that is k from 1 to m).

For an ideal solute, γ_j is unity and the activity of species j

$$a_j = \frac{C_j}{C_w + \sum C_k} \tag{3.17}$$

Activity coefficients for charged species can be appreciable less than unity because of the importance of electrical interactions.

The term $\upsilon_j P$ in Eq. (3.15) represents the effect of hydrostatic pressure on chemical potential. Since essentially all measurements in plant physiology and ecology are made on systems subjected to atmospheric pressure, it is convenient to define P as the pressure in excess of this, and we will adopt such a convention here. υ_j is the differential increase in volume of a system when a differential amount of species j is added, with other species, temperature, pressure, electrical potential, and gravitational position remaining constant:

$$\upsilon_j = \left(\frac{\partial \upsilon}{\partial n_j} \right)_{n_i, T, P, E, h} \tag{3.18}$$

The subscript n_j on the partial derivative in Eq. (3.18) means that the number of moles of each species presented, other than species j, is held constant when the derivative is

taken; the other four subscripts are included to remind us of the additional parameters that must be held constant.

υ_j is called the partial molar volume of species j. It is often nearly equal to the volume of a mole of that species, but because there is in general a slight change in total volume when substances are mixed, υ_j is not exactly equal to it.

To justify the form of pressure term, let us imagine that the solution containing species j is built up by adding small volumes of species j while the system is maintained at a constant pressure P. the work done to add a mole of species j would then be the existing pressure times some volume change of the system characterizing a mole of that species, namely, υ_j.

The influence of electrical potential on the μ_j of an ion is expressed by the term $z_j FE$ in Eq. (3.15), where z_j is an integer representing the charge number of species j, F is a constant known as the faraday, and E is the electrical potential. Because water is uncharged ($z_w = 0$), the electrical term does not contribute to its chemical potential. But electrical potential is of central importance when discussing ions and the origin of membrane potentials. The full expression for chemical potential given by Eq. (3.15), including $z_j FE$, is often referred to as electrochemical potential when discussing the properties of chard particles.

Finally, Eq. (3.15) includes a gravitational term $m_j gh$ expressing the amount of work required to raise an object of mass m_j per mole to a vertical height h, where g is the gravitational acceleration. The gravitational term in the chemical potential is not only important for the fall of rain, snow, or hail, but also it affects the percolation of water downward through porous soil and the upward movement of water in a tree (Nobel, 1983).

In food processing engineering, in the calculation of chemical potential, the last two terms, $z_j FE$ and $m_j gh$ will not be involved because only non-electrolytes will be

discussed and the samples are so small that the difference in vertical direction can be always ignored.

Let us now return to the theoretical treatment of previous problem, the transport of solute and water.

3.3 Transport across Membrane

3.3.1 The Phenomenological Equations of Irreversible Thermodynamics

In nature, there are many examples of linear relations between fluxes and their conjugate forces. For example, the rate of diffusion of a substance is proportional to the negative gradient of its concentration. Extensive studies of the relations between flows and their conjugate forces revealed, however, a flow and a non-conjugate force. For example, a temperature gradient in a bimetallic system produced a current flow. Thus, any theoretical treatment of the relation between flows and forces must include not only the coupling between fluxes and their conjugated forces but also possible coupling between flows and non-conjugate forces. First, any flow J_i may be expressed as a power series in X_i and if the system is relatively close to equilibrium (X_i small) then all powers of X_i larger than the first may be ignored. This approximation is certainly invalid when the range of values of X_i is extended beyond certain limits. Secondly, the relation between J_i and the non-conjugate force X_i has been assumed to be linear too and in 1931 Onsager embodied both of these relations between flows and forces in a set of equations known as the phenomenological equations. These equations can be expressed concisely in the form

$$J_i = \sum_{i=1}^{n} L_{ij} X_j \quad (i = 1, 2, 3, \cdots n) \tag{3.19}$$

or in the extended form

$$
\begin{aligned}
J_1 &= L_{11}X_1 + L_{12}X_2 + L_{13}X_3 + \cdots + L_{1n}X_n \\
J_2 &= L_{21}X_1 + L_{22}X_2 + L_{23}X_3 + \cdots + L_{2n}X_n \\
J_3 &= L_{31}X_1 + L_{32}X_2 + L_{33}X_3 + \cdots + L_{3n}X_n \\
&\cdots \\
J_n &= L_{n1}X_1 + L_{n2}X_2 + L_{n3}X_3 + \cdots + L_{nn}X_n
\end{aligned}
\tag{3.20}
$$

This system of equations describes n different flows in terms of n forces. $L_{11}, L_{12}, \cdots L_{nn}$ are the classical coefficients signifying the relations between the fluxes and their corresponding conjugate forces. On the other hand, L_{ij} $(i \neq j)$ are the cross coefficients signifying the dependence of fluxes on non-conjugate forces. Provided that the fluxes and conjugate forces are chosen so that the sum of their products, that is, $\sum_{i=1}^{n} J_i X_i$, is equal to the rate of entropy production in the system, then the cross coefficients must satisfy the Onsager reciprocal relations, namely

$$L_{ij} = L_{ji} \quad (i \neq j) \tag{3.21}$$

An important consequence of the expression (3.21) is that instead of the n^2 coefficients apparently required to describe n flows in Eq. (3.20) only $n(n+1)/2$ independent coefficients are required. Hence, if we wish to describe the flows of, say, water and glucose across a membrane then only three independent transport coefficients are required.

The phenomenological equations of irreversible thermodynamics describe the relations between fluxes and forces in continuous systems. For example, these equations can be applied to the analysis of isothermal diffusion of solute in a volume of solvent. As these equations are applied to membrane transport, they are probably the most useful equations we have at present (House, 1973).

3.3.2 Transport of Solute and Solvent

Consider a membrane system given in Fig. 3.1. The system consists of two compartments separated by a homogeneous membrane of thickness Δx and area A, and

the compartments are filled with different aqueous solutions of the same solute (non-electrolyte) s. The outer and inner compartments are designated by the superscripts o and i respectively. Let us assume that there is no difference of temperature across the membrane but there is a difference of hydrostatic pressure, Δp , and of solute concentration, Δc_s , across the membrane. The permeation of solute and water which results from these gradients involves discontinuous transitions; that is, both species have to cross phase boundaries between the membrane and the solutions. In addition, the driving forces on solute and water are established within the membrane.

In order to facilitate the adaptation of the thermodynamic formalism, developed for continuous systems, to this discontinuous system several conditions must be satisfied. It must be assumed that each compartment is so well agitated that no local concentration gradients of s exist at the surfaces of the membrane. Moreover, it must be assumed that our discontinuous system is in a state of stationary flow; that is, the net fluxes of solute and water across the membrane are independent of time. The latter condition implies, for example, that the flux of s has the same magnitude and direction at all points in the membrane. Under these circumstances, certain 'forces' cause flows of water and solute across the membrane.

Before embarking on the simple mathematics of this case, let us guess what the final result might look like. First, one would expect that Δp will produce a hydraulic flow of water and Δc_s might establish an osmotic flow. Secondly, Δc_s will produce a diffusional flux of s and Δp might generate an ultrafiltration of s across the membrane. Putting these predictions into the framework of the phenomenological Eqs. (3.20) and expressing them as simply as possible, we expect to find that

$$\text{water flow} = \textbf{hydraulic flow} + \text{osmotic flow}$$

and

$$\text{solute flow} = \text{ultrafiltration} + \textbf{diffusion}$$

where the bold type signifies the flows driven by their conjugate forces. Before we start the theoretical treatment of this problem, we need to know some basic concepts (House, 1973).

Let us denote the net fluxes of solute and solvent across the membrane from outside to inside by J_s and J_w respectively. These fluxes represent the number of moles passing across unit area of membrane in unit time.

The chemical potential for an ideal non-electrolytes solution can be expressed as:

$$\mu_s = \mu_s^0 + RT \ln \frac{C_s}{C_w + \sum C_k} + \upsilon_s P \tag{3.22}$$

where μ_s in J/mole is the total chemical potential of species s, μ_s^0 in J/mole is the total chemical potential of species s when P=0, υ_s in m^3/mole is the partial molar volume of species s, P in N/m^2 is the hydrostatic pressure, R=8.314 J/(mole K) is the universal gas constant, T in K is the absolute temperature, C_s, C_w, C_k in mole/m^3 are the concentrations of species s, solvent and species k respectively.

Note that for any solution the concentrations of species and solvent satisfy:

$$C_w \upsilon_w + \sum C_k \upsilon_k = 1 \tag{3.23}$$

where υ_w and υ_k in m^3/mole are the partial molar volume of the solvent and species k respectively. Hence, any change in the concentration of one particular species will result in the changes of the concentrations of other species, as well as the solvent. The differentiation of Eq. (3.22) leads to:

$$\Delta\mu_s = \upsilon_s \Delta p + RT\left(\frac{\Delta C_s}{C_s} - \frac{\Delta C_w + \sum \Delta C_k}{C_w + \sum C_k}\right) \tag{3.24}$$

Using Eq. (3.23) and noting that:

$$\Delta C_w = -\frac{1}{\upsilon_w} \sum \upsilon_k \Delta C_k \tag{3.25}$$

Eq. (3.24) can be simplified as:

$$\Delta\mu_s = \upsilon_s \Delta P + \frac{RT}{C_s} \Delta C_s \tag{3.26}$$

Similarly to the solute, the chemical potential of the solvent in the solution can be expressed by:

$$\mu_w = \mu_w^0 + RT \ln \frac{C_w}{C_w + \sum C_k} + \upsilon_w P \tag{3.27}$$

where μ_w in J/mole is the total chemical potential of the solvent and μ_w^0 in J/mole is the initial chemical potential of the solvent when P=0.

Eq. (3.27) can be simplified as:

$$\Delta\mu_w = \upsilon_w \Delta P - RT\upsilon_w \sum \Delta C_k \tag{3.28}$$

In Appendix A, the detailed formula transfer about chemical potential is introduced. Eqs. (3.26) and (3.28) are well known and have been widely applied in the field of physical chemistry.

3.3.3 Flux Expressions based on Irreversible Thermodynamics

The conventional description of transport through membranes makes use of two equations, one for the flow of solution and one for the flow of ionic species. Consider a volume element of unit area and thickness dx within a membrane. If this volume is homogeneous, the dissipation function, Φ_m, for the element can be expressed as:

$$\begin{aligned} \Phi_m &= J_w \Delta\mu_w + \sum J_k \Delta\mu_k \\ &= \left(\upsilon_w J_w + \sum \upsilon_k J_k\right) X_V + \sum \left(\frac{J_k}{C_k} - \frac{J_w}{C_w}\right) X_{Dk} \end{aligned} \tag{3.29}$$

where J_w and J_k in mole/(m^2 s) are the molar fluxes of water and species k, respectively, X_v and X_{Dk} in J/m^3 are the corresponding driving forces, which have the following expressions:

$$X_V = C_w \Delta\mu_w + \sum C_k \Delta\mu_k \tag{3.30}$$

$$X_{Ds} = C_s \Delta\mu_s - C_s \upsilon_s \left(C_w \Delta\mu_w + \sum C_k \Delta\mu_k\right) \quad (s=1, 2, \ldots, m) \tag{3.31}$$

For the dilute solution, Eqs. (3.26) and (3.28) can be utilized to replace the chemical potential gradients of water and species s in Eqs. (3.30) and (3.31). In this way, Eqs. (3.30) and (3.31) lead to:

$$X_V = \Delta P \tag{3.32}$$

$$X_{Ds} = RT\Delta C_s \quad (s=1, 2, \ldots, m) \tag{3.33}$$

With the driving forces (3.32) and (3.33), the flows defined in Eq. (3.29) may be rewritten in the form of the phenomenological equations as follows:

$$J_V = L_p X_V - L_p \sum \sigma_k X_{Dk} \tag{3.34}$$

$$J_{Ds} = -L_p \sigma_s X_V + \sum L_{Dsk} X_{Dk} \quad (s=1, 2, \ldots, m) \tag{3.35}$$

where L_p in $m^3/(N\ s)$ is the hydraulic conductivity coefficient, σ_k is the reflection coefficient of the species k, L_{Dsk} in $m^3/(N\ s)$ is the permeability coefficient, J_v and J_{Ds} in $m^3/(m^2\ s)$ are the volume flow and exchange flow defined as:

$$J_V = \upsilon_w J_w + \sum \upsilon_k J_k \tag{3.36}$$

$$J_{Ds} = \frac{J_s}{C_s} - \frac{J_w}{C_w} \quad (s=1, 2, \ldots, m) \tag{3.37}$$

Substituting Eqs. (3.32) and (3.33) into Eqs. (3.34) and (3.35) yields:

$$J_V = L_p \Delta P - L_p \sum \sigma_k RT\Delta C_k \tag{3.38}$$

$$J_{Ds} = -L_p \sigma_s \Delta P + \sum L_{Dsk} RT\Delta C_k \quad (s=1, 2, \ldots, m) \tag{3.39}$$

Note that for the dilute solution the molar flux of species s can be approximately expressed as:

$$\begin{aligned} J_s &= (J_V + J_{Ds})C_s \\ &= (1-\sigma_s)J_V C_s + \sum \omega_{sk} RT\Delta C_k \end{aligned} \tag{3.40}$$

where ω_{sk} is the new permeability coefficient, expressed as:

$$\omega_{sk} = C_s\left(L_{Dsk} - L_p\sigma_s\sigma_k\right) \tag{3.41}$$

As the dominant interaction in the solution is one between ions and solvent, it is generally reasonable to assume $\omega_{sk} << \omega_{ss}$ for $s \neq k$, that is, the non-conjugate permeability coefficients are much smaller than the conjugate permeability coefficients. Under this assumption Eq. (3.40) can be simplified to:

$$J_s = \left(1-\sigma_s\right)J_V C_s + \omega_s RT\Delta C_s \quad (s=1, 2, \ldots, m) \tag{3.42}$$

where $\omega_s = \omega_{ss}$ is the conjugate permeability coefficient.

Eq. (3.38) can be rewritten as:

$$J_V = L_p\left(\Delta P - \sum \sigma_s RT\Delta C_s\right) \tag{3.43}$$

The transport coefficients specified in this chapter have been introduced in section 3.1. With the practical coefficients L_p, ω_s and σ_s it is now possible to express the Eqs. (3.42) and (3.43) in the relatively more useful forms of equations for J_v and J_s.

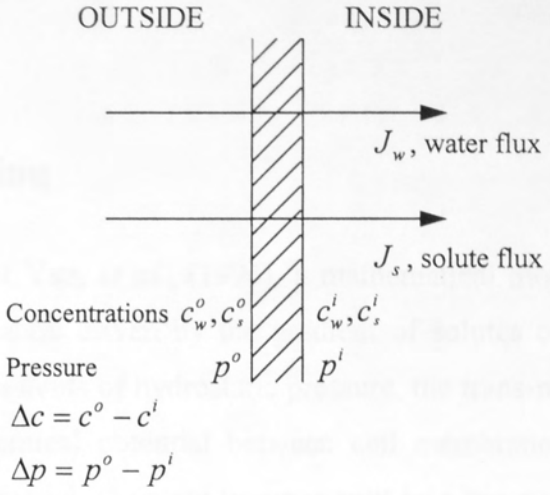

Figure 3.1 Basic transport system showing flows of solute and water across a homogeneous membrane

Chapter 4 MASS TRANSFER MODEL ONE

4.1 Introduction

Based on the work of Yao, *et al.*, (1996), a mathematical model is developed, which incorporates the diffusion driven by the gradient of solutes concentrations, the bulk-flow driven by the gradients of hydrostatic pressure, the trans-membrane flux driven by the difference of chemical potential between cell membranes and shrinkage of the whole matrix. In the model, the plant tissue is split into two parts: intracellular volume and extra-cellular volume. The intracellular volume includes cytoplasm and vacuole and all components inside the cell membranes. The extra-cellular volume includes cell wall fibre volume and free space among the individual cells (see Fig. 4.1). The cell membranes are generally considered as volumeless, but with higher rigidity than other parts. In each part, the mass balance equations and volume balance equations are built and solved by using numerical methods. Unlike the Yao's model, the diffusion in the present model is also considered in the intracellular volume as well as in the extra-cellular volume. Moreover, the volume flux is employed to express the shrinkage of the tissue. Some additional equations are also modified to simplify the process, which are given in the following sections.

4.2 Mathematical Model

4.2.1 Tissue Structure Model

A simplified two-layer model is developed to represent a thin slab of tissue and is shown in Fig. 4.2. Due to the symmetric properties, only half of the tissue slab is considered. The structural model consists of intracellular and extra-cellular volumes separated by a 'semi-permeable' membrane. All individual cellular volumes are collected and combined into the intracellular volume to form one layer of the model and the same to the extra-cellular volume to form the other layer. The individual cell

membranes in the tissue are combined into one single equivalent membrane in this model.

The intracellular and extra-cellular volumes and the membrane area are determined according to the average cellular properties of the tissue. The height of the model (H) is equal to half of the physical thickness of the slice. The dimension of the model in the y-direction (E, Fig. 4.2) is calculated from the total membrane area and the height of the model. The total membrane area is calculated through the average diameter of spherical cells, that is,

$$A_m = N \cdot S = N \cdot \pi \cdot d^2 \tag{4.1}$$

$$E = \frac{A_m}{H} \tag{4.2}$$

where A_m is the total area of membranes, which is regarded as an aggregation of N cells, each of which has the same structure, N is the total number of cells in the model, H is the height of the model, which is the half of the physical thickness of the tissue sample, S and d are the surface area and the diameter of the average cell, respectively.

The dimensions in the x-direction for each volume were determined from the relationship between the individual volumes and the dimensions in the y- and z-directions.

4.2.2 Equations of Mass Balance

The solutions in both intracellular and extra-cellular volumes are assumed incompressible and dilute so that the partial molar volumes of all components are constant. It is also assumed that there is no concentration gradient in the xy-plane and that the concentration gradient exists only in the z-direction. This is because the x-dimension is very small compared to other two-directions. By making a mass balance on a small segment of the conceptual model along the z-direction (Fig. 4.2), the following equations are obtained:

For intracellular volume ($s = 1, 2, \ldots, M$):

$$\frac{\partial[C_s^c A^c]}{\partial t} = \frac{\partial}{\partial z}[A^c D_s^c \frac{\partial C_s^c}{\partial z}] - \frac{\partial[C_s^c V^c A^c]}{\partial z} + J_s^{fc} E \tag{4.3}$$

For extra-cellular volume ($s = 1, 2, \ldots, M$):

$$\frac{\partial[C_s^f A^f]}{\partial t} = \frac{\partial}{\partial z}[A^f D_s^f \frac{\partial C_s^f}{\partial z}] - \frac{\partial[C_s^f V^f A^f]}{\partial z} - J_s^{fc} E \tag{4.4}$$

where t is the time, C_s^c and C_s^f are the concentrations of species s in the intracellular and extra-cellular volumes, A^c and A^f are the cross section area, D_s^c and D_s^f are the diffusion coefficients of species s in the intracellular and extra-cellular volumes, V^c and V^f are the bulk velocities of solutions in the intracellular and extra-cellular volumes, E is the model dimension in the y-direction, J_s^{fc} is the apoplastic transport flux of species s from the extra-cellular volume into the intracellular volume through cell membrane (plasmalemma) and M is the total number of the solutes considered in the solution.

Eqs. (4.3) and (4.4) represent the concentration changes at a fixed position in the intracellular and extra-cellular volume due to three mechanisms: the first relates to diffusion, the second describes the transport by bulk flow, and the last is a generation term which represents the contribution from the trans-membrane flux. The trans-membrane flux is defined as positive when it flows from the extra-cellular volume to the intracellular volume and it couples the changes in the intracellular and extra-cellular volumes.

The change of the intracellular and extra-cellular volumes can be determined by considering the volumes balance in the intracellular and extra-cellular volumes. Note that for ideal dilute solutions the volume change due to diffusion can be ignored. Therefore, the following volume conservation equations can be established,

$$\frac{\partial A^c}{\partial t} = -\frac{\partial[V^c A^c]}{\partial z} + J_v^{fc} E \tag{4.5}$$

$$\frac{\partial A^f}{\partial t} = -\frac{\partial[V^f A^f]}{\partial z} - J_v^{fc} E \tag{4.6}$$

where J_v^{fc} is the volume flux, including water flux and solutes fluxes from extra-cellular volume into the intercellular volume through cell membrane.

Eqs. (4.5) and (4.6) represent the concentration changes at a fixed position in the intracellular and extra-cellular volume due to two mechanisms. The first represents the variation with bulk flow along the z-axis, and the negative sign indicates that an increase in cross section leads to a decrease in flow rate. The second is the contribution of the trans-membrane flux.

The bulk flow velocities of solutions in the intracellular and extra-cellular volumes, V^c and V^f, and the model dimension in the y-direction, E, will be determined by the following additional equations. The three stages concept model is also adopted in this model to simplify the analysis.

As mentioned before, in stage 1, the extra-cellular volume is assumed to be constant. Consequently, we have:

$$A^f = A_0^f = const. \tag{4.7}$$

The total shrinkage was assumed to be distributed proportionally in three dimensions. According to Yao *et al.*, (1994), and based on this proportionality the local shrinkage rate (δ) is given by:

$$\delta = \frac{dV^c}{dz} = \frac{1}{2A^t}\frac{dA^t}{dt} = \frac{1}{(A^c + A^f)}\frac{d(A^c + A^f)}{dt} \tag{4.8}$$

where A^t is the total cross sectional area.

Then the shrinkage velocity at a position z from the centre is:

$$V^c = \int_0^z \delta \, dz \tag{4.9}$$

As discussed in the development of this model, the dimension in the y-direction is determined by the cell membrane area and the dimension in the z-direction. The cell

membrane, like the rubber sheet of a balloon, changes its surface area with the pressure in the intracellular volume. The higher the pressure, the larger the area. When the pressure in the intracellular volume approaches the pressure in the extra-cellular volume, the cell membrane area becomes constant. Therefore, the cell membrane area decreases in stage 1 as a function of the internal pressure or intra-cellular volume and stays constant after stage 1, till to a critical volume (Yao *et al.*, 1996).

In stage 1, the *y*-dimension (E) can be shown to vary according to the following equation (Yao *et al.*, 1996):

$$\frac{\partial E}{\partial t} = \frac{4}{d}\left(A^c \delta + \frac{\partial A^c}{\partial t} \right) - E\delta \tag{4.10}$$

where d is the average cell diameter, A^c is the cross sectional area of the intracellular volume, t is the time and δ is the local shrinkage rate.

In stages 2 and 3, the membrane area is constant, and again after mathematical manipulation, overall dimension change in the *y*-dimension in stage 2 and 3 is:

$$\frac{\partial E}{\partial t} + E\delta = 0 \tag{4.11}$$

As mentioned in the earlier chapter, the equations derived from irreversible thermodynamics to describe volume and solute flows are

$$J_v^{fc} = L_p(\Delta P - \sum \sigma_s \Delta \pi_s) \tag{4.12}$$

$$J_s^{fc} = \omega_s \Delta \pi_s + J_v \overline{C}_s (1 - \sigma_s) \tag{4.13}$$

where L_p is hydraulic conductivity of membrane, ω_s is the solute permeability of membrane, and σ_s is reflection coefficient of membrane. The methods used to obtain these parameters have been introduced in chapter 3. ΔP is the difference in hydrostatic pressure across the membrane, that is:

$$\Delta P = P^c - P^f \tag{4.14}$$

where P_f is the pressure in extra-cellular volume which is assumed to be equal to the atmosphere pressure. P_c is the pressure in intracellular volume, which is evaluated in

relation to the change of cellular volume, through a measure of the reversible elastic properties of the cell walls in the form of an empirical modulus, ξ, that is (Dainty, 1976; Nobel, 1983):

$$dP_c = \xi \frac{dV^c}{V^c} \tag{4.15}$$

It is assumed that ξ is not a function of P_c, integration of Eq. (4.15) yields:

$$P_c = \xi \ln \frac{V^c}{V_0^c} + P_c^0 \tag{4.16}$$

where P_c^0 is given by:

$$P_c^0 = RT \sum_k \left(C_{k_0}^c - C_{k_0}^f \right) \tag{4.17}$$

where the summation is performed for all the non-permeating solutes present in the intracellular and extra-cellular volumes at full turgor.

Eqs. (4.3) and (4.4) are the governing equations for determining concentrations, C_s^c and C_s^f, and cross sections, A^c and A^f can be determined by Eqs. (4.5) and (4.6) respectively in which the mass exchange between the intracellular and extra-cellular volumes is defined by Eqs. (4.12) and (4.13), and the bulk velocities of the solution in the intracellular and extra-cellular volumes and the model dimension in the y-direction E are defined by Eqs. (4.8) - (4.11). For given initial and boundary conditions the solute concentrations and volume fractions at any time and any place can be determined by solving the governing Eqs. (4.3) - (4.6).

4.3 Initial and Boundary Conditions

4.3.1 Initial Conditions

Initially, the plant tissue is assumed to have uniform composition over the whole domain. However, the initial concentration in the intracellular volume ($C_{s,0}^c$) and the

initial concentration in the extra-cellular volume ($C_{s,0}^{f}$) are different, but both are constant, that is,

$$C_{s,0}^{c}\,|_{z=[0,H]} = const. \tag{4.18}$$

$$C_{s,0}^{f}\,|_{z=[0,H]} = const. \tag{4.19}$$

The initial cross section areas in intracellular and extra-cellular and the model dimension in y-direction E are taken as constants:

$$A_0^c\Big|_{z=[0,H]} = const. \tag{4.20}$$

$$A_0^f\Big|_{z=[0,H]} = const. \tag{4.21}$$

$$E_0\Big|_{z=[0,H]} = const. \tag{4.22}$$

4.3.2 Boundary Conditions

Boundary conditions at the surfaces

Let us assume that there is no resistance at the surface, so the concentrations on the surfaces ($C_s^c\Big|_{Z=H}$ and $C_s^f\Big|_{Z=H}$) are equal to the concentration in the osmotic solution (C_s^l), that is,

$$C_s^c\Big|_{z=H} = C_s^f\Big|_{Z=H} = C_s^l \tag{4.23}$$

Boundary conditions at the centre

According to the symmetrical properties of the slab, the boundary conditions of concentrations and bulk flow velocities at the centre (z=0) are:

$$\left.\frac{\partial C_s^c}{\partial z}\right|_{z=0} = \left.\frac{\partial C_s^f}{\partial z}\right|_{z=0} = 0 \tag{4.24}$$

$$\left.\frac{\partial V^c}{\partial z}\right|_{z=0} = \left.\frac{\partial V^f}{\partial z}\right|_{z=0} = 0 \tag{4.25}$$

$$\left.V^c\right|_{z=0} = \left.V^f\right|_{z=0} = 0 \tag{4.26}$$

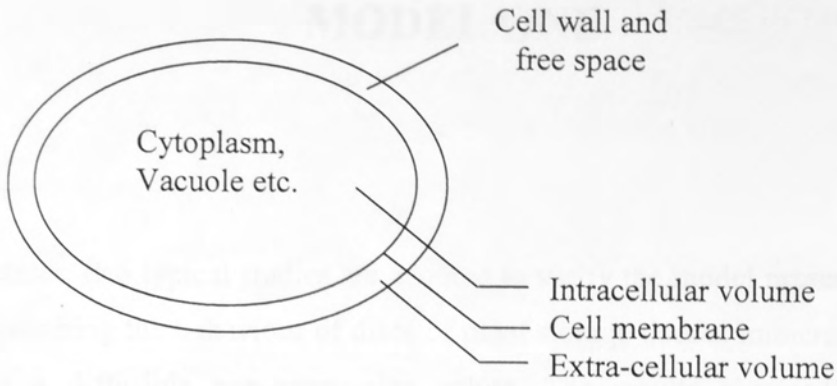

Figure 4.1 Schematic diagram of a simplified plant cell

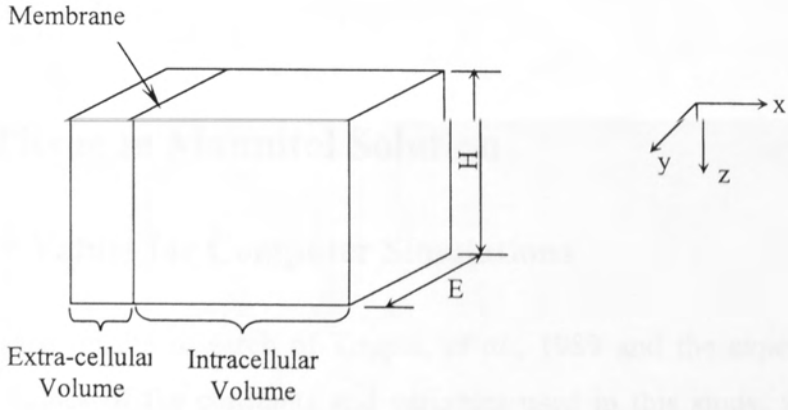

Figure 4.2 Conceptual model of a cellular tissue

Chapter 5 NUMERICAL ANALYSES FOR MODEL ONE

In this chapter, two typical studies are adopted to verify the model presented in chapter 4, each describing the behaviour of discs of plant storage tissues immersed in solutions containing a diffusible non-permeating solute. The results obtained by presented mathematical model are compared with the results gained by other mathematical model and original experimental data. Some parameters and the sensitivity of parameters are analyzed in this chapter. Potato tissue is used to validate the model because of the availability of literature data. The governing equations are solved numerically by using one-dimensional finite difference method.

5.1 Potato Tissue in Mannitol Solution

5.1.1 Parameter Values for Computer Simulations

This analysis is based on the research of Toupin, *et al.*, 1989 and the experiment of Stuart, 1973. The values of the constants and variables used in this study, which are summarized in Table 5.1, are obtained from literature sources. However, for properties the values of which are either unknown or available only in order of magnitude, sensitivity analyses are performed to determine which of these properties need precise adjustments in order to achieve a good agreement between observed and predicted data.

As reported by Stuart (1973), discs of 1.4×10^{-2} m in diameter and 1.0×10^{-3} m thick are used in the experiment (Fig. 5.1). According to Poole (1976), a corrected thickness of 0.8×10^{-3}m is used in the calculations to take account of a layer of about 0.1×10^{-3} m thick of dead cells formed at each surface by slicing. The average cell diameter is obtained from diameter measurements performed by Walker *et al.*, (1976), leading to an approximate value of 6.0×10^{-5} m. Before the discs are used in the experiment, they have

been washed in running tap water, are transferred to aerated distilled water in which they are stored for at least 48 hours. The initial extra-cellular free space and cell wall volume fractions are taken as representing, respectively, 3% (Sterling, 1966; Crapiste & Rotstein, 1982) and 5% of the total tissue volume (Hayden, 1969; Reeve, 1973). The tortuosity within the cell wall is estimated at 2 (Toupin *et al.*, 1989). This value should represent at least an upper limit since the tortuosity of the cellulosic matrix could be greater (Nobel, 1983). The elastic modulus of cell wall is assumed constant at 2.1×10^{6} N/m^2 according to Dainty (1963a). The solutions within the potato system are regarded as equivalent mannitol solutions, since this is the diffusible non-permeating solute used by Stuart in his analysis. Accordingly, 0.535 $kmol/m^3$ and 0.1 $kmol/m^3$ are computed for the extra-cellular and initial intracellular concentrations, respectively.

The initial mass of the piece is taken as 1.67×10^{-4} kg, which corresponds to $1/6^{th}$ of the weight of the '6-discs' samples ($\approx 10^{-3}$ kg fresh weight) used by Stuart in his experiment. Since the main component of potato is starch (68%, Crapiste & Rotstein, 1982), the dry matter density of potato is chosen equal to the density of starch of 1650 kg/m^3.

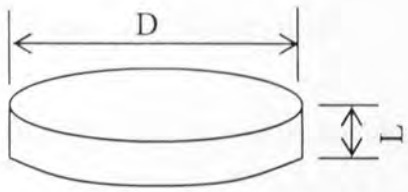

Figure 5.1 A potato slice sample

As mentioned before, hydraulic conductivity of membrane L_p may be determined, by measuring J_v for a given Δp (chapter 3). However, due to the unavailability of experiment for this study, L_p can only be determined by optimized method. The value of conductivity of membrane in this study is 6.5×10^{-14} m/(Pa s), which satisfies the range of previous researches (House, 1973).

The volume at the incipient plasmolysis and the critical volume also need adjustment. Their values are given as a range and reported to have strong effect on the mass transfer

(Toupin & Le Maguer, 1989). According to former researches, the volume at incipient plasmolysis and critical volume are chosen at 0.88 and 0.8 to obtain the optimum results. The resistance force from cell walls is also ignorable. In the model, the one-dimensional mass transfer in the thickness direction is assumed. The one-dimensional case is easy to manipulate mathematically, and allows the analysis of the general mass transfer mechanism, rather than focusing on individual cases (Yao, *et al.*, 1997).

5.1.2 Results and Discussions

Fig. 5.2 shows the best fit between the simulation and experimental results after the optimization. In conclusion, the adjustable parameters are well within the range given in the literature and the optimization of the parameters is successful. Considering that this model is based on Toupin's model and most of parameters used in this model is obtained from Toupin's model, so this model could be considered more effective than Toupin's model, as some of parameters in Toupin's model have been optimized.

5.2 Potato Tissue in Sucrose Solution

5.2.1 Parameter Values for Computer Simulations

This case is based on the research of Yao, *et al.*, 1997. The potato tubers are immersed in 60% (w/w), 2.277 kmol/m^3, sucrose solution at 40℃. The volume fraction of the potato cell wall is taken to be 5% (Hayden, *et al.*, 1969; Reeve, *et al.*, 1973). The volume fraction of the free space is reported between 1% and 4% (Burton & Spragg, 1955; Davis, 1962; Crapiste & Rotstein, 1982) and 4% is chosen in the simulation. The same as previous case, the tortuosity within the cell wall is estimated as 2. The elastic modulus of potato is taken as 2.1×10^{6} N/m^2 and the hydraulic conductivity is assumed as 6.5×10^{-14} kmol/(Pa s). According to Yao, *et al.*, the dimensionless volumes based on the initial volume of potato can be recalculated as 0.94 ± 0.03 for incipient plasmolysis volume and 0.43 ± 0.15 for the critical volume. In this study, 0.91 is used for incipient plasmolysis volume as Yao's model, after modification, the critical volume is chosen as 0.67. The overall values used in this study are summarized in Table 5.2.

5.2.2 Results and Discussions

Fig. 5.3 shows the comparison of weight fraction of sucrose between the model prediction, Yao's prediction and the experimental measurement for potato tissue contacted with a 60% (w/w) sucrose solution at 40℃ for 1 hour. In this figure, the value of sucrose in each cross section is described. There is some difference in the values from this model and Yao's model at the surface due to the boundary effect, surface resistance, damaged cells, etc. reasons. Apart from the boundary, these values well fit in with the experimental data.

5.3 Parameters Analyses

The independent variables (position and time) are plotted in dimensionless form in all figures. The distance in the thickness direction measured from the symmetrical plane divided by the half thickness of the slice is used as dimensionless distance. The dimensionless time is the ratio of time to an equivalent diffusion time corresponding to the initial conditions, that is, the square of initial half thickness of the slice divided by the diffusivity of mannitol at infinite dilution.

5.3.1 Concentration in the Extra-cellular Volume

The dimensionless mannitol concentration in the extra-cellular volume versus dimensionless distance and time is plotted in Fig. 5.4. The dimensionless concentration is the ratio of the concentration at time t to the concentration in the solution. The concentration in the solution is assumed to be constant during the whole osmotic dehydration process.

At a specific time, in general, there are three distinct regions on the graph (as shown in Fig. 5.4). There is a flat high concentration region on the right, keeping constant, a flat low concentration region on the left, and in between, a transient region with a steep concentration gradient. The location of the transient region moves from the surface (x/L=1) towards the symmetrical plane (x/L=0) as the dehydration progresses. The transient region becomes wider as it moves towards the symmetrical plane, and the

concentration gradient decreases. The high concentration region is absent at the beginning, and the low concentration and transient regions disappears at the end of the process. The location close to symmetrical plane takes less time to reach the equilibrium.

5.3.2 Cross-sectional Area of Extra-cellular Volume

The extra-cellular volume can be divided into cell wall fibre volume and free volume as introduced in former chapter. The variation of the free volume is exactly the same as the extra-cellular volume because the cell wall fibre volume is constant. The free volume is the true flowing channel and has a strong impact on the bulk flow velocity, an important parameter in the analysis of mass transfer in osmotic dehydration (Yao and Le Maguer, 1996a).

The variation of the cross-sectional area of the extra-cellular volume against time and position is simulated and shown in Fig. 5.5. The cross-sectional area of the extra-cellular volume is plotted as the ratio of the cross-sectional area of the free volume at time t to its initial value. There are three regions in Fig. 5.5. A low value region (ratio = 1) on the left corresponds to the low concentration region in Fig. 5.4, where cells are in stage 1; a transition region corresponds to the steep gradient region in Fig. 5.4, where cells are in stage 2; a high value region corresponds to the high concentration region in Fig. 5.4, where cells are in stage 3. The cross-sectional area of extra-cellular volume increases quickly from a small value to a large value in transient region. In other two regions, the cross-sectional area of extra-cellular keeps constant. The increase in the cross-sectional area is most rapid at the surface and slowest at the symmetrical plane.

5.3.3 Cross-sectional Area of Intracellular Volume

The variation of the cross-sectional area of the intracellular volume against time and position is simulated in Fig. 5.6. Similar to the cross-sectional area of extra-cellular volume, the cross-sectional area of the intracellular volume is plotted as the ratio of the cross-sectional area of intracellular volume at time t to its initial value as well.

The cross-sectional area of the intracellular volume decreases in the whole dehydration process. At a specific time, the cross-sectional area is largest in the symmetrical plane and gradually decreases to the lowest value at the surface. In another word, the decrease in the cross-sectional area is most rapid at the surface and slowest at the symmetrical plane.

5.3.4 Trans-membrane Volume Flux

Trans-membrane volume flux is important in the analysis of mass transfer in osmotic dehydration because it indicates the amount of water and solutes removed from the intracellular volume where up to 90% of tissue water is located (Nobel, 1983). The trans-membrane flux forms a bulk flow in the direction from the tissue to the osmotic solution, and the presence of this bulk flow greatly complicates the modelling of osmotic dehydration progress (Yao and Le Maguer, 1996a, b). When the solutes are impermeable, the trans-membrane volume flux only indicates trans-membrane water flux. Analysis of trans-membrane flux is fundamental to the study of bulk flow in osmotic dehydration.

The trans-membrane volume flux as a function of dimensionless time and distance is shown in Fig. 5.7. At a particular location, the trans-membrane flux increases from zero at the beginning to a maximum and then decreases to zero. At the surface (x/L=1), the peak and the rates of increase and decrease of the trans-membrane flux reaches to the highest values, and at the symmetrical plane (x/L=0), the peak and the rates are the lowest values. All the cells lose the same amount of volume through the membrane to reach equilibrium, regardless of their locations. That means that the area under the curve along the time axis is the same at all locations in the tissue. However, different cells take different amounts of time to reach this point, depending on their location. The cells closer to surface take less time to reach the point. The location of the maximum of the trans-membrane volume flux (the ridge) corresponds to the beginning of the transient region in Fig. 5.4 where cells are at the interface between stage 1 and stage 2.

5.3.5 Bulk Flow Velocity

As mentioned before, bulk flow plays an important role in osmotic dehydration. The bulk flow velocity determines the amount of solutes washes out, and is affected by the trans-membrane flux in the whole tissue and the change of the cross-sectional area of the free volume in the extra-cellular volume.

The bulk flow velocity versus dimensionless time and distance is simulated and then plotted in Fig. 5.8. At the beginning, the bulk flow velocity increases from zero at the symmetrical plane (x/L=0) to a maximum near the surface (x/L=1). Then, the velocity reaches a peak somewhere between the symmetrical plane and the surface. After this peak, it reduces to a very small value, increasing only slightly afterwards. The location of the peak is shifted from the surface towards the symmetrical plane as the process continues, and disappears in a certain time. After that, the velocity increases very slowly from zero at the symmetrical plane until it reaches the surface.

The peak of the trans-membrane flux is caused by the rapid increase of the mannitol concentration in the extra-cellular volume. When the cells enter stage 2, the cross-sectional area of the extra-cellular volume increases rapidly to its maximum. This results in the bulk flow velocity falling down quickly from its maximum to a small value as the cells pass through stage 2. Due to the large cross-sectional area of the extra-cellular volume, the bulk flow velocity in the area where cells are in stage 3 is very slow and increases slightly from the ridge to the surface.

Bulk flow controls diffusion by affecting the concentration gradient. In the beginning of the transient region where cells are just entering stage 2, the bulk flow velocity is largest at a specific position (Fig. 5.8), which results in the steepest gradient in this region as shown in Fig. 5.4. As the transient region moves from the surface towards the centre, the peak of the bulk flow velocity decreases, resulting in a reduced steepness of the concentration curve in the transient zone as shown in Fig. 5.4. The influence of the bulk flow is consequently considerable, and indicates that attempting to interpret osmotically driven processes on the basis of pure diffusion would lead to serious underestimation of the time.

5.4 Sensitivity Analyses

The influence of specific variables on the overall behaviour can be illustrated effectively by using the model to predict the response of the system studied to changes in the values of these variables.

Some major properties will be examined in the following analyses. They are the concentration of solution, diffusion coefficient, the diffusivity of solute in extra-cellular volume, membrane conductivity coefficient and cell critical volume.

The parameters in case study one are adopted as the reference parameters to the sensitivity analyses. These parameters will be increased and decreased either by a certain factor or to a certain value, so that the change of the weight reduce ratio can be shown.

5.4.1 Concentration of Solution

A mannitol solution is chosen at a reference concentration of 0.535 kmol/m^3 which is increased and decreased by a factor of two, so that three concentrations of mannitol are used (0.2675, 0.535 and 1.07 kmol/m^3). As mentioned before, mannitol is assumed to be unable to permeate through the cell membrane and therefore it is restricted in the extra-cellular volume (Yao, *et al.*, 1996). In addition, it is assumed that all mannitol is dissolved in water and there is no recrystallization at the three concentrations used in this simulation.

The concentration effect of mannitol solution on mass reduction and mannitol gain in tissue are shown in Fig. 5.9 and Fig. 5.10. The weight reduction and rate of loss increase as the concentration increases. Similarly, the rate of mannitol infusion and the maximum mannitol content at equilibrium increase at higher concentrations of mannitol in the solution.

5.4.2 Diffusion Coefficient

The description of the concentration-dependence of the diffusion coefficient of solute in water is found by fitting a polynomial of the following form to measurements obtained at different concentrations (Landolt-Bornstein Table, 1969):

$$\ln\left(D_i / D_i^{\infty}\right) = \sum_k a_k C_i^k \quad (k=0, 1, \ldots, n) \tag{5.1}$$

where D_i is the diffusivity of species i at a concentration C_i in water, D_i^{∞} is the diffusivity at infinite dilution and a_k is the k^{th} coefficient of the polynomial of degree n (Toupin *et al.*, 1989). The detailed values for these parameters are summarized in Table 5.1 and Table 5.2.

The effect of the diffusion coefficient on the course of osmotic dehydration is considered in this section. The diffusion coefficient is first decreased and then increased by a factor of 2 from its reference value, while keeping constant for all other parameters. The results are shown in Fig. 5.11.

As expected, an increase or decrease in the diffusion coefficient significantly affects the rate of dehydration. With the increase of the diffusion coefficient, the tissue loses more weight. This also shows that the higher diffusion coefficient will lead the process to complete more quickly. This indicates diffusion plays a very important role in osmotic dehydration process.

5.4.3 Membrane Conductivity Coefficient

As mentioned before, the plant cell is under considerable hydrostatic pressure (turgor pressure) and this additional parameter plays an important role in the osmotic relations of plant cells.

When a plant cell is bathed by a solution of some non-permeating solute, the trans-membrane volume flux is given by

$$J_v = L_p(\Delta p - \Delta \pi) \tag{5.2}$$

where Δp and $\Delta \pi$ represent the differences in hydrostatic and osmotic pressure between the intracellular and extra-cellular volume. This relation offers a method of determining L_p. Many researches have been done to obtain the values for L_p. According to previous results, it is found that L_p of plants lying in the range $1.8\text{-}300 \times 10^{-14}$ m/(Pa s) (House, 1973). The L_p for potato tissue is obtained by optimization in this model, which is 6.5×10^{-14} m/(Pa s). Fig. 5.12 illustrates the effect of varying the conductivity coefficient on the course of osmotic exchanges in potato tissue. To carry out this simulation, the conductivity is first increased and then decreased by a factor of two from its reference value.

As expected, an increase or decrease in the conductivity of the cell membrane affects the rate of dehydration of the potato tissue. For instance, in Fig. 5.12, it can be observed that for the bigger value of conductivity, the tissue reduces the mass quicker and takes less time to reach equilibrium and for the smaller value of conductivity, the tissue reduces the mass slower and takes more time to reach equilibrium.

5.4.4 Diffusibility of Cell Wall

The effect of varying the cell wall diffusibility on the course of osmotic dehydration is considered in this section. Values of 0.1, 0.3 and 0.6 are ascribed successively to the diffusivity of the cell wall, yielding the range of curves shown in Fig. 5.13.

As can be seen, the course of osmotic exchange is not altered to the extent observed previously when the membrane conductivity is modified (see Fig. 5.13).

These results tend to explain that the response of the tissue is more sensitive to changes in the cell membrane conductivity than in the diffusibility of the cell wall. This suggests that the cell membrane represents the major resistance to mass transfer. It is important however to realize that this statement does not lessen the role in the overall transport phenomena of the apoplast microstructure or the symplast. It simply grades the contribution of each factor to the overall response of the tissue.

5.4.5 Elastic Modulus of the Cell Wall

The influence of elastic modulus of cell wall is discussed in this section. As known, the cell is under the full turgor pressure, which is held by the cell wall, when the osmotic dehydration process starts. Therefore, the elastic modulus of the cell wall will affect the change of the cell volume in the process of osmotic dehydration. The cell volume will change relatively less when the elastic modulus of the cell wall is a relatively bigger value. On the contrary, the cell volume will change relatively more when the elastic modulus of the cell wall is a relatively smaller value.

Just as expected, when the elastic modulus of the cell wall is reduced and increased by a factor of two, a dramatic change is seen in Fig. 5.14. The increase of the elastic modulus of the cell wall will reduce the rate of mass reduction, and the decrease of the elastic modulus of the cell wall will increase the rate of mass reduction rapidly. This is because with the same change of hydrostatic pressure, the increase of elastic modulus will reduce the change of volume, that is, reduce the rate of mass reduction.

5.4.6 Cell Critical Volume

As shown in former chapter, this description assumes all the cells, during osmotic dehydration, experience three stages, each having a direct influence on the behaviour of the whole structure. The second stage of dehydration lying between the limits of the point of incipient plasmolysis and the point where the cell reached the critical cell volume is the most crucial. During that stage it is assumed that any volume lost by the cell is simply compensated by a proportional increase in inter-cellular free space, so that the total volume of the tissue remains constant.

As stated previously, this upper limit of the second stage of dehydration corresponds to the point of incipient plasmolysis, that is, the point where the intracellular hydrostatic pressure vanishes. Since intracellular pressure and cellular volume are linked through equations involving the elastic modulus of the cell wall, this state of the cell can be related directly to a limiting volume for any tissue. If these relationships are solved for P_c=0, potato tissue is found to have a reduced volume of 0.88. On the other hand, the

equilibrium volume the cell will eventually reach for the forces involved in the system can be obtained by Boyle-Van't Hoff law. The critical cell volume lies therefore between the cellular volume at incipient plasmolysis and the equilibrium volume of the cell. For potato tissue, the critical cell volume (V_{cr}) lies between 0.88 and 0.22 (Toupin *et al.*, 1989).

The effect of varying the critical cell volume for that system is shown in Fig. 5.15, where, V_{cr} values of 0.7, 0.8, and 0.85 are used and the results are compared. As shown, the extent of weight loss increased as this limit is reduced. This response of the tissue indicatesd that mass transport in this system depends on the structural rearrangement occurring in the tissue as dehydration progresses.

5.5 Summary for Model One

According to the analyses of parameters and sensitivity, the osmotic dehydration process is affected not only by tissue properties (hydraulic conductivity of cell membrane, diffusibility of cell wall, etc.) but by solution characteristics (concentration etc.). Therefore the effective diffusivity coefficient, which is used in modelling osmotic dehydration with the macroscopic approach, depends on both tissue and solution characteristics. This imparts the difficulties in rationalizing from one type of tissue to another, from one kind of solution to another, and from one concentration to a different concentration. The cell membrane is the main barrier to mass transfer in osmotic dehydration for single cells or slices of tissue with a few layers of cells.

The good agreement between the prediction by the proposed model and the experimental measurement indicates that the mechanism postulated to describe the mass transfer in cellular tissue under the osmotic dehydration process condition is realistic, and the numerical simulation procedure to solve the model equation is successful. The model is mechanistic and possesses the capacity to predict the concentration profiles of solute and water in cellular tissue as a function of time and space. In addition, the model can provide information about the trans-membrane flux, the bulk flow velocity in the extra-cellular volume and the shrinkage behaviour of the tissue.

The mass transport of solutes by diffusion is considered and in the expression of volume changes, the trans-membrane volume flux is adopted instead of the summation of each solute and water in this model. These modifications make the equations express the process more general and integrated.

Therefore, the model contributes a useful tool to investigate the mechanism of mass transfer phenomena in osmotic dehydration. The model can also be used by plant physiologists and cytologists in the study of the transport of water and solutes in cells and plants.

However, in this model, the three stages assumption of osmotic dehydration process is employed. That is, some parameters have been assumed during the process, such as the critical cell volume. Actually, these parameters are hard to obtain or predict, of course, it is impossible to be verified.

Moreover, this model is limited in one-dimensional analyses. It is always abstract when the problem is solved as one-dimension. It is necessary to extend the osmotic dehydration problem to multi-dimension analyses in order to obtain more intuitionistic, compatible results.

Table 5.1 Value of Constants and Variables used in Potato Tissue in Mannitol Solution

Quantity	Units	Value
Osmoticum Characteristics		
Temperature	K	298.15
universal gas constant	J/kmol-K	8.31×10^{3}
partial molar volume	m^3/kmol	
Water		0.018
Mannitol		0.119
molecular weights	kg/kmol	
Water		18
Mannitol		182.17
diffusivity of sucrose in water		
D^{∞}	m^2/s	6.67×10^{-10}
a_0	Dimensionless	1.509×10^{-5}
a_1	Dimensionless	-0.317
mannitol concentration	$kmol/m^3$	0.535
Initial Tissue Characteristics		
disc diameter	m	1.4×10^{-2}
corrected thickness	m	8×10^{-4}
tissue volume fractions	%	
cell wall		5
free space		3
mass of disc	kg	1.67×10^{-4}
Density	kg/m^3	
water		997.5
dry matter		1650
extra-cellular sucrose concentration	$kmol/m^3$	0
Initial Cell Characteristics		
diameter d	m	6.0×10^{-5}
volume at incipient plasmolysis	Dimensionless	0.88[a]
critical volume	Dimensionless	0.8[a]
cell wall diffusibility	Dimensionless	0.3
cell wall tortuosity	Dimensionless	2
elastic modulus	N/m^2	2.1×10^{6}
hydraulic conductivity of membrane	m/s-Pa	6.5×10^{-14}[a]
intracellular solution concentration		0.1
composition	$kmol/m^3$	
starch	kg/kg dry matter	0.68
proteins		0.11
glucose		0.02
cellulose		0.03
fructose		0.02
sucrose		0.015
others		0.125

[a] Value adjusted by optimization.

Table 5.2 Value of Constants and Variables used in Potato Tissue in Sucrose Solution

Quantity	Units	Value
Osmoticum Characteristics		
Temperature	K	313.15
universal gas constant	J/kmol-K	8.31×10^{3}
partial molar volume	m^3/kmol	
Water		0.018
Sucrose		0.211
molecular weights	kg/kmol	
Water		18
Sucrose		342.3
diffusivity of sucrose in water		
D^{∞}	m^2/s	7.53×10^{-10}
a_0	Dimensionless	0
a_1	Dimensionless	-0.71479
sucrose concentration	$kmol/m^3$	2.277
Initial Tissue Characteristics		
disc diameter	m	1.4×10^{-2}
corrected thickness	m	8×10^{-4}
tissue volume fractions	%	
cell wall		5
free space		4
mass of disc	kg	2.5×10^{-4}
Density	kg/m^3	
water		997.5
dry matter		1650
extra-cellular sucrose concentration	$kmol/m^3$	0
Initial Cell Characteristics		
diameter d	m	6.1×10^{-5}
volume at incipient plasmolysis	Dimensionless	0.91
critical volume	Dimensionless	0.67[a]
cell wall diffusibility	Dimensionless	0.3
cell wall tortuosity	Dimensionless	2
elastic modulus	N/m^2	2.10×10^{-6}
hydraulic conductivity of membrane	m/s-Pa	6.5×10^{-14}
intracellular solution concentration		0.1
composition	$kmol/m^3$	
starch	kg/kg dry matter	0.68
proteins		0.11
glucose		0.02
cellulose		0.03
fructose		0.02
sucrose		0.015
others		0.125

[a] Value adjusted by optimization.

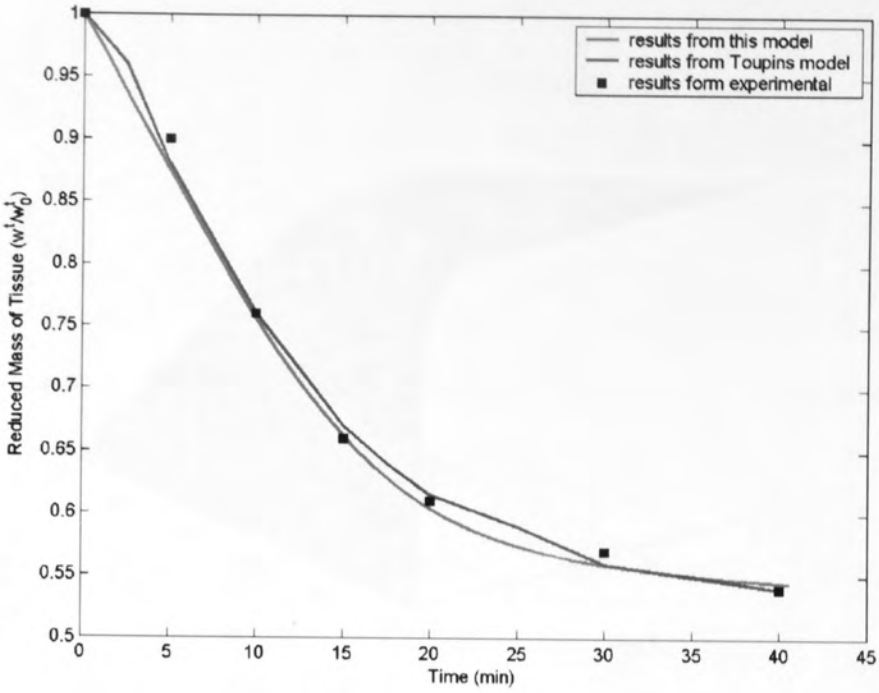

Figure 5.2 Comparison of mass reduction of tissue between predictions from this model, Toupin's model (1989) and experimental measurement for potato slices contacted with 0.535 m mannitol solution at 25°C for 42 minutes.

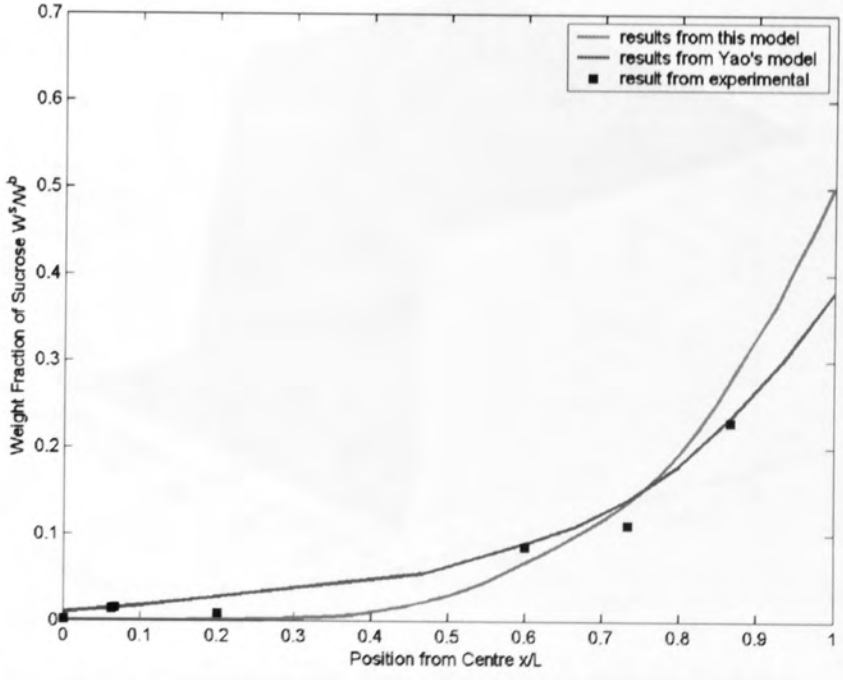

Figure 5.3 Comparison of weight fraction of sucrose between simulations from this model, Yao's model (1997) and experimental measurement for potato tubers contacted with 60% (w/w) sucrose solution at 40°C for 1 hour.

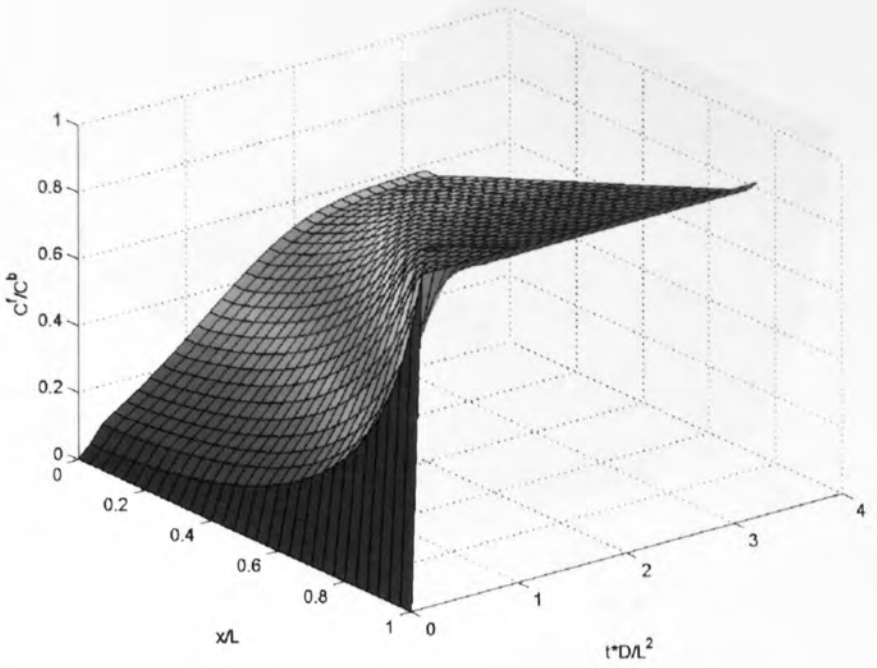

Figure 5.4 Concentration Profiles of Mannitol in Extra-cellular Volume

(C^f – Concentration of mannitol in the extra-cellular volume; C^b – Concentration of mannitol in the osmotic solution; x – Distance in the thickness direction measured from the symmetrical plane; L - Half thickness of the tissue slice; D – Diffusivity of mannitol at infinite dilution; t - time)

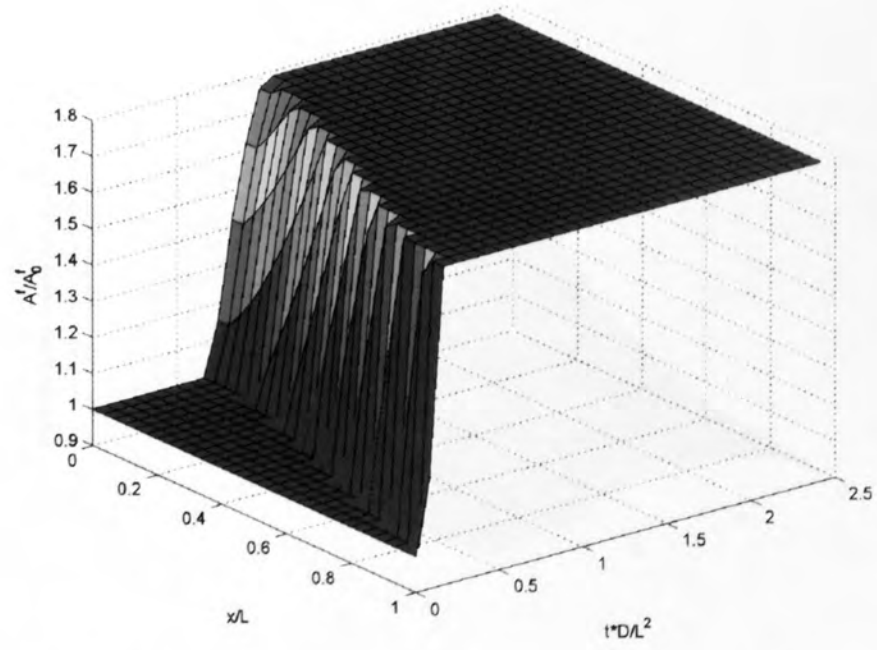

Figure 5.5 Cross-sectional Area of the Extra-cellular Volume

(A^f – Cross-sectional area of the extra-cellular volume; A_0^f - Initial cross-sectional area of the extra-cellular volume; x – Distance in the thickness direction measured from the symmetrical plane; L - Half thickness of the tissue slice; D – Diffusivity of mannitol at infinite dilution; t - Time)

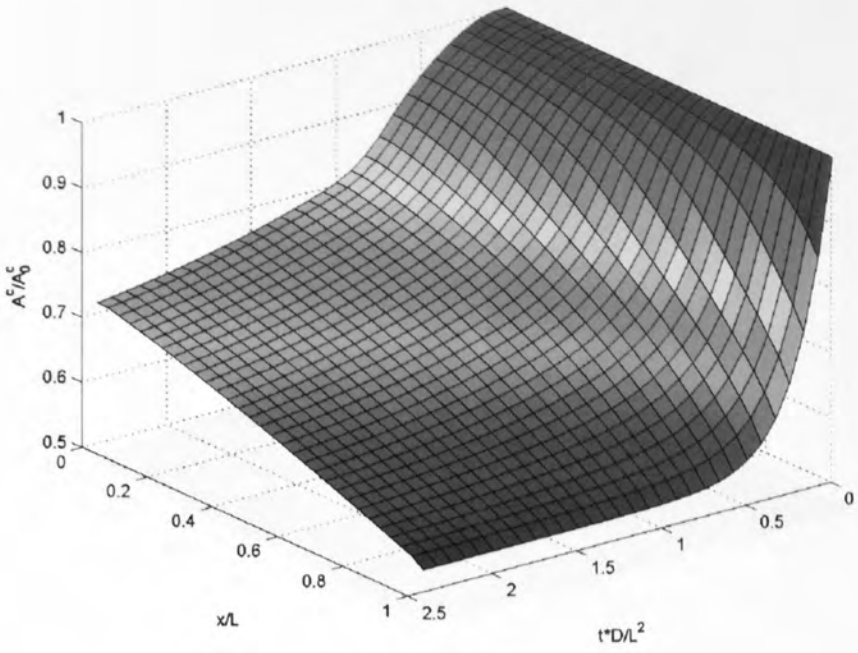

Figure 5.6 Cross-sectional Area of the Intracellular Volume

(A^c – Cross-sectional area of the intracellular volume; A_0^c - Initial cross-sectional area of the intracellular volume; x – Distance in the thickness direction measured from the symmetrical plane; L - Half thickness of the tissue slice; D – Diffusivity of mannitol at infinite dilution; t - Time)

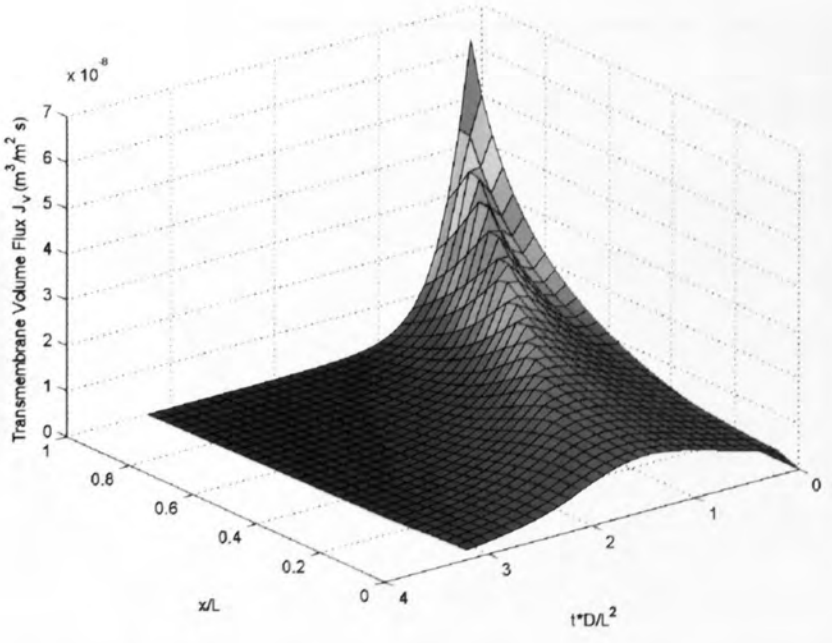

Figure 5.7 Flux of Volume across the Cell Membrane

(J_v – Trans-membrane volume flux; x – Distance in the thickness direction measured from the symmetrical plane; L - Half thickness of the tissue slice; D – Diffusivity of mannitol at infinite dilution; t - Time)

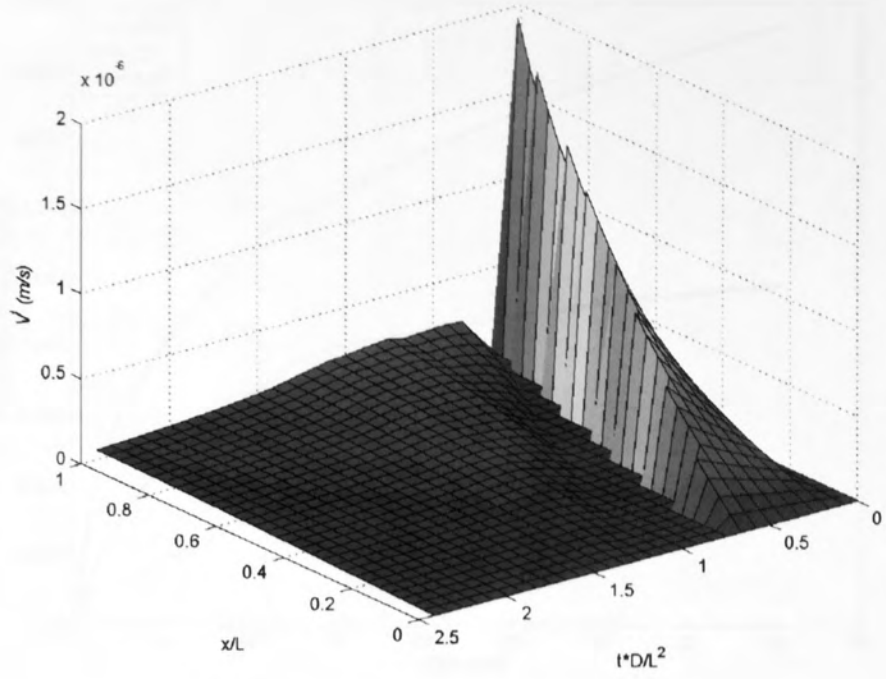

Figure 5.8 Bulk Flow Velocity in the Extra-cellular Volume

(v^f – Bulk flow velocity in the extra-cellular volume; x – Distance in the thickness direction measured from the symmetrical plane; L - Half thickness of the tissue slice; D – Diffusivity of mannitol at infinite dilution; t - Time)

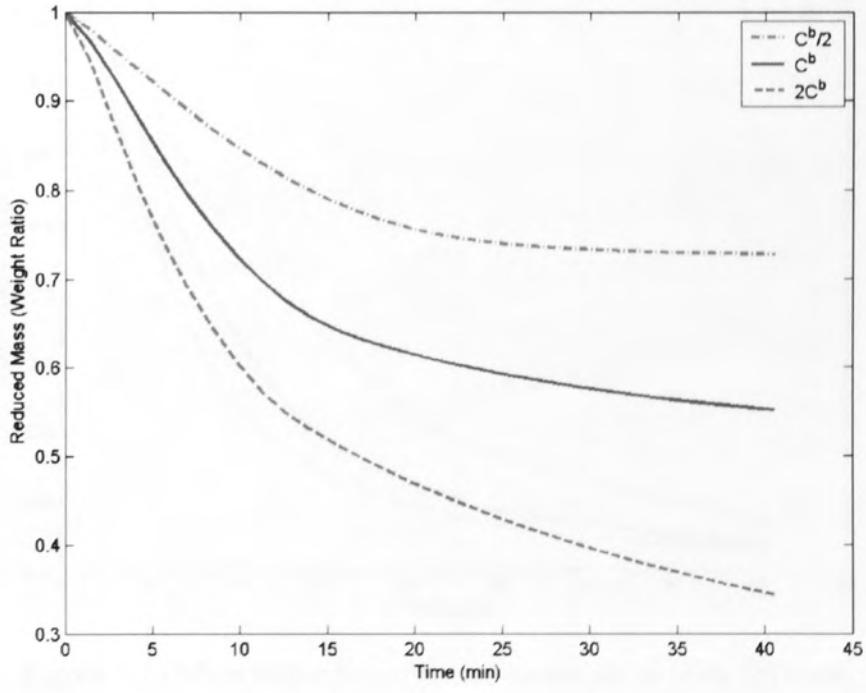

Figure 5.9 Mass reduction of potato tissue slices immersed in solutions of different concentration

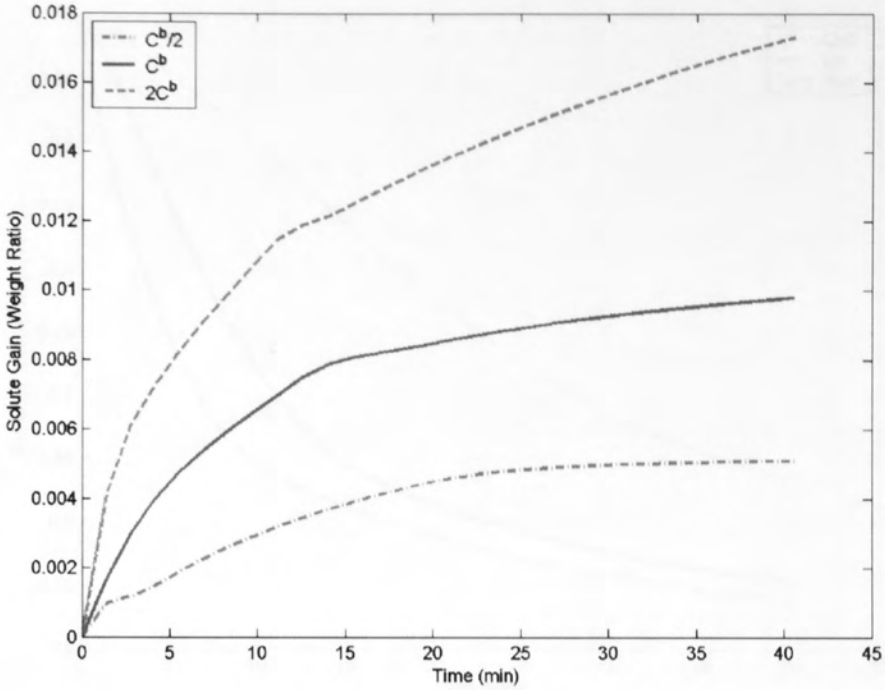

Figure 5.10 Solute gain in potato tissue slices immersed in solutions of different concentration

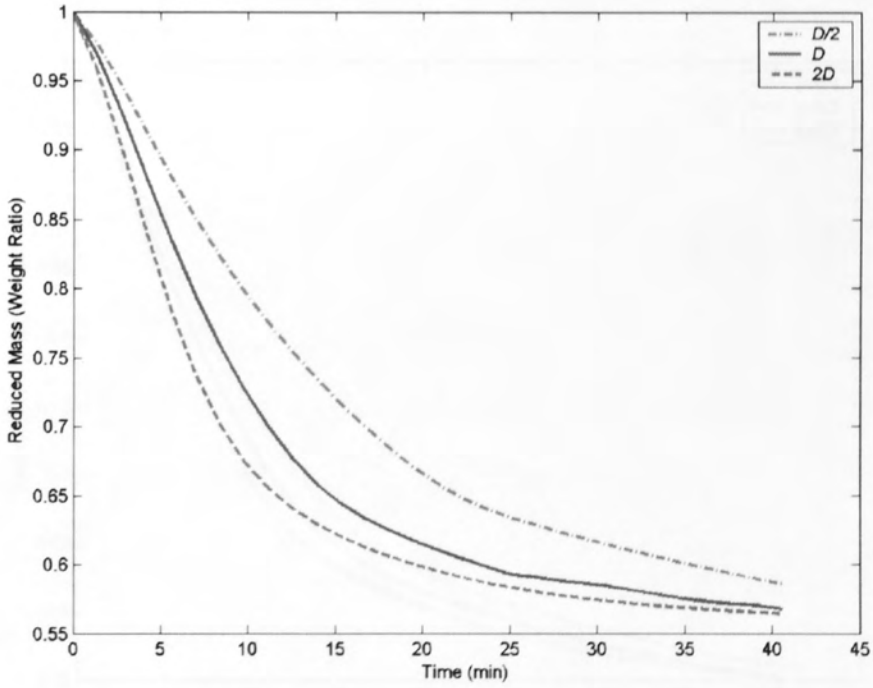

Figure 5.11 Mass reduction of potato tissue slices with different diffusion coefficients immersed in a mannitol solution

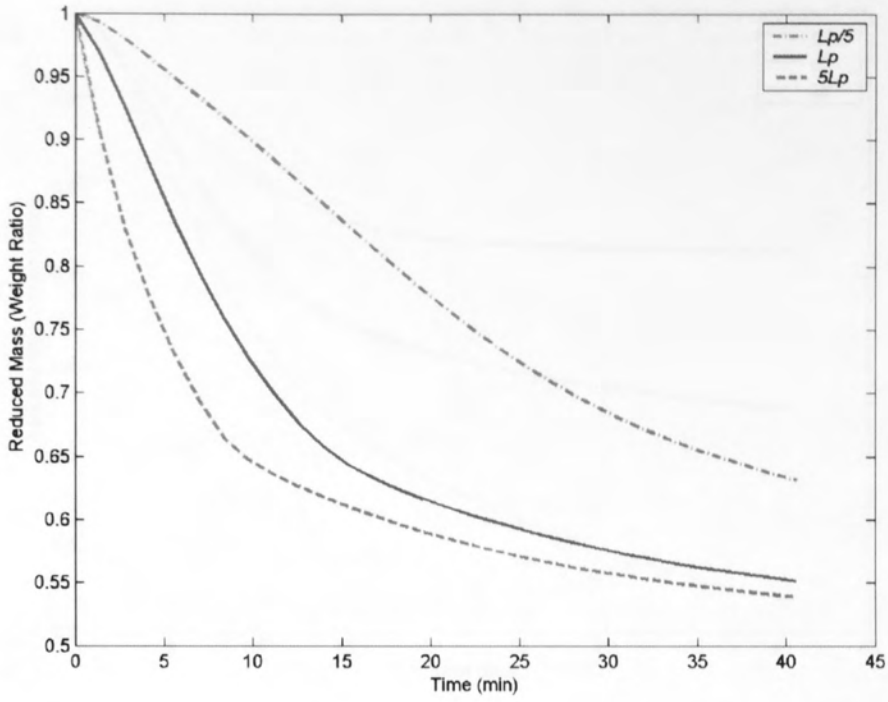

Figure 5.12 Mass reduction of potato tissue slices with different cell membrane conductivity immersed in a mannitol solution

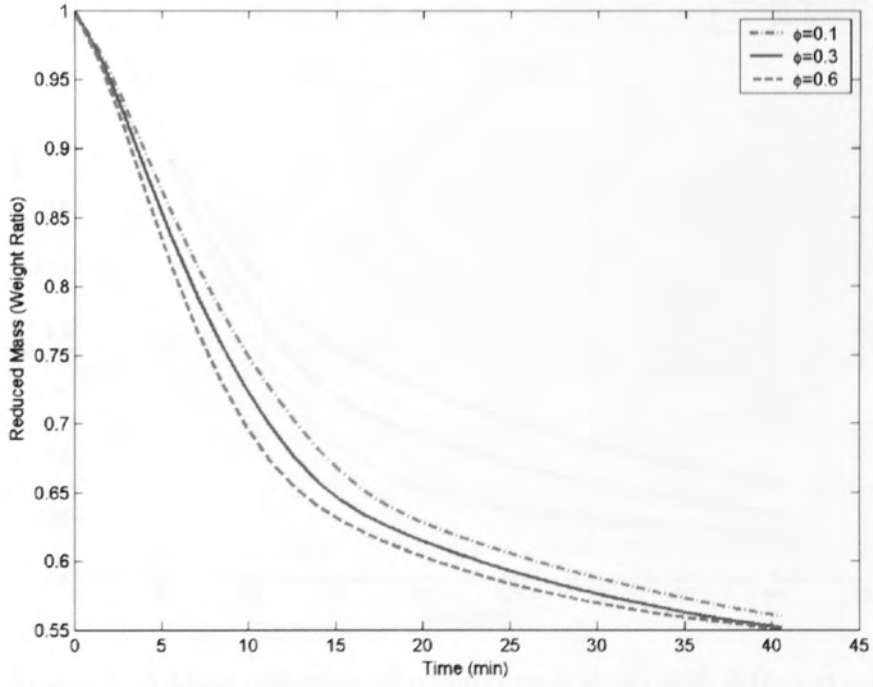

Figure 5.13 Mass reduction of potato tissue slices with different cell wall diffusibility immersed in a mannitol solution

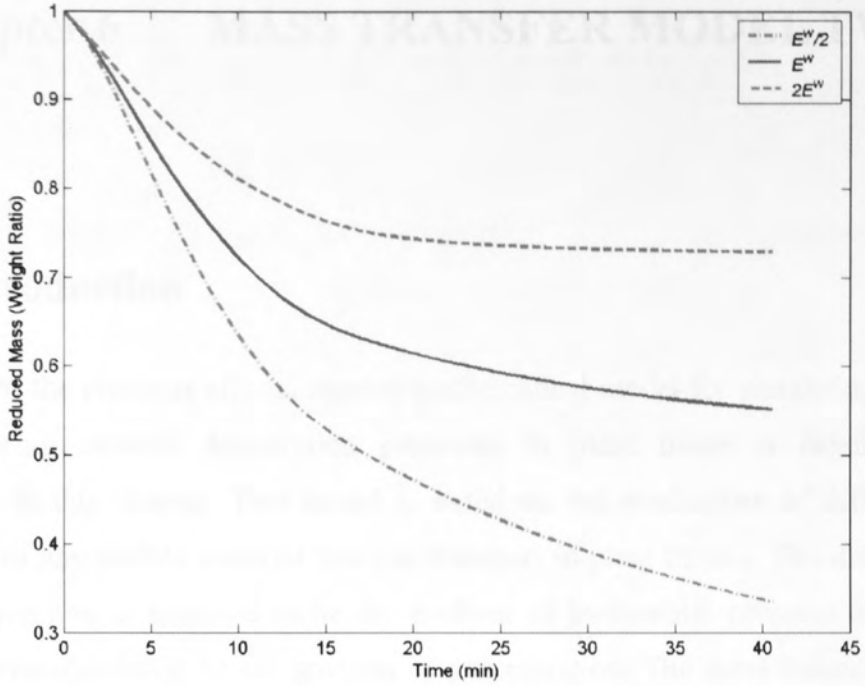

Figure 5.14 Mass reduction of potato tissue slices with different cell wall elastic modulus immersed in a mannitol solution

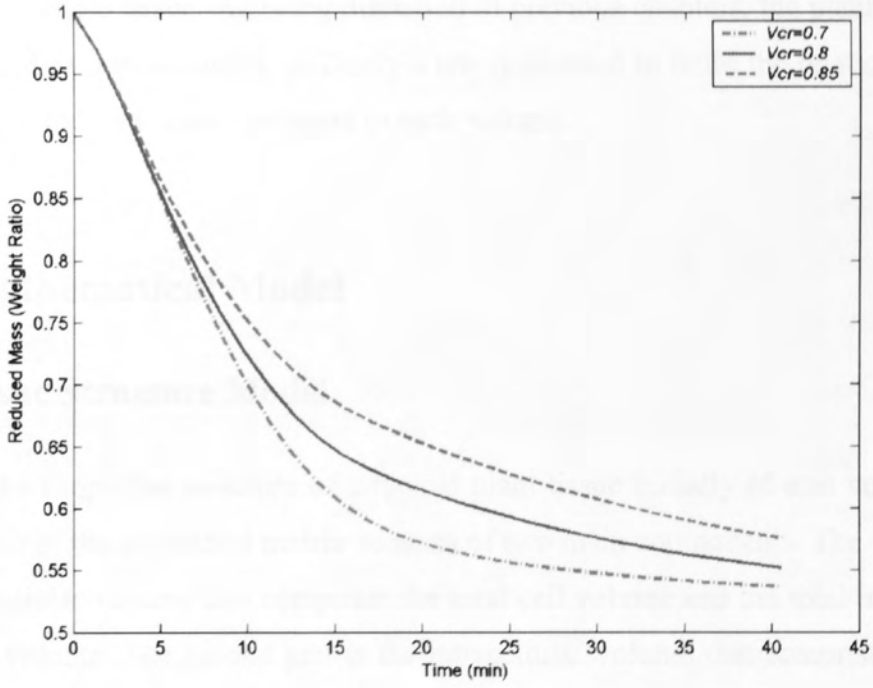

Figure 5.15 Mass reduction of potato tissue slices with different cell critical volume immersed in a mannitol solution

Chapter 6 MASS TRANSFER MODEL TWO

6.1 Introduction

According to the previous efforts, another mathematical model for simulating the mass transfer during osmotic dehydration processes in plant tissue is developed and represented in this chapter. This model is based on the mechanism of diffusion and convection of any mobile material that can transport in plant tissues. The driving force for the convection is assumed to be the gradient of hydrostatic pressure and for the diffusion is considered to be the gradient of concentration. The mass balance equation for the transport of each constituent is established separately for intracellular and extra-cellular volumes but with taking into account the mass exchange across the cell membrane between the intracellular and extra-cellular volumes. The mass transfer results in not only the change of intracellular and extra-cellular volumes but also the shrinkage of whole tissue. As being discussed in previous chapters, the plant tissue can be considered as porous media, so Darcy's law is adopted to build the relation between bulk velocity and hydrostatic pressure in each volume.

6.2 Mathematical Model

6.2.1 Tissue Structure Model

Consider the simplified structure of a typical plant tissue initially of unit volume. The total volume of the simplified matrix consists of two main components. The first part is the extra-cellular volume that comprises the total cell volume and the total intercellular free space volume. The second part is the intracellular volume that comprises the total cellular volume. The actual tissue thus can be regarded as an aggregation of N cells each of which has an identical volume (see Fig. 6.1 a), that is:

$$N\Omega_0 = N(\Omega_0^c + \Omega_0^f) \equiv 1 \tag{6.1}$$

where N is the total number of cells in the referenced frame, Ω_0 is the initial value of the average cell, Ω_0^c and Ω_0^f are the intracellular and extra-cellular volumes of the average cell.

To make the mathematical treatment feasible, it is assumed that the actual tissue is represented approximately by a homogeneous and isotropic cubic arrangement of representative spherical cells. Therefore the intercellular and extra-cellular volumes for the average cell can be expressed as follows:

$$\Omega = \Omega^c + \Omega^f \tag{6.2}$$

$$\Omega^c \equiv \varepsilon^c \Omega_0 \tag{6.3}$$

$$\Omega^f \equiv \varepsilon^f \Omega_0 \tag{6.4}$$

where Ω is the volume of the average cell, Ω^c and Ω^f are the intracellular and extra-cellular volumes of the average cell, ε^c and ε^f are the intracellular and extra-cellular volumes in the referenced unit volume respectively.

Note that, $\varepsilon^c + \varepsilon^f = 1$ if the volume change only involves the volume exchange between the intracellular and extra-cellular volumes and $\varepsilon^c + \varepsilon^f \neq 1$ if the volume change also involves the change of the average cell size. Therefore, the value of $\varepsilon^c + \varepsilon^f$ actually represents the change of the average cell volume during the osmotic process.

The diameter of the sphere representing the intracellular volume of the average cell can be calculated based on the spherical arrangement model as follows:

$$d^c = \left(\frac{6\Omega^c}{\pi}\right)^{1/3} = \left(\frac{6\varepsilon^c \Omega_0}{\pi}\right)^{1/3} \tag{6.5}$$

$$S^c = \pi\left(\frac{6\varepsilon^c \Omega_0}{\pi}\right)^{2/3} \tag{6.6}$$

where d^c is the diameter of the sphere representing the intracellular volume of the average cell and S^c is the corresponding surface area of the sphere. The interface

surface between the intracellular and extra-cellular volumes in the referenced unit volume thus is $NS^c = S^c/\Omega_0$.

6.2.2 Equations of Mass Balance

When a plant tissue is immersed in a concentrated osmotic solution containing one or more solutes, the solute in the solution will diffuse into the tissue. The penetration of the solute creates concentration gradients within the intracellular and extra-cellular volumes as well as between the intracellular and extra-cellular volumes, which drive the water out from the cellular structure. Consequently, there are at least two simultaneous, counter-current flows occurring in three different paths during the osmotic process. The two simultaneous, counter-current flows are the solute flow from the concentrated solution into the tissue and the water flow out from the tissue into the solution. The three paths are the transport within the intracellular volume, namely symplastic transport, the transport within the extra-cellular volume, namely free-space transport, and the transport across the cell membrane, namely apoplastic transport. In addition, the tissue shrinks because the amount of water flowing out, in general, is more than that of solutes diffusing in. This in turn leads to the change of hydrostatic pressures in the intracellular and extra-cellular volumes, which causes the convection of solutions in the intracellular and extra-cellular volumes.

The equations of mass balance for each species (solute) within the referenced frame can be expressed as (Li, 2005),

In the intracellular volume ($s=1, 2, \ldots, M$):

$$\frac{\partial}{\partial t}\left(\varepsilon^c C_s^c\right) = -\nabla J_s^c + \frac{S^c}{\Omega_0} J_s^{fc} \tag{6.7}$$

In the extra-cellular volume ($s=1, 2, \ldots, M$):

$$\frac{\partial}{\partial t}\left(\varepsilon^f C_s^f\right) = -\nabla J_s^f - \frac{S^c}{\Omega_0} J_s^{fc} \tag{6.8}$$

where t is the time, C_s^c and C_s^f are the concentrations of species s in the intracellular and extra-cellular volumes, J_s^c and J_s^f are the molar flux of species s in the intracellular and extra-cellular volumes, J_s^{fc} is the flux of species s from the extra-cellular volume into the intracellular volume through cell membrane (plasmalemma) and M is the total number of the solutes considered in the solution. The fluxes of species s in the intracellular and extra-cellular volumes can be expressed as

$$J_s^c = -D_s^c \varepsilon^c \overline{\nabla} C_s^c + V^c \left(\varepsilon^c C_s^c\right) \tag{6.9}$$

$$J_s^f = -D_s^f \varepsilon^f \overline{\nabla} C_s^f + V^f \left(\varepsilon^f C_s^f\right) \tag{6.10}$$

where D_s^c and D_s^f are the diffusion coefficients of species s in the intracellular and extra-cellular volumes, V^c and V^f are the bulk velocities of solutions in the intracellular and extra-cellular volumes. Note that the gradient operator in Eqs. (6.7) and (6.8) is different from that in Eqs. (6.9) and (6.10). For the former the derivatives are with respect to the referenced coordinates. The relationship between these two gradients can be expressed as follows (Li, 2005),

$$\overline{\nabla}(\cdots) = \frac{1}{\varepsilon^c + \varepsilon^f} \nabla(\cdots) \tag{6.11}$$

During the mass transport the intracellular and extra-cellular volumes vary with both time and position. The change of the intracellular and extra-cellular volumes can be determined by considering the conservation of the total volumes of solutes and solutions in the intracellular and extra-cellular volumes. Note that for ideal dilute solutions the volume change due to diffusion can be ignored. Therefore, the following volume conservation equations can be established,

$$\frac{\partial \varepsilon^c}{\partial t} = -\nabla\left(V^c \varepsilon^c\right) + \frac{S^c}{\Omega_0} J_0^{fc} \tag{6.12}$$

$$\frac{\partial \varepsilon^f}{\partial t} = -\nabla\left(V^f \varepsilon^f\right) - \frac{S^c}{\Omega_0} J_0^{fc} \tag{6.13}$$

where J_0^{fc} is the apoplastic transport flux of the water from the extra-cellular volume into the intercellular volume through cell membrane.

The bulk velocities of solutions in the intracellular and extra-cellular volumes can be determined by employing Darcy's law in terms of the pressure gradients in the intracellular and extra-cellular volumes as follows (Vankan *et al.*, 1997; Li *et al.*, 2002):

$$V^c = -\frac{K^c}{\mu^c}\overline{\nabla}P^c \tag{6.14}$$

$$V^f = -\frac{K^f}{\mu^f}\overline{\nabla}P^f \tag{6.15}$$

where K^c and K^f are the medium permeabilities for the solution in the intracellular and extra-cellular volumes, μ^c and μ^f are the corresponding dynamic viscosities, P^c and P^f are the hydrostatic pressures in the intracellular and extra-cellular volumes, respectively.

The hydrostatic pressures in the intracellular and extra-cellular volumes are related to their volumes and thus can be assumed as the functions of the intracellular and extra-cellular volumes as follows:

$$P^f = E^f \ln\frac{\Omega^f}{\Omega_0^f} + P_0^f \tag{6.16}$$

$$P^c = E^c \frac{\Omega^c - \Omega_0^c}{\Omega_0^c} + P_0^c \tag{6.17}$$

where E^f is the elastic modulus of the extra-cellular volume, which is considered as a constant. However, the empirical modulus E^c, which is strongly affected by the internal pressure (Nilsson *et al.*, 1958; Dainty, 1963a), varies due to the existence of the turgor pressure. E^c is considered as the elastic modulus of the cell membrane when the turgor pressure is vanished, and the composite of the elastic moduli of cell wall and cell membrane when the cell is under the turgor. In this model, the higher value is used when the cell is under the turgor pressure because the elastic modulus of cell wall is much bigger than the elastic modulus of cell membrane, and the lower value is used when the turgor pressure is vanished. P_0^c and P_0^f are the initial values of P^c and P^f, respectively. P_0^f is assumed to be the atmospheric pressure, and P_0^c is assumed to be

the summation of full turgor pressure and the initial pressure in extra-cellular volume. Therefore,

$$P_0^c = P_0^t + P_0^f \tag{6.18}$$

where P_0^t is the initial turgor pressure, can be expressed as

$$P_0^t = RT\sum_i \Delta C_i \tag{6.19}$$

where the summation is performed for all the non-permeating solutes present in the intracellular and extra-cellular volumes at full turgor.

The turgor pressure P^t, starting from full turgor and vanishing when incipient plasmolysis starts and is expressed as:

$$P^t = E^w \ln\frac{\Omega^c}{\Omega_0^c} + P_0^t \tag{6.20}$$

where E^w is the elastic module of cell wall, P_0^t is the initial torpor pressure. Equation (6.16), (6.17) and (6.20) are developed on the assumptions made by Dainty (1976) and Nobel (1983) for biological tissues, which are based on the experimentally found relationship between turgor pressure and cell volume change.

6.2.3 Mass Exchange across Cell Membrane

The driving force for the apoplastic transport of solutes and water across the cell membrane is the chemical potential difference between the solutions in the intracellular and extra-cellular volumes, which can be characterised using irreversible thermodynamics with phenomenological equations of Kedem and Katchalsky (1958) as follows (see, also, Li, 2004; Li, 2005):

$$J_0^{fc} = L_p\left(\Delta P - \sum_{s=1}^{M}\sigma_s RT\Delta C_s\right) \tag{6.21}$$

$$J_s^{fc} = (1-\sigma_s)\overline{C}_s J_0^{fc} + \omega_s RT\Delta C_s \tag{6.22}$$

where L_p is the membrane hydraulic conductivity, σ_s is the membrane reflection coefficient to solute s, ω_s is the membrane permeability to solute s, ΔP and ΔC_s are the

differences in pressures and concentrations (solute s) between the intracellular and extra-cellular volumes, $\overline{C}_s$ is the average concentration (solute s) of intracellular and extra-cellular volumes, R is the universal gas constant, T is the absolute temperature. The sign convention used in Eqs. (6.21) and (6.22) is defined as follows. Net fluxes of water and solutes from extra-cellular volume into intracellular volume are taken as positive. The differences in solute concentrations and in pressures across the membrane are calculated by the extra-cellular values minus the intracellular values. The two terms in Eq. (6.21) are called hydraulic flow and osmotic flow; while the two terms related to the solute flux in Eqs. (6.22) are called ultrafiltration and diffusion, respectively (Thain, 1967).

Eqs. (6.7), (6.8), (6.12) and (6.13) are the governing equations for determining concentrations, C_s^c and C_s^f, and volume fractions, ε^c and ε^f, in which the mass fluxes in the intracellular and extra-cellular volumes are defined by Eqs. (6.9) and (6.10), and the mass exchange between the intracellular and extra-cellular volumes is defined by Eqs. (6.21) and (6.22). For given initial and boundary conditions the solute concentrations and volume fractions at any time, at any place can be determined by solving the governing Eqs. (6.7), (6.8), (6.12) and (6.13).

6.3 Initial and Boundary Conditions

6.3.1 Initial Conditions

It will be assumed that initially the tissue is at full turgor, that is, it has been equilibrated with pure water. This supposes that initially all the constituent cells are identical, that is, on average their dimensions and their contents are equal, as are the elastic and permeability properties of their walls and membranes.

However, the initial concentration in the intracellular volume ($C_{s,0}^c$) and the initial concentration in the extra-cellular volume ($C_{s,0}^f$) are different, although they are constants, that is,

$$C^c_{s,0} = const. \tag{6.23}$$

$$C^f_{s,0} = const. \tag{6.24}$$

The initial intracellular and extra-cellular volumes are defined by the initial tissue characteristics, but total volume can be assume to be unity, that is,

$$\varepsilon^c_0 = const. \tag{6.25}$$

$$\varepsilon^c_0 + \varepsilon^f_0 \equiv 1 \tag{6.26}$$

The initial pressure in extra-cellular volume is considered as the atmospheric pressure. However, the initial pressure in intracellular volume will not be the atmospheric pressure due to the existence of turgor pressure. The initial turgor pressure is considered as the full turgor pressure. These pressures are expressed as:

$$P^f_0 = 1 atm \tag{6.27}$$

$$P^t_0 = RT\sum_{i=1}^{k} \Delta C_i \tag{6.28}$$

$$P^c_0 = P^f_0 + P^t_0 \tag{6.29}$$

where R is universal gas constant, T is the absolute temperature and ΔC_i is the concentration difference of impermeable solute i between intracellular and extra-cellular volumes.

6.3.2 Boundary Conditions

Boundary conditions on the surfaces

Let us assume that there is no resistance at the surfaces, so the concentrations on the surfaces of intracellular and extra-cellular volumes ($C^c_s\big|_{Surface}$ and $C^f_s\big|_{Surface}$) are equal to those in the osmotic solution (C^l_s), that is,

$$C^c_s\big|_{Surface} = C^f_s\big|_{Surface} = C^l_s \tag{6.30}$$

The volumes on the surfaces are considered constants, the values of which are dependent on individual case,

$$\varepsilon^c|_{Surface} = const. \tag{6.31}$$

$$\varepsilon^f|_{Surface} = const. \tag{6.32}$$

where $\varepsilon^c|_{Surface}$ and $\varepsilon^f|_{Surface}$ are the intracellular and extra-cellular volumes on the surfaces, respectively.

Boundary conditions at the centre

If there is a symmetrical boundary, then the boundary conditions for concentrations at the symmetrical boundary (z=0) are:

$$\left.\frac{\partial C_s^c}{\partial z}\right|_{z=0} = \left.\frac{\partial C_s^f}{\partial z}\right|_{z=0} = 0 \tag{6.33}$$

$$\left.\frac{\partial \varepsilon^c}{\partial z}\right|_{z=0} = \left.\frac{\partial \varepsilon^f}{\partial z}\right|_{z=0} = 0 \tag{6.34}$$

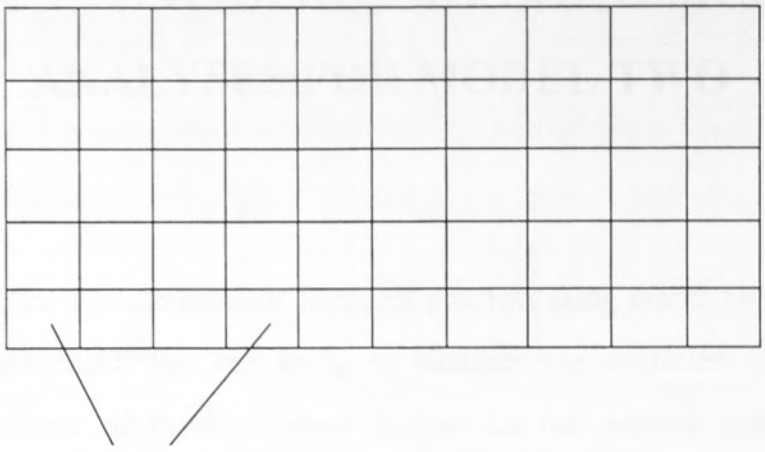

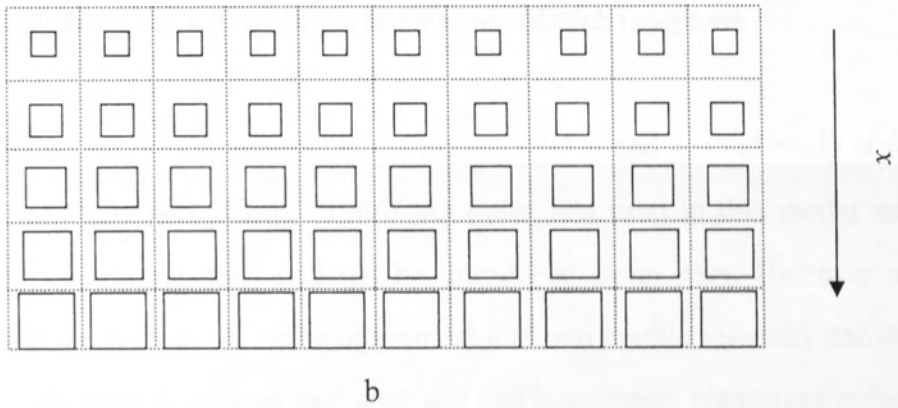

Figure 6.1 The Simplified Tissue Structure Model

a) The original tissue structural
b) The dehydrated tissue structure (1D)

Chapter 7 ONE-DIMENSIONAL NUMERICAL ANALYSES FOR MODEL TWO

In this chapter, the one-dimensional transport problem using model two developed in chapter 6 is presented, the aim being to simulate the evolution of the osmotic dehydration process of discs of plant tissues. Let us assume that the osmotic dehydration only happens in x-direction (Fig. 6.1 b). Two typical studies are adopted to verify the model. The results will be compared with the experimental data. Moreover, some important parameters employed in this model will also be analyzed in this chapter. The governing equations are solved numerically using Matlab programs.

The first study is based on the experiment of Stuart, (1973) and second study is based on the research of Kohn and Dainty, (1966). As most data used in this model are the same as used in model one, they will not be introduced again here. However, some important parameters, such as the ratios of permeability to dynamic viscosity and elastic moduli in the extra-cellular volume, cell wall and cell membrane, membrane reflection coefficients, etc., are obtained by a trial-and-error method and verified with the previous related studies.

7.1 Parameter Values for Computer Simulations

It is assumed that there are two solutes ($s=1, 2$) in the osmotic solution and therefore there are six coupled partial differential equations that need to be solved. The values used for defining initial conditions (at $t=0$), boundary conditions at one side of the disc ($x=L=0.5$cm) and transport parameters employed in the numerical computations are given in Table 7.1. The boundary at $x=0$ is assumed as the symmetric boundary.

All the values of constants and variables used in this model are summarized in Table 7.1 as well. They are obtained from literature sources (see table 7.2). However, for the parametrical values which are either unknown or available only quantitatively, sensitivity analyses are performed to determine which of these properties needed precise adjustment in order to achieve a good agreement with experimental data.

Before the discs of the plant tissue sample are used in the experiment, they have been washed in running tap water, are transferred to aerated distilled water in which they are stored for at least 48 hours. The initial pressure in intracellular volume is considered at full turgor. The ratios of permeability to dynamic viscosity are obtained by best fitting the numerical solution with experimental data.

7.2 Numerical Results

7.2.1 Concentrations in Intracellular and Extra-cellular Volumes

When the disc is immersed in the concentrated osmotic solutions, the solutes in the solution start to diffuse into the disc through both intracellular and extra-cellular volumes unless the cell membrane is impermeable to the solutes. Fig. 7.1 shows the concentration distribution profiles of the two solutes at four different times.

It can be seen that the concentrations are higher in the extra-cellular volume than in the intracellular volume for solute s_1. This is because the diffusion coefficients assumed in the extra-cellular volume are generally higher than those assumed in the intracellular volume. Due to the assumption that solute s_2 is non-permeable, the solute can only diffuse within the intracellular and extra-cellular volumes and cannot go through the cell membrane. The concentration in the intracellular volume changes with the change of intracellular volume. The intracellular volume changes mostly at the boundary, so the concentration close to boundary changes most obviously.

7.2.2 Intracellular and Extra-cellular Volumes and Hydraulic Pressures in Intracellular and Extra-cellular Volumes

The concentration difference between the intracellular and extra-cellular volumes creates a chemical potential difference across the cell membrane, which drives water to flow from the intracellular volume into the extra-cellular volume (that is so-called osmotic flow). As a consequence of this osmotic flow, the intracellular volume will decrease whereas the extra-cellular volume increases. The volume changes in the intracellular and extra-cellular volumes alter the distributions of hydrostatic pressures, which in turn cause the convective flow of solutions in both the intracellular and extra-cellular volumes and the hydraulic flow of water through the cell membrane.

Fig. 7.2 shows the distribution profiles of the volume fractions and corresponding hydrostatic pressures in the intracellular and extra-cellular volumes. As is to be expected, the extra-cellular volume increases with time, while the intracellular volume decreases with time. It is noticed from the figure that the distributions of hydrostatic pressures in the intracellular and extra-cellular volumes are quite different. The hydrostatic pressure in the intracellular volumes gets its maximum value when the tissue is under the full turgor, afterwards it reduces with time. However, the hydrostatic pressure in the extra-cellular volume increases slightly with time. This is mainly because the elastic modulus of the extra-cellular volume is much smaller than that of the cell wall and cell membrane.

Any significant difference in hydrostatic pressures between the intracellular and extra-cellular volumes will lead to the change of the intracellular volume and thus the pressure difference will immediately be compensated by the changed intracellular volume.

7.2.3 Average Cell Volume

Note that the trans-membrane water flow changes only the relative values of the intracellular and extra-cellular volumes. It does not change the whole cell volume. The change of cell volume is due to the convective flows caused by the gradients of hydrostatic pressures and the diffusion caused by gradients of the concentrations taking place in both intracellular and extra-cellular volumes

Fig. 7.3 shows the evolution of the change of the average cell volume during the process. At the beginning, the average cell volume is 1.0 and the volume is getting smaller and smaller with the time going on. It is noticed that the volume change starts from the place close to the side exposed to the osmotic solution and gradually moves to the centre when the time goes on.

The proposed mathematical model needs to be verified before we have the sensitivity analyses.

7.3 Cases Analyses

To verify the proposed mathematical model two, the following two case studies are carried out. The results for both case studies obtained from the simulation of this model are compared with the experimental data. In the end of this section, the results are validated.

7.3.1 Potato Tissue in Mannitol Solution

The same as the numerical analysis for mathematical model one, the first case study is according to the research of Toupin, *et al.*, 1989. The experimental result reported by Stuart (1973) for a potato discs subjects in mannitol solution is employed to be

compared with the present numerical simulation.

There is only one solute (Mannitol) in solution. According to Toupin *et al.*, the initial concentration in intracellular volume is assumed to be 0.1 kmol/m^3. The extra-cellular solution is taken as pure water since the potato discs used in this experiment, after being washed in running tap water, were transferred to aerated distilled water in which they were stored for at least 48 hours. This pretreatment not only ensures that the tissue is initially at full turgor, but also that the extra-cellular volume is likely to be pure water (Dainty, 1997; Green *et al.*, 1979). Assume that Mannitol is the solute s_1 and the non-permeating solutes in intracellular volume are s_2. All of the values of constants and variables used in this model are summarized in Table 7.3.

Fig. 7.4 provides a comparison between the present numerical simulation from model one, two and the experimental results reported by Stuart (1973) for a potato sample. It is seen that the present numerical results obtained by both models are reasonably good. By adjusting the parameters proposed in these models, the results obtained by both of these models can give a good agreement with the experimental data.

7.3.2 Red Beet Tissue in Sucrose Solution

This second numerical analysis is based on Kohn and Dainty (1966)'s measurement on red beet discs in contact with 0.4048 kmol/m^3 sucrose solution at 25°C for half an hour. The intracellular concentration at full turgor is taken as 0.2863 kmol/m^3, which corresponds to a value quoted by Ferrier and Dainty (1978) for red beet cells. All the values of constants and variables used in this study are listed in Table 8.4 as follow.

Fig. 7.5 provides the comparison between the present numerical simulation and the experimental results reported by Ferrier and Dainty (1966) for red beet samples. As is shown, the simulation results are well fit with the experimental data. Therefore, it can

be concluded that the present model is reasonable to simulate the osmotic dehydration process.

7.4 Sensitivity Analyses

As having been described in chapter 5, the influence of specific variables on the overall behaviour can be illustrated effectively by using the model to predict the response of the system studied to changes in the values of these variables.

Only one solute is employed (s_1) in the sensitivity analyses. Six same values are adopted to examine all these properties. They are:

- the concentration in intracellular volume
- the concentration in extra-cellular volume
- intracellular volume
- extra-cellular volume
- hydrostatic pressure in intracellular volume
- hydrostatic pressure in extra-cellular volume

The parameters employed for the sensitivity analyses are:

- diffusion coefficient
- the ratio of permeability to dynamic viscosity
- membrane hydraulic conductivity
- membrane permeability
- membrane reflection coefficient

- the elastic modulus in extra-cellular volume
- the elastic modulus of cell membrane
- the elastic modulus of the cell wall

The results influenced by the increasing or decreasing each value of parameters are shown in Figs. 7.6–7.13 (all these values are the results after 36 minutes' process).

7.4.1 Diffusion Coefficient

The effect of varying diffusion coefficient on the course of osmotic dehydration is considered in this section. Fig. 7.6 shows the results corresponding to three different diffusion coefficients (factor 5.0 is used as the changing ratio), while all other parameters remain unchanged (given in Table 7.1).

As is expected, an increase or decrease in the diffusion coefficient significantly affects the rate of dehydration. The concentrations in both intracellular and extra-cellular volume are changed dramatically. The higher the diffusion coefficient, the higher the concentrations in both volumes. The volume and hydrostatic pressure in intracellular volume reduce significantly when the diffusion coefficient is increased. However, the volume and hydrostatic pressure in extra-cellular volume increases significantly when the diffusion coefficient is increased. This means that the diffusion coefficient plays a very important role in osmotic dehydration process. This also shows that the higher diffusion coefficient will lead the process to complete more quickly.

7.4.2 Permeability / Dynamic Viscosity

Fig. 7.7 shows the results influenced by the change of the ratio of permeability to dynamic viscosity (the changing factor is chosen as 5.0). As is seen, the concentration in intracellular volume decreases while the concentration in extra-cellular volume

increases when the ratio is increased. This is because that the ratio can significantly affect the convective flow. However, the direction of convective flow is decided by the pressure gradient (see equation 6.14 and 6.15). From Fig. 7.7, it can be seen that with the increase of the ratio of permeability to dynamic viscosity, the intracellular volume and the hydrostatic pressure in intracellular volume will be dramatically decreased and the extra-cellular volume and the hydrostatic pressure in the extra-cellular volume are also been changed slightly. Because the value of elastic modulus in extra-cellular volume is much smaller than the one in intracellular volume, normally the hydrostatic pressure in extra-cellular volume does not change significantly.

7.4.3 Membrane Constants

Figs. 7.8-7.10 show the influence of the membrane constants on the transport of solutes and solution. These constants include the membrane hydraulic conductivity, the membrane reflection coefficient and the membrane permeability. It is seen from Fig. 7.8 that the increase of the membrane hydraulic conductivity has a little influence on the transport of solutes but has more influence on the water flow between the intracellular and extra-cellular volumes. In comparing to the membrane hydraulic conductivity, the influence of the membrane reflection coefficient (see Fig. 7.9) and the membrane permeability (see Fig. 7.10) seems not very significant. When the membrane reflection coefficient is changed from 0.7 to 1.0, the results seems to be similar. Only when the coefficient is reduced to 0.1, the change becomes noticeable. This feature is also applied to the membrane permeability, when it is increased by a factor of 20, a slight difference can be seen.

7.4.4 Elastic Modulus

The influence from elastic modulus of extra-cellular volume, cell wall and cell membrane is shown in Figs. 7.11-7.13. The elastic modulus of extra-cellular volume has

almost no influence on the values of intracellular volume as can be seen from Fig. 7.11. However, it has significant influence on the concentration in extra-cellular volume and the extra-cellular volume. The elastic modulus of cell membrane has a significant influence on the hydrostatic pressure in intracellular volume, but has slight influence on other variables (seen Fig. 7.12). The elastic modulus of cell wall does not give much contribution to the results after 36 minutes' process (see Fig. 7.13). This is because the elastic modulus of the cell wall only contributes to the turgor pressure, which influences the initial pressure in the intracellular volume, and after 36 minutes' process, the turgor pressure is vanished.

7.5 Summary for Model Two

According to the case studies, the good agreement between the simulated results by the proposed model and the experimental measurement indicates that the mathematic model to describe the mass transfer in cellular tissue under the osmotic dehydration process is reasonable, and the numerical simulation procedure to solve the model equations is successful.

The model allows us to quantitatively simulate the time evolution of intracellular and extra-cellular volumes and pressures as well as the concentrations.

The total volume reduction in potato tissue obtained by both of these two models is listed in Fig. 7.4 and is compared with the experimental data. The good agreement between the simulation results and experimental data is shown in this figure. This means both of these two models are reasonable and efficient to simulate the process of osmotic dehydration in plant tissue although many parameters are employed in each model. The mathematical model two avoids the limitation of three stages assumption in the osmotic dehydration process. More highly effective than the first model proposed in chapters 4 and 5, this model can be easily extended to two- or three-dimensional analyses which

can generalize the osmotic dehydration process and achieve the more effective and intuitionistic results.

Table 7.1 Value of Constants and Variables used in Calculations

Parameter	Value in Intracellular Volume	Value in Extra-cellular Volume	Unit
Diffusion Coefficients	$D_1^c = 0.01\, D_1^f$	$D_1^f = 9.0\times10^{-10}$	m^2/s
	$D_2^c = 0.01\, D_2^f$	$D_2^f = 4.0\times10^{-10}$	
Permeability/Dynamic Viscosity	$\frac{K^c}{\mu^c} = 0.05\frac{K^f}{\mu^f}$	$\frac{K^f}{\mu^f} = 5.0\times10^{-14}$	$m^4/(N\text{-}s)$
Elastic modulus	$E^c = 6.0\times10^5$	$E^f = 2.0\times10^4$	N/m^2
	$E^c = 1.8\times10^5$		
Membrane Hydraulic Conductivity	$L_p = 1.0\times10^{-14}$		$m^3/(N\text{-}s)$
Membrane Reflection Coefficient	$\sigma_1 = 0.7;\ \sigma_2 = 1.0$		dimensionless
Membrane Permeability	$RT\omega_1 = 7.0\times10^{-10};\ RT\omega_2 = 1.0\times10^{-9}$		m/s
Initial Concentrations	$C_1^c = 0.001$	$C_1^f = 0.001$	$kmol/m^3$
	$C_2^c = 0.1$	$C_2^f = 0.001$	
Initial Volume Fractions	$\varepsilon_0^c = 0.9$	$\varepsilon_0^f = 0.1$	dimensionless
Initial Pressures	$P_0^c = P_0^f + P_0^t$	$P_0^f = 1.0\times10^5$	N/m^2
Concentrations at Boundary	$C_1^{cb} = 0.5$	$C_1^{fb} = 0.5$	$kmol/m^3$
	$C_2^{cb} = 0.1$	$C_2^{fb} = 0.001$	
Volume Fractions at Boundary	$\varepsilon_b^c = 0.2$	$\varepsilon_b^f = 0.1$	dimensionless
Universal Gas Constant	$R = 8314$		(N-m)/(K-kmol)
Temperature	$T = 298$		K
Initial Spherical Diameter of Intracellular volume	$d_0^c = 6.0\times10^{-5}$		m
Full Turgor Pressure	$P_0^t = RT\sum\Delta C = RT\times 0.1$		$kmol/m^3$

Table 7.2 Sources of Constants and Variables used in Calculations

Parameters	References
Diffusion Coefficient	Marcotte (1988); Toupin & Le Maguer (1989); Yao & Le Maguer (1997)
Permeability/Dynamic Viscosity	RILEM (1965); Scheidegger (1957); Li (2005)
Membrane Hydraulic Conductivity	House (1973); Lüttge & Pitman (1976); Toupin & Le Maguer (1989); Yao & Le Maguer (1997); Li (2005)
Membrane Reflection Coefficient	Lüttge & Pitman (1976); Toupin & Le Maguer (1989); Yao & Le Maguer (1997); Li (2005)
Membrane Permeability	Lüttge & Pitman (1976); Toupin & Le Maguer (1989); Yao & Le Maguer (1997); Li (2005)
Initial Cell Diameter	Lüttge & Pitman (1976); Toupin & Le Maguer (1989)
Elastic Moduli	Lüttge & Pitman (1976); Toupin & Le Maguer (1989); Yao & Le Maguer (1997)

Table 7.3 Value of Constants and Variables used in Potato Tissue in Mannitol Solution

Parameter	Value in Intracellular Volume	Value in Extra-cellular Volume	Unit
Diffusion Coefficients	$D_1^c = 0.01\, D_1^f$	$D_1^f = 6.7 \times 10^{-10}$	m^2/s
	$D_2^c = 0.01\, D_2^f$	$D_2^f = 4.0 \times 10^{-10}$	
Permeability/Dynamic Viscosity	$\frac{K^c}{\mu^c} = 0.05 \frac{K^f}{\mu^f}$	$\frac{K^f}{\mu^f} = 1.5 \times 10^{-14}$	$m^4/(N\ s)$
Elastic modulus	$E^c = 6.0 \times 10^5$	$E^f = 2.0 \times 10^4$	N/m^2
	$E^c = 1.8 \times 10^5$		
Membrane Hydraulic Conductivity	$L_p = 1.0 \times 10^{-14}$		$m^3/(N\ s)$
Membrane Reflection Coefficient	$\sigma_1 = 0.7;\ \sigma_2 = 1.0$		dimensionless
Membrane Permeability	$RT\omega_1 = 7.0 \times 10^{-10}; RT\omega_2 = 1.0 \times 10^{-9}$		m/s
Initial Concentrations	$C_1^c = 0.0$	$C_1^f = 0.0$	$kmol/m^3$
	$C_2^c = 0.1$	$C_2^f = 0.0$	
Initial Volume Fractions	$\varepsilon_0^c = 0.9$	$\varepsilon_0^f = 0.1$	dimensionless
Initial Pressures	$P_0^c = P_0^f + P_0^t$	$P_0^f = 1.0 \times 10^5$	N/m^2
Concentrations at Boundary	$C_1^{cb} = 0.535$	$C_1^{fb} = 0.535$	$kmol/m^3$
	$C_2^{cb} = 0.1$	$C_2^{fb} = 0.0$	
Volume Fractions at Boundary	$\varepsilon_b^c = 0.2$	$\varepsilon_b^f = 0.1$	dimensionless
Universal Gas Constant	$R = 8314$		(N m)/(K kmol)
Temperature	$T = 298$		K
Initial Spherical Diameter of Intracellular volume	$d_0^c = 6.0 \times 10^{-5}$		M
Full Turgor Pressure	$P_0^t = RT \sum \Delta C = RT \times 0.1$		$kmol/m^3$

Table 7.4 Value of Constants and Variables used in Red Beet Root Tissue in Sucrose Solution

Parameter	Value in Intracellular Volume	Value in Extra-cellular Volume	Unit
Diffusion Coefficients	$D_1^c = 0.05\, D_1^f$	$D_1^f = 5.23\times10^{-10}$	m^2/s
	$D_2^c = 0.05\, D_2^f$	$D_2^f = 4.0\times10^{-10}$	
Permeability/Dynamic Viscosity	$\frac{K^c}{\mu^c} = 0.05\frac{K^f}{\mu^f}$	$\frac{K^f}{\mu^f} = 3.5\times10^{-14}$	$m^4/(N\ s)$
Elastic modulus	$E^c = 4.0\times10^5$	$E^f = 2\times10^4$	N/m^2
	$E^c = 2\times10^5$		
Membrane Hydraulic Conductivity	$L_p = 2.5\times10^{-14}$		$m^3/(N\ s)$
Membrane Permeability	$RT\omega_1 = 7.0\times10^{-10}$; $RT\omega_2 = 1.0\times10^{-9}$		m/s
Membrane Reflection Coefficient	$\sigma_1 = 0.7$; $\sigma_2 = 1.0$		dimensionless
Initial Concentrations	$C_1^c = 0.0$	$C_1^f = 0.0$	$kmol/m^3$
	$C_2^c = 0.2863$	$C_2^f = 0.0$	
Initial Volume Fractions	$\varepsilon_0^c = 0.9$	$\varepsilon_0^f = 0.1$	dimensionless
Initial Pressures	$P_0^c = P_0^f + P_0^t$	$P_0^f = 1.0\times10^5$	N/m^2
Concentrations at Boundary	$C_1^{cb} = 0.4088$	$C_1^{fb} = 0.4088$	$kmol/m^3$
	$C_2^{cb} = 0.2863$	$C_2^{fb} = 0.0$	
Volume Fractions at Boundary	$\varepsilon_b^c = 0.4$	$\varepsilon_b^f = 0.2$	dimensionless
Universal Gas Constant	$R = 8314$		(N m)/(K kmol)
Temperature	$T = 298$		K
Initial Spherical Diameter of Intracellular volume	$d_0^c = 6.1\times10^{-5}$		m
Full Turgor Pressure	$P_0^t = RT\sum\Delta C = RT \times 0.2863$		$kmol/m^3$

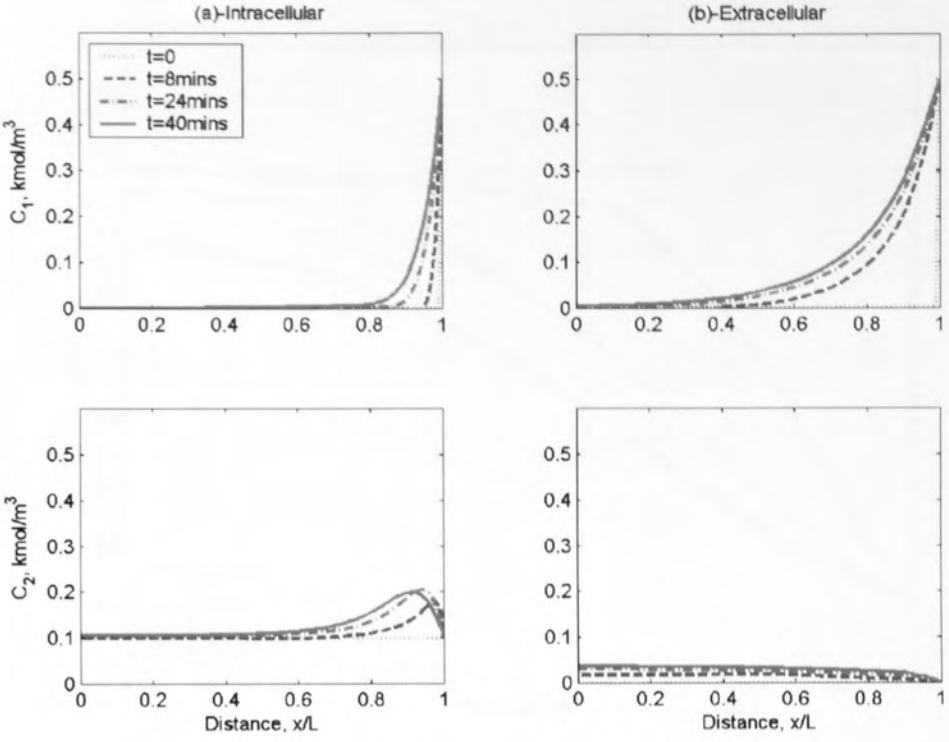

Figure 7.1 Concentration distribution profiles of solutes at different times

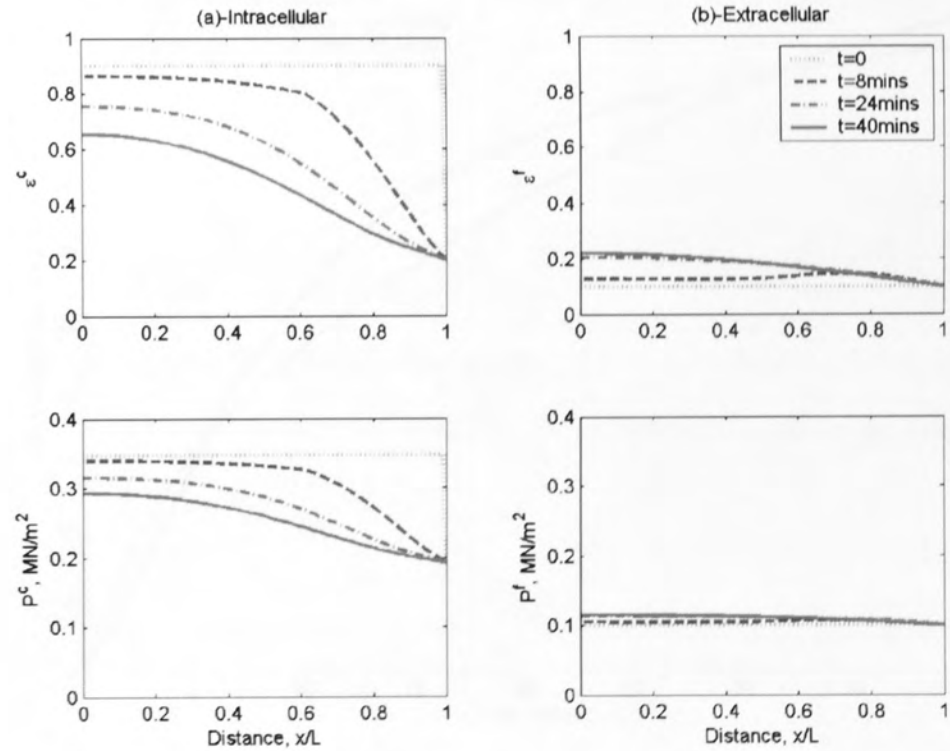

Figure 7.2 Volume fraction and hydrostatic pressure distribution profiles at different times

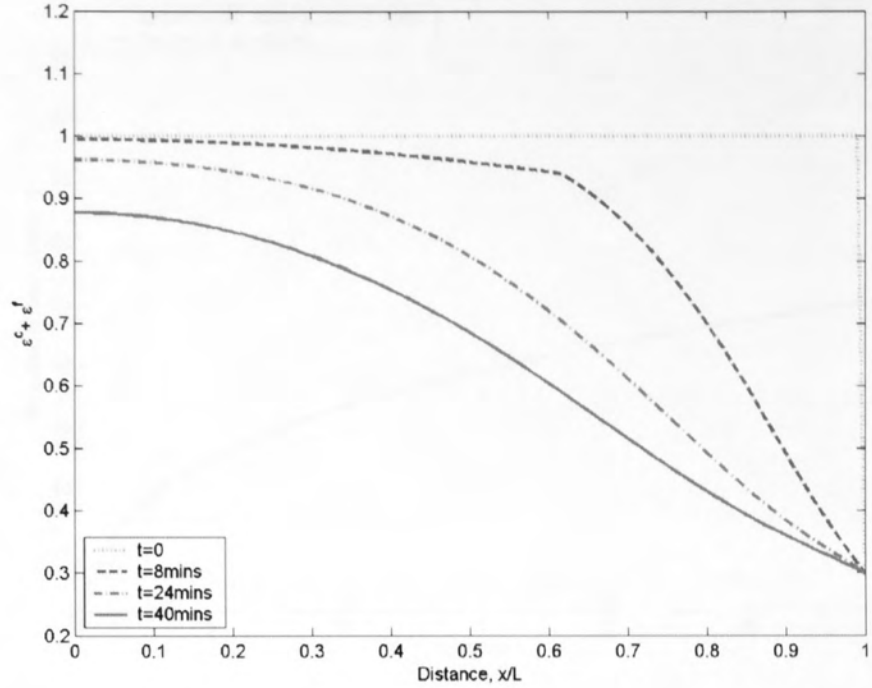

Figure 7.3 Evolution of the cell volume during the process of osmotic dehydration

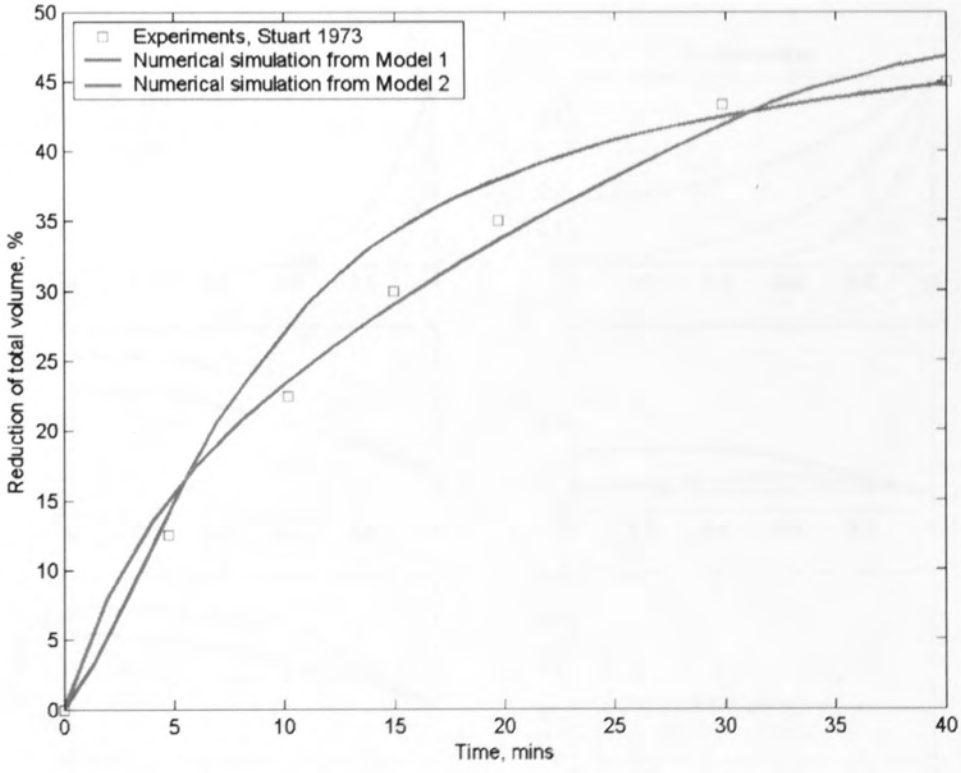

Figure 7.4 Comparison of the cell volume between the simulations from model 1, 2 and the experimental results reported by Stuart (1973)

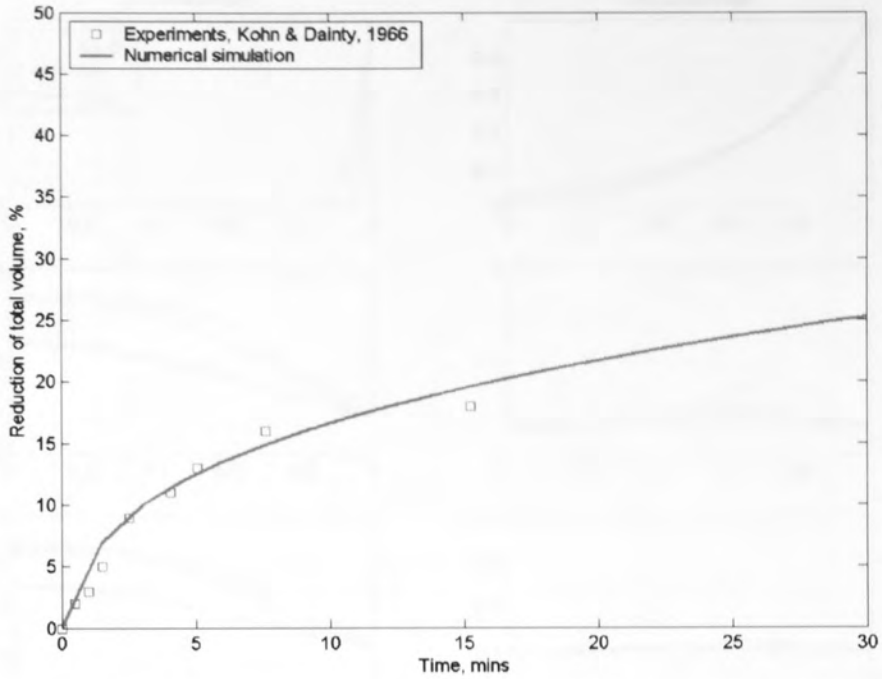

Figure 7.5 Comparison of the red beet root cell volume between present simulation and the experimental results reported by Kohn & Dainty (1966)

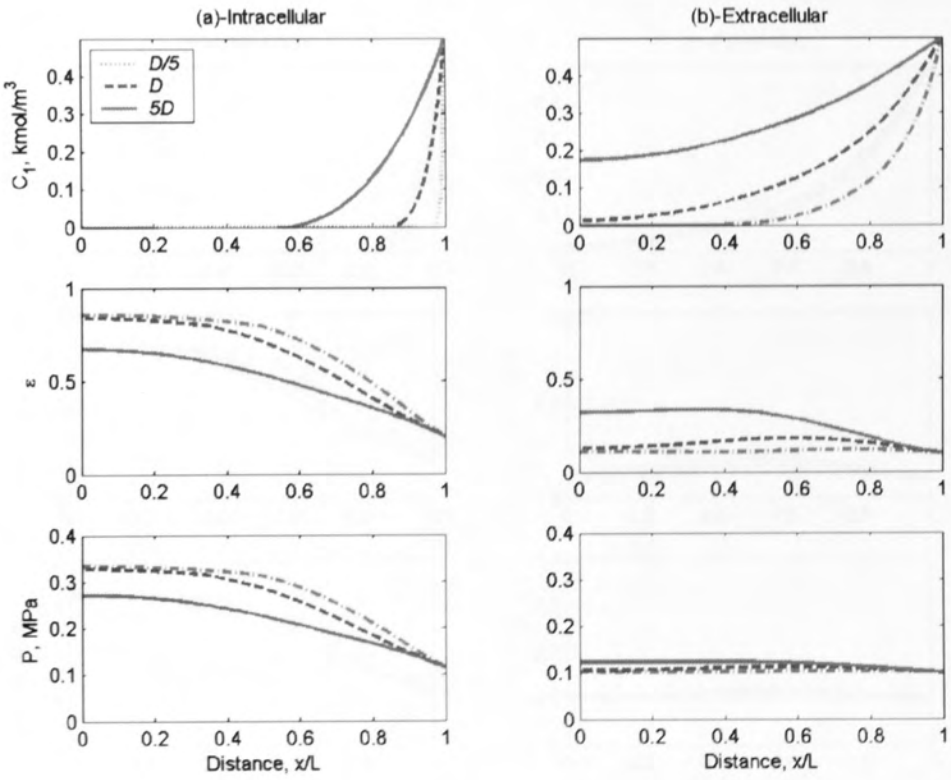

Figure 7.6 Influence of diffusion coefficient on the process (t=36 mins)

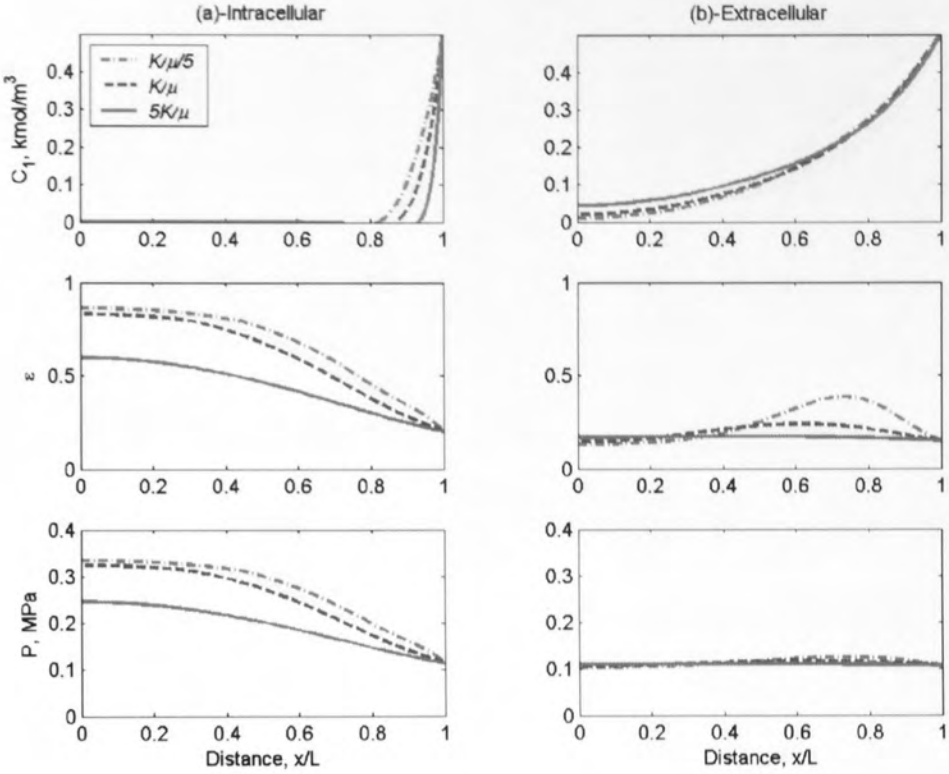

Figure 7.7 Influence of permeability/dynamic viscosity on the process (t=36 mins)

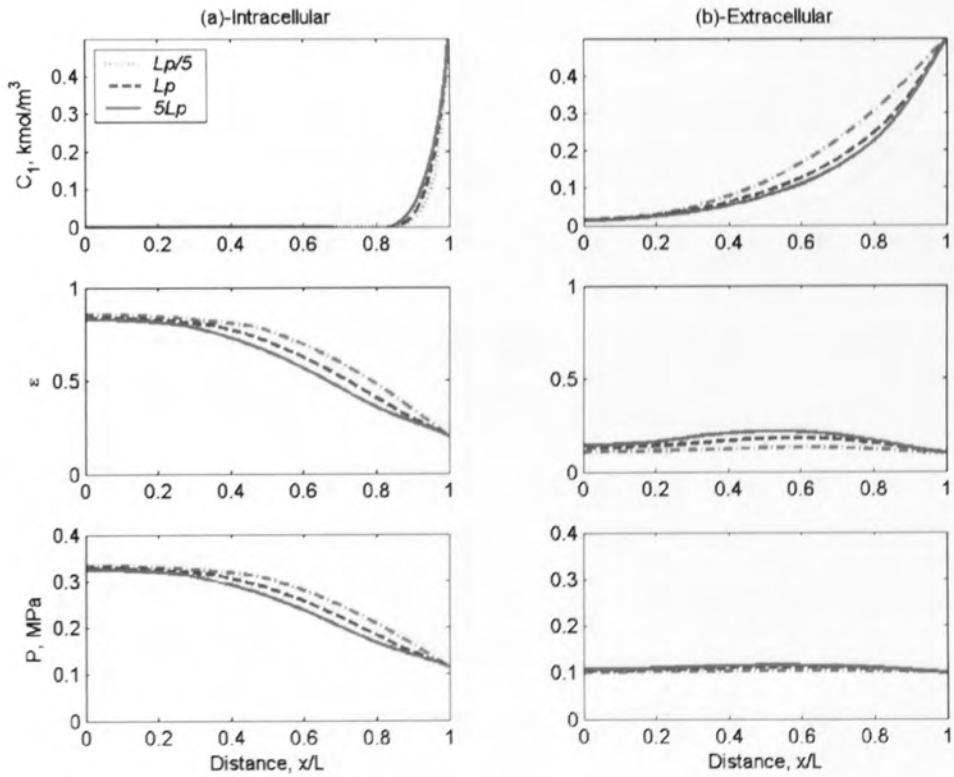

Figure 7.8 Influence of membrane hydraulic conductivity on the process (t=36 mins)

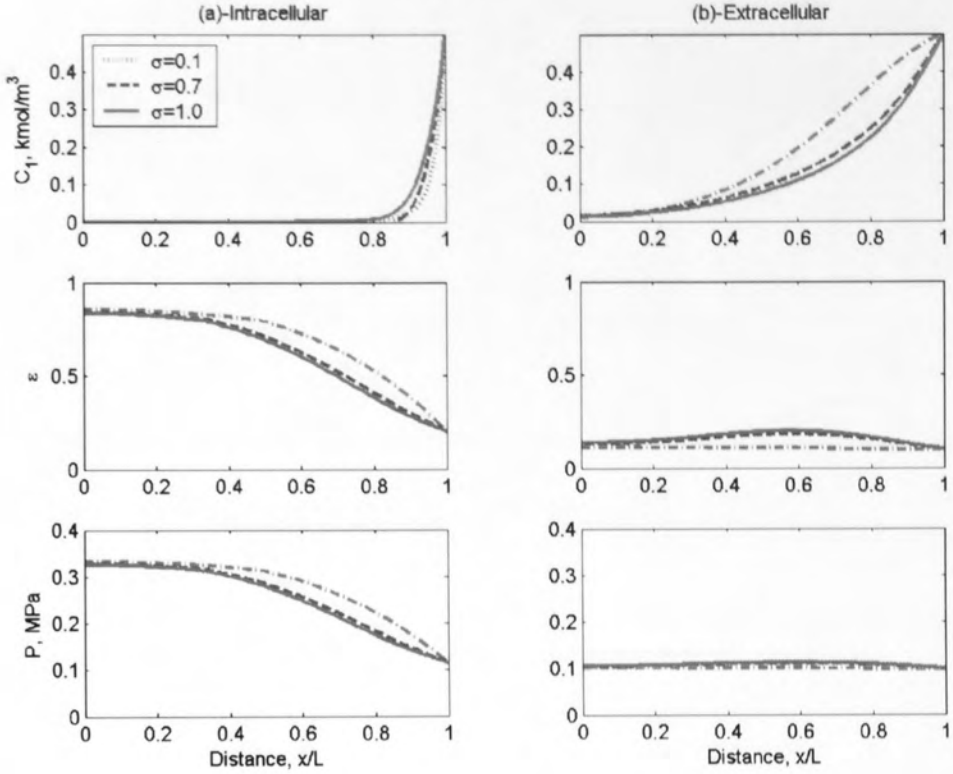

Figure 7.9 Influence of membrane reflection coefficients on the process (t=36 mins)

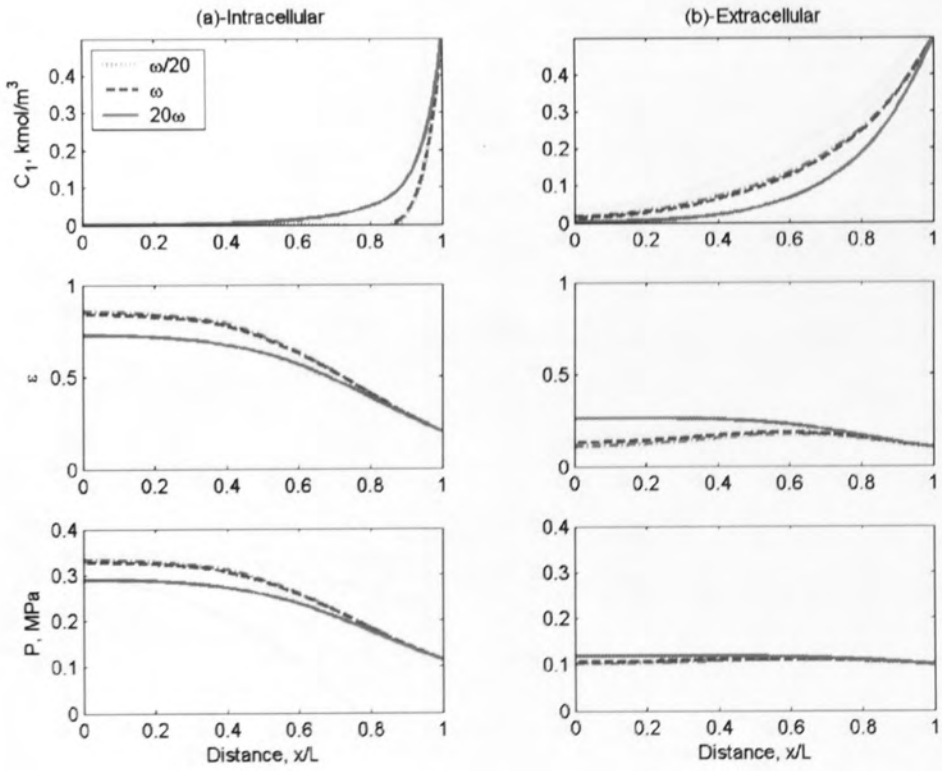

Figure 7.10 Influence of membrane permeability on the process (t=36 mins)

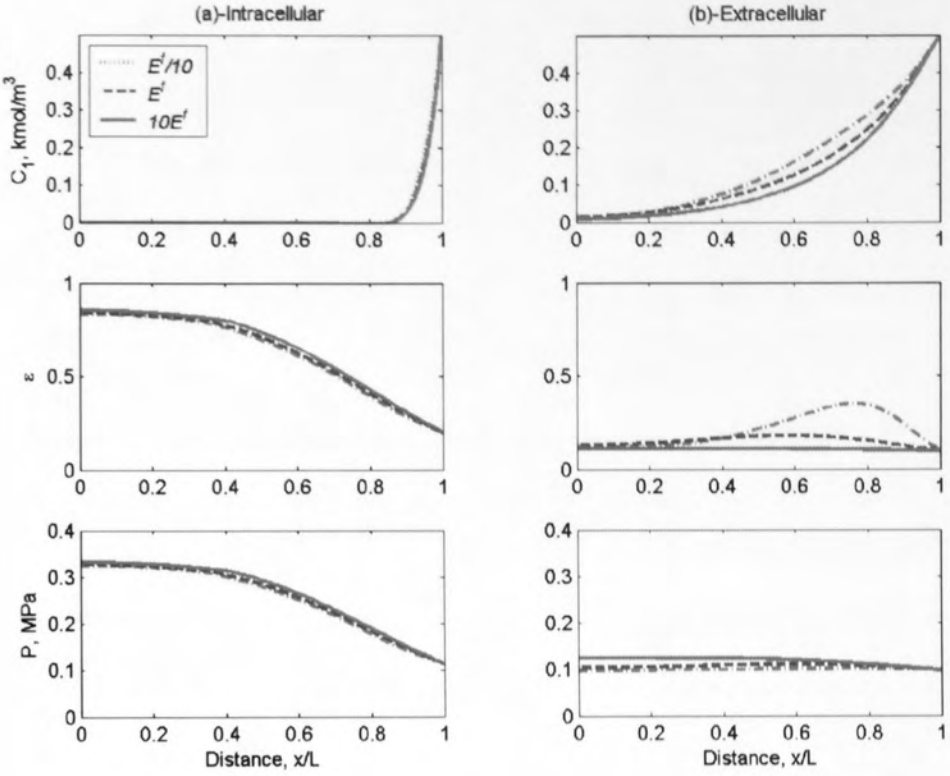

Figure 7.11 Influence of elastic modulus of extra-cellular volume (t=36 mins)

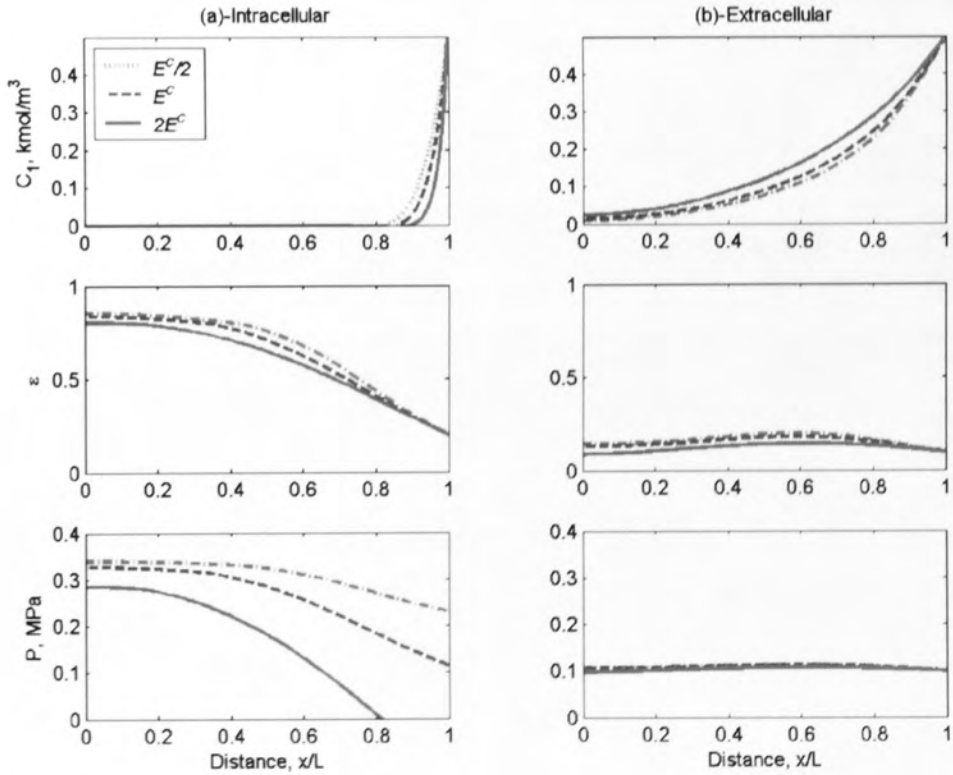

Figure 7.12 Influence of elastic modulus of cell membrane (t=36 mins)

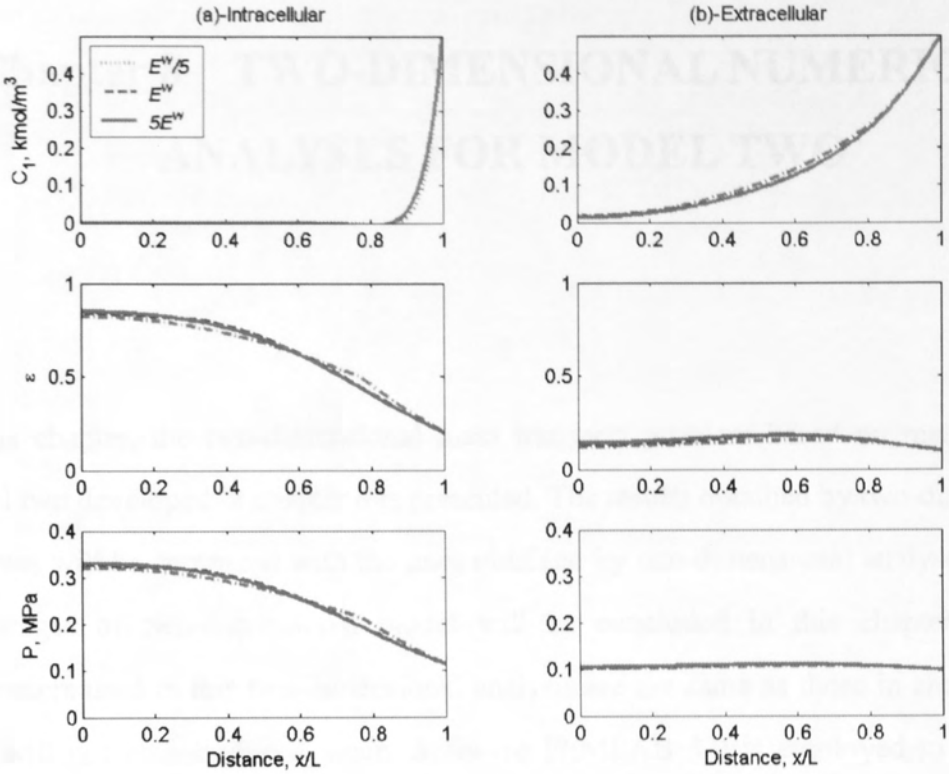

Figure 7.13 Influence of elastic modulus of cell wall (t=36 mins)

Chapter 8 TWO-DIMENSIONAL NUMERICAL ANALYSES FOR MODEL TWO

In this chapter, the two-dimensional mass transport problem based on mathematical model two developed in chapter 6 is presented. The results obtained by two-dimensional analyses will be compared with the ones obtained by one-dimensional analyses and the advantages of two-dimensional model will be concluded in this chapter. All the parameters used in this two-dimensional analysis are the same as those in chapter 7, so they will not be introduced again. Software FEMLAB 3.0 is employed to solve the partial differential equations (PDEs).

8.1 Introduction to the Two-dimensional Governing Equations

As presented in chapter 6, the governing equations of mass balance and volume conservation for each species (solute) within the referenced frame can be expressed as (Li, 2005),

$$\frac{\partial}{\partial t}\left(\varepsilon^c C_s^c\right) = -\nabla J_s^c + \frac{S^c}{\Omega_0} J_s^{fc} \tag{6.7}$$

$$\frac{\partial}{\partial t}\left(\varepsilon^f C_s^f\right) = -\nabla J_s^f - \frac{S^c}{\Omega_0} J_s^{fc} \tag{6.8}$$

$$\frac{\partial \varepsilon^c}{\partial t} = -\nabla\left(V^c \varepsilon^c\right) + \frac{S^c}{\Omega_0} J_0^{fc} \tag{6.12}$$

$$\frac{\partial \varepsilon^f}{\partial t} = -\nabla\left(V^f \varepsilon^f\right) - \frac{S^c}{\Omega_0} J_0^{fc} \tag{6.13}$$

where $s=1, 2, \ldots, M$ (M is the total number of species);

$$J_s^c = -D_s^c \varepsilon^c \overline{\nabla} C_s^c + V^c \left(\varepsilon^c C_s^c \right) \tag{6.9}$$

$$J_s^f = -D_s^f \varepsilon^f \overline{\nabla} C_s^f + V^f \left(\varepsilon^f C_s^f \right) \tag{6.10}$$

$$\overline{\nabla}(\cdots) = \frac{1}{\varepsilon^c + \varepsilon^f} \nabla(\cdots) \tag{6.11}$$

When substitute Eqs. (6.9) - (6.11) to Eqs. (6.7) and (6.8), the following equations can be obtained:

$$\frac{\partial}{\partial t}\left(\varepsilon^c C_s^c \right) - \nabla \left[\frac{D_s^c \varepsilon^c}{\varepsilon^c + \varepsilon^f} \nabla C_s^c - V^c (\varepsilon^c C_s^c) \right] = \frac{S^c}{\Omega_0} J_s^{fc} \tag{8.1}$$

$$\frac{\partial}{\partial t}\left(\varepsilon^f C_s^f \right) - \nabla \left[\frac{D_s^f \varepsilon^f}{\varepsilon^c + \varepsilon^f} \nabla C_s^f - V^f (\varepsilon^f C_s^f) \right] = -\frac{S^c}{\Omega_0} J_s^{fc} \tag{8.2}$$

$$\begin{aligned} &\frac{\partial}{\partial t}\left(\varepsilon^c C_s^c \right) - \frac{\partial}{\partial x}\left[\frac{D_s^c \varepsilon^c}{\varepsilon^c + \varepsilon^f} \frac{\partial}{\partial x} C_s^c - V_x^c (\varepsilon^c C_s^c) \right] \\ &\quad - \frac{\partial}{\partial y}\left[\frac{D_s^c \varepsilon^c}{\varepsilon^c + \varepsilon^f} \frac{\partial}{\partial y} C_s^c - V_y^c (\varepsilon^c C_s^c) \right] = \frac{S^c}{\Omega_0} J_s^{fc} \end{aligned} \tag{8.3}$$

$$\begin{aligned} &\frac{\partial}{\partial t}\left(\varepsilon^f C_s^f \right) - \frac{\partial}{\partial x}\left[\frac{D_s^f \varepsilon^f}{\varepsilon^c + \varepsilon^f} \frac{\partial}{\partial x} C_s^f - V_x^f (\varepsilon^f C_s^f) \right] \\ &\quad - \frac{\partial}{\partial y}\left[\frac{D_s^f \varepsilon^f}{\varepsilon^c + \varepsilon^f} \frac{\partial}{\partial y} C_s^f - V_y^f (\varepsilon^f C_s^f) \right] = -\frac{S^c}{\Omega_0} J_s^{fc} \end{aligned} \tag{8.4}$$

Let us rewrite these governing equations in standard two-dimensional form:

$$\begin{aligned} &\frac{\partial}{\partial t}\left(\varepsilon^c C_s^c \right) - \frac{\partial}{\partial x}\left[\frac{D_s^c}{\varepsilon^c + \varepsilon^f} \left[\frac{\partial}{\partial x}\left(\varepsilon^c C_s^c \right) - C_s^c \frac{\partial}{\partial x} \varepsilon^c \right] - V_x^c (\varepsilon^c C_s^c) \right] \\ &\quad - \frac{\partial}{\partial y}\left[\frac{D_s^c}{\varepsilon^c + \varepsilon^f} \left[\frac{\partial}{\partial y}\left(\varepsilon^c C_s^c \right) - C_s^c \frac{\partial}{\partial y} \varepsilon^c \right] - V_y^c (\varepsilon^c C_s^c) \right] = \frac{S^c}{\Omega_0} J_s^{fc} \end{aligned} \tag{8.5}$$

$$\frac{\partial}{\partial t}\left(\varepsilon^f C_s^f\right)-\frac{\partial}{\partial x}\left[\frac{D_s^f}{\varepsilon^c+\varepsilon^f}\left[\frac{\partial}{\partial x}\left(\varepsilon^f C_s^f\right)-C_s^f\frac{\partial}{\partial x}\varepsilon^f\right]-V_x^f(\varepsilon^f C_s^f)\right]$$
$$-\frac{\partial}{\partial y}\left[\frac{D_s^f}{\varepsilon^c+\varepsilon^f}\left[\frac{\partial}{\partial y}\left(\varepsilon^f C_s^f\right)-C_s^f\frac{\partial}{\partial y}\varepsilon^f\right]-V_y^f(\varepsilon^f C_s^f)\right]=-\frac{S^c}{\Omega_0}J_s^{fc} \tag{8.6}$$

$$\frac{\partial\varepsilon^c}{\partial t}-\frac{\partial}{\partial x}\left(-V_x^c\varepsilon^c\right)-\frac{\partial}{\partial y}\left(-V_y^c\varepsilon^c\right)=\frac{S^c}{\Omega_0}J_0^{fc} \tag{8.7}$$

$$\frac{\partial\varepsilon^f}{\partial t}-\frac{\partial}{\partial x}\left(-V_x^f\varepsilon^f\right)-\frac{\partial}{\partial y}\left(-V_y^f\varepsilon^f\right)=-\frac{S^c}{\Omega_0}J_0^{fc} \tag{8.8}$$

where V_x^c, V_y^c, V_x^f and V_y^f can be obtained from Eqs. (6.14) and (6.15).

$$V^c=-\frac{K^c}{\mu^c}\overline{\nabla}P^c \tag{6.14}$$

$$V^f=-\frac{K^f}{\mu^f}\overline{\nabla}P^f \tag{6.15}$$

that is:

$$V_x^c=-\frac{K^c}{\mu^c(\varepsilon^c+\varepsilon^f)}\frac{\partial P^c}{\partial x} \tag{8.9}$$

$$V_y^c=-\frac{K^c}{\mu^c(\varepsilon^c+\varepsilon^f)}\frac{\partial P^c}{\partial y} \tag{8.10}$$

$$V_x^f=-\frac{K^f}{\mu^f(\varepsilon^c+\varepsilon^f)}\frac{\partial P^f}{\partial x} \tag{8.11}$$

$$V_y^f=-\frac{K^f}{\mu^f(\varepsilon^c+\varepsilon^f)}\frac{\partial P^f}{\partial y} \tag{8.12}$$

Eqs. (8.5) – (8.8) are the governing equations for determining concentrations, C_s^c and C_s^f, and volume fractions, ε^c and ε^f.

8.2 PDE Formations in FEMLAB

The PDE formation of diffusion and convection used in FEMLAB is:

$$d_a \frac{\partial u}{\partial t} - \nabla(c\nabla u + au - \gamma) + \alpha u + \beta \nabla u = f \tag{8.13}$$

where

- d_a is the mass coefficient.
- c is the diffusion coefficient.
- α is the conservative flux convection coefficient.
- β is the convection coefficient.
- a is the absorption coefficient.
- γ is the conservative flux source term.
- f is the source term.

Let us assume that there are two solutes in the osmotic solution and therefore there are six independent variables that need to be considered. Assume:

$$\begin{aligned} u_1 &= \varepsilon^c C_{s1}^c \\ u_2 &= \varepsilon^f C_{s1}^f \\ u_3 &= \varepsilon^c C_{s2}^c \\ u_4 &= \varepsilon^f C_{s2}^f \\ u_5 &= \varepsilon^c \\ u_6 &= \varepsilon^f \end{aligned} \tag{8.14}$$

Then the coefficient matrices can be expressed as:

$$d_a = \begin{bmatrix} 1 & 0 & 0 & 0 & 0 & 0 \\ 0 & 1 & 0 & 0 & 0 & 0 \\ 0 & 0 & 1 & 0 & 0 & 0 \\ 0 & 0 & 0 & 1 & 0 & 0 \\ 0 & 0 & 0 & 0 & 1 & 0 \\ 0 & 0 & 0 & 0 & 0 & 1 \end{bmatrix} \tag{8.15}$$

$$c = \begin{bmatrix} \frac{D_{s1}^c}{u_5+u_6} & 0 & 0 & 0 & -\frac{D_{s1}^c \cdot \frac{u_1}{u_5}}{u_5+u_6} & 0 \\ 0 & \frac{D_{s1}^f}{u_5+u_6} & 0 & 0 & 0 & -\frac{D_{s1}^f \cdot \frac{u_2}{u_6}}{u_5+u_6} \\ 0 & 0 & \frac{D_{s2}^c}{u_5+u_6} & 0 & -\frac{D_{s2}^c \cdot \frac{u_3}{u_5}}{u_5+u_6} & 0 \\ 0 & 0 & 0 & \frac{D_{s2}^f}{u_5+u_6} & 0 & -\frac{D_{s2}^f \cdot \frac{u_4}{u_6}}{u_5+u_6} \\ 0 & 0 & 0 & 0 & 0 & 0 \\ 0 & 0 & 0 & 0 & 0 & 0 \end{bmatrix} \tag{8.16}$$

$$a = \begin{bmatrix} -V_x^c - V_y^c & 0\ 0 & 0\ 0 & 0\ 0 & 0\ 0 & 0\ 0 \\ 0\ 0 & -V_x^f - V_y^f & 0\ 0 & 0\ 0 & 0\ 0 & 0\ 0 \\ 0\ 0 & 0\ 0 & -V_x^c - V_y^c & 0\ 0 & 0\ 0 & 0\ 0 \\ 0\ 0 & 0\ 0 & 0\ 0 & -V_x^f - V_y^f & 0\ 0 & 0\ 0 \\ 0\ 0 & 0\ 0 & 0\ 0 & 0\ 0 & -V_x^c - V_y^c & 0\ 0 \\ 0\ 0 & 0\ 0 & 0\ 0 & 0\ 0 & 0\ 0 & -V_x^f - V_y^f \end{bmatrix} \tag{8.17}$$

$$f = \begin{bmatrix} \frac{S^c}{\Omega_0} J_{s1}^{fc} \\ -\frac{S^c}{\Omega_0} J_{s1}^{fc} \\ \frac{S^c}{\Omega_0} J_{s2}^{fc} \\ -\frac{S^c}{\Omega_0} J_{s2}^{fc} \\ \frac{S^c}{\Omega_0} J_0^{fc} \\ -\frac{S^c}{\Omega_0} J_0^{fc} \end{bmatrix} \tag{8.18}$$

$$\gamma = \mathrm{O} \tag{8.19}$$

$$\alpha = \mathrm{O} \tag{8.20}$$

$$\beta = \mathrm{O} \tag{8.21}$$

8.3 Numerical Results

To verify the extended two-dimensional mathematical model, two same series of data as used in chapter 7 are adopted again. They are the experimental results of potato tissue in mannitol solution (Stuart, 1973) and red beet root tissue in sucrose solution (Kohn & Dainty, 1966).

8.3.1 Case Study I: Potato Tissue in Mannitol Solution

As mentioned before, potato discs of 1.4×10^{-2} m in diameter and 1.0×10^{-3} m in thickness were used in Stuart (1973)'s experiment. Due to the symmetrical characteristics, a quarter of the disc is adopted to the two-dimensional analyses (see Fig. 8.1). The boundary conditions of this case for the two-dimensional analyses are the same as those used in chapter 6 (see Section 6.3) for the one-dimensional analyses. The only

difference is, for the two-dimensional case, there are two outer surfaces and two symmetrical planes and the boundary conditions will be applied to all these boundaries. That is:

- for the symmetric boundaries:

$$\left.\frac{\partial C_s^c}{\partial x}\right|_{x=0} = \left.\frac{\partial C_s^f}{\partial x}\right|_{x=0} = 0 \tag{8.22a}$$

$$\left.\frac{\partial C_s^c}{\partial y}\right|_{y=0} = \left.\frac{\partial C_s^f}{\partial y}\right|_{y=0} = 0 \tag{8.22b}$$

$$\left.\frac{\partial \varepsilon^c}{\partial x}\right|_{x=0} = \left.\frac{\partial \varepsilon^f}{\partial x}\right|_{x=0} = 0 \tag{8.23a}$$

$$\left.\frac{\partial \varepsilon^c}{\partial y}\right|_{y=0} = \left.\frac{\partial \varepsilon^f}{\partial y}\right|_{y=0} = 0 \tag{8.23b}$$

- for the boundaries attached to the external solution:

$$C_s^c\big|_{Surface} = C_s^f\big|_{Surface} = C_s^l \tag{8.24}$$

$$\varepsilon^c\,|_{Surface} = const. \tag{8.25}$$

$$\varepsilon^f\,|_{Surface} = const. \tag{8.26}$$

where $C_s^c\big|_{Surface}$ and $C_s^f\big|_{Surface}$ are the concentrations on the surfaces of intracellular and extra-cellular volumes, C_s^l is the concentration in external solution, $\varepsilon^c\,|_{Surface}$ and $\varepsilon^f\,|_{Surface}$ are the intracellular and extra-cellular volumes on the surfaces, respectively.

All the parameters for the case study I are the same as those used in chapter 7 (see Table 7.3), so they are not introduced here again.

8.3.1.1 Concentrations in Intracellular and Extra-cellular Volumes

Fig. 8.2 and Fig. 8.3 show the concentration distribution profiles of one solute in intracellular volume and extra-cellular volume at different times (t=0, 10, 20, 30, 40 minutes) respectively. The evolution of concentrations in both intracellular and extra-cellular volumes can be seen generally. With the increase of the treatment time, in each cross-section, the value of concentration is getting bigger and bigger. For the same location, the concentration is higher in the extra-cellular volume than in the intracellular volume due to the higher solute diffusion coefficient in the extra-cellular volume than the diffusion coefficient in the intracellular volume. For both intracellular and extra-cellular volumes, in each cross-section, the concentration significantly reduces from the boundaries to the centers (symmetrical planes). The solute diffuses more quickly in the y-direction than in the x-direction due to the concentration gradient in the y-direction is higher than that in the x-direction. Fig. 8.4 shows the concentration distribution profiles of one solute in extra-cellular volume after 30 minutes treatment. The concentration in each cross-section in extra-cellular volume can be seen more clearly from this figure.

8.3.1.2 Hydrostatic Pressures in Intracellular and Extra-cellular Volume

Fig. 8.5 and Fig. 8.7 show the distribution profiles of hydrostatic pressures in the intracellular and extra-cellular volumes at different times (t=0, 10, 20, 30, 40 minutes), respectively. It can be noticed that the distributions of hydrostatic pressures in the intracellular and extra-cellular volumes are quite different. The hydrostatic pressure in the intracellular volumes gets its maximum value when the tissue is under the full turgor (at time t=0), afterwards it reduces with the increased time. At the same time, the hydrostatic pressure in intracellular volume reduces most at the surfaces and least in the centre (symmetrical planes). However, the hydrostatic pressure in the extra-cellular

volume increases slightly with time. At the same time, the hydrostatic pressure in extra-cellular volume increases most at the surface and least in the centre (symmetrical planes). This is mainly because the elastic modulus of the extra-cellular volume is much smaller than that of the cell wall and cell membrane. Fig. 8.6 and Fig. 8.8 show the distribution profiles of hydrostatic pressures in the intracellular and extra-cellular volumes after 30 minutes' treatment. It shows that, from outer boundaries to the centers, the hydrostatic pressure in intracellular volume decreases generally. However, the hydrostatic pressure in extra-cellular volume increases slightly to a higher value and decreases slowly from the boundaries to the centers. In a certain zone close to the two outer boundaries, the hydrostatic pressure in extra-cellular volume reaches to its peak value. This is the result of combination effect of the osmotic dehydration from both x- and y-directions.

8.3.1.3 Intracellular and Extra-cellular Volumes

As has been introduced in chapter 7 (Section 7.2.2), the concentration difference between the intracellular and extra-cellular volumes creates a chemical potential difference across the cell membrane between the two volumes, which drives water to flow from the intracellular volume into the extra-cellular volume. As a result, the intracellular volume will decrease whereas the extra-cellular volume increases. Fig. 8.9 and Fig. 8.10 show the evolution of the intracellular and extra-cellular volumes at different times (t=0, 10, 20, 30, 40 minutes), respectively. It can be seen that, with the increase of the treatment time, the intracellular volume decreases significantly whereas the extra-cellular volume increases slightly. Figs. 8.11 – 8.14 shows the evolution of the intracellular volume and extra-cellular volume at one cross-section of x-direction and y-direction at three different times (t=10, 20, 40 minutes). Fig. 8.15 and Fig. 8.16 show the evolution of total volume at one cross-section of x-direction and y-direction at three different times (t=10, 20, 40 minutes), respectively. These figures describe that the intracellular volume decreases rapidly and the extra-cellular volume increases slightly

with the time. In any cross-section, both intracellular volume and extra-cellular volume change more slowly in x-direction than in y-direction because the size of tissue in x-direction is much bigger than that in y-direction. Note that, the peak value of the extra-cellular volume is found to locate at a place close to the outer boundary in y-direction (see Fig. 8.13). This is the results of the combination effect of osmotic dehydration from both x- and y-directions. Fig. 8.17 shows the evolution of the total volume at different times (t=0, 10, 20, 30, 40 minutes). From this figure, the total volume change in both directions at different treatment times can be seen generally. Fig. 8.18 shows the comparison of total volume reduction of potato tissue after three different time treatments (t=8, 24 and 40 minutes) obtained by one-dimensional and two-dimensional numerical simulations. The cross-section in y-direction is adopted as $x=3.5\times10^{-3}$ m. It can be seen that the results obtained by one-dimensional and two-dimensional analyses are quite similar.

8.3.1.4 Common Geometric Tissue Structure Analyses

The common geometric structure of potato tissue is simulated to test the model because the disc size in the experiments of Stuart (1973) is very special (the diameter of the tissue structure is over 10 times the thickness) and may not be reasonable to explain the common geometric tissue structures. The plant tissue sample is assumed to be 7.0×10^{-3} m in diameter and 5.0×10^{-3} m in thickness and is immerged in the solution with one solute. All the parameters used in this analysis are exactly the same as those used in thin slab structure (see Table 7.3). Therefore, they will not be introduced here again.

Because the total volume of the tissue is reduced during the whole osmotic dehydration process, shrinkage phenomena will be shown in the process. Figs. 8.19 – 8.23 show the shrinkage phenomena of the tissue sample at different times (t=1, 2, 3, 4, 5 hours) separately. As we know, the initial volume is considered as 1.0 in the whole tissue sample. It can be seen that the shrinkage phenomena occur when the osmotic

dehydration starts; with the increase of the treatment time, more and more zones of the tissue shrink and shrinkage phenomena happen in the boundary firstly and move to the centre gradually. Many ellipses are shown in these figures because the shrinkage phenomena occur in all directions. Fig. 8.24 is the combination of Figs. 8.19 – 8.23. The shrinkage phenomena of the tissue sample at different times (t=1, 2, 3, 4, 5 hours) are shown in this figure, from which the evolution of the shrinkage of the tissue can be seen clearly. The changes of intracellular and extra-cellular volumes of the tissue in different times (t=1, 2, 3, 4, 5 hours) are illustrated in Fig. 8.25 and Fig. 8.26 which make the shrinkage phenomena seen more clearly and completely. Fig. 8.27 – 8.31 are the contour analyses of shrinkage phenomena of the tissue sample at separately different times (t=1, 2, 3, 4, 5 hours). The whole shrinkage phenomena can be seen and the value of total volume in each treatment time can be obtained from these figures. Fig. 8.32 is the comparison of total volume reduction of potato tissue between the simulations from the mathematical model 2 (1D, 2D thin slab, 2D rectangular) and the experimental results reported by Stuart (1973). It can be seen that the results obtained by 1D and 2D (thin slab structure) are close to the reported experimental data. The results obtained by 2D (thin slab structure) are slightly bigger than those obtained by 1D analyses. This is because the osmotic dehydration will happen in x-direction as well as in y-direction, although the cross-section area normal to x-axis is much smaller than that normal to y-axis. With the same treatment time, the reduction ratio of total tissue volume obtained by 2D (rectangular structure) analyses is much less than those obtained by 1D and 2D (thin slab structure). This is because the size of the rectangular structure is much bigger than that of thin slab structure (5 times), although the osmotic dehydration happened in both x- and y-directions is considered.

8.3.2 Case Study II: Red Beet Root Tissue in Sucrose Solution

Another set of experimental data based on Kohn and Dainty (1966)'s measurement on red beet root discs is adopted in order to further demonstrate the two-dimensional

analyses. All the experimental data and model parameters used in this simulation are exactly the same as those used in one-dimensional analyses which have been introduced in chapter 7 (see Table 7.4), and the boundaries conditions for both symmetric boundaries and outer surfaces are also the same as those introduced in case study I (see Section 8.3.1 in this chapter), so they will not be presented here again.

Figs. 8.33 - 8.35 simulate the evolutions of the total volume, the intracellular volume and the extra-cellular volume of red beet root tissue at different times (t=0, 10, 20 and 30 minutes), respectively. Figs. 8.36 shows the distribution profiles of total volume at time t=30 minutes. From these figures, the similar images can be seen as obtained in case study I in this chapter. The concentrations and hydrostatic pressures in intracellular and extra-cellular volumes can be also obtained by the two-dimensional analyses. Considering all these results are much similar to those shown in case study I, they are not illustrated and explained here again. Fig. 8.37 shows the comparison of total volume reduction of red beet root tissue after three different time treatments (t=10, 20 and 30 minutes) obtained by one-dimensional and two-dimensional numerical simulations. The cross-section in y-direction is adopted as $x=2.0\times10^{-3}$ m. It can be seen that the results obtained by one-dimensional and two-dimensional analyses (thin slab structure) are close.

Case study II is also extended to the common geometric structure. The tissue is assumed as 7.0×10^{-3} m in diameter and 5.0×10^{-3} m in thickness which is the same as the dimensions used in case study I for the common geometric tissue structure. The parameters used here are exactly the same as those used for the thin slab structure analyses. The pattern images are found to be much similar to those in case study I, so that they are not illustrated here again. Fig. 8.38 shows the total volume reduction of the tissue sample at different times. The evolution of the shrinkage of the tissue can be seen clearly from this figure. The comparison of total volume reduction of red beet root tissue between the simulations from the mathematical model 2 (1D, 2D thin slab, 2D rectangular) and the experimental results reported by Kohn and Dainty (1966) is shown

in Fig. 8.39. The results obtained by 1D and 2D (thin slab structure) are found to well fit with the experimental data. The total volume reduction of the tissue obtained by 2D (thin slab structure) is slightly bigger than that obtained by 1D analyses. With the same treatment time, the reduction ratio of total tissue volume obtained by 2D (rectangular structure) analyses is much less than those obtained by 1D and 2D (thin slab structure) analyses. This is again due to the thickness of 2D model is much greater than that of 1D model.

8.4 Summary

In this chapter the mass transport mathematical model two presented in chapter 6 and chapter 7 has been extended to analyze the two-dimensional problems. The concentrations and hydrostatic pressures in intracellular and extra-cellular volumes in both x-direction and y-direction and the total volumes at different treatment times are simulated and discussed. The shrinkage phenomena in different treatment times are also shown and analyzed in this chapter.

Two sets of previous used experimental data are employed again to verify the extension of the mathematical model two. The results are reasonable by comparing with the one-dimensional data obtained in chapter 7 and the original experimental data for the thin slab tissue samples.

Both sets of data and parameters are employed again to analyze the common geometric tissue structure. The results obtained by one-dimensional, two-dimensional (both thin slab structure and rectangular structure) and the original experimental data are compared. It shows that the results obtained by 2D (thin slab structure) are slightly bigger than those obtained by 1D analyses due to the combination effect of osmotic dehydration in both x- and y- directions.

Therefore, it can conclude that the two-dimensional model developed here is reliable. The numerical examples shown in this chapter also demonstrated that the two-dimensional model can handle more general osmotic dehydration problems which existing one-dimensional models cannot.

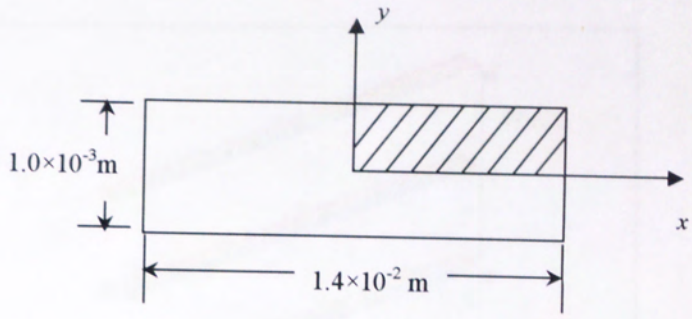

Figure 8.1 A sample of potato tissue (a quarter of disc is used in this model)

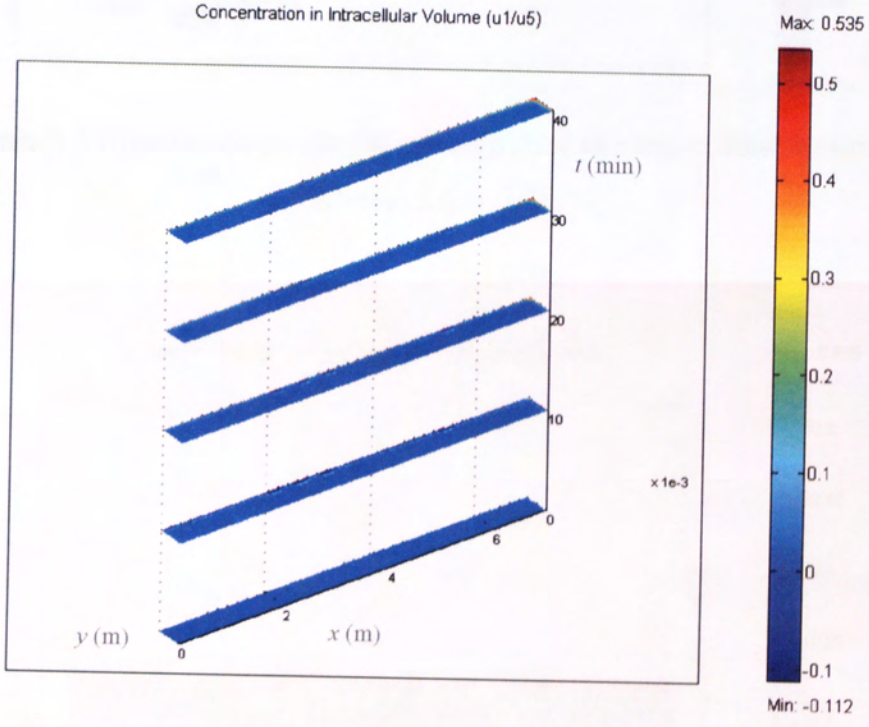

Figure 8.2 Distribution profiles of concentration in intracellular volume at different times (mins)

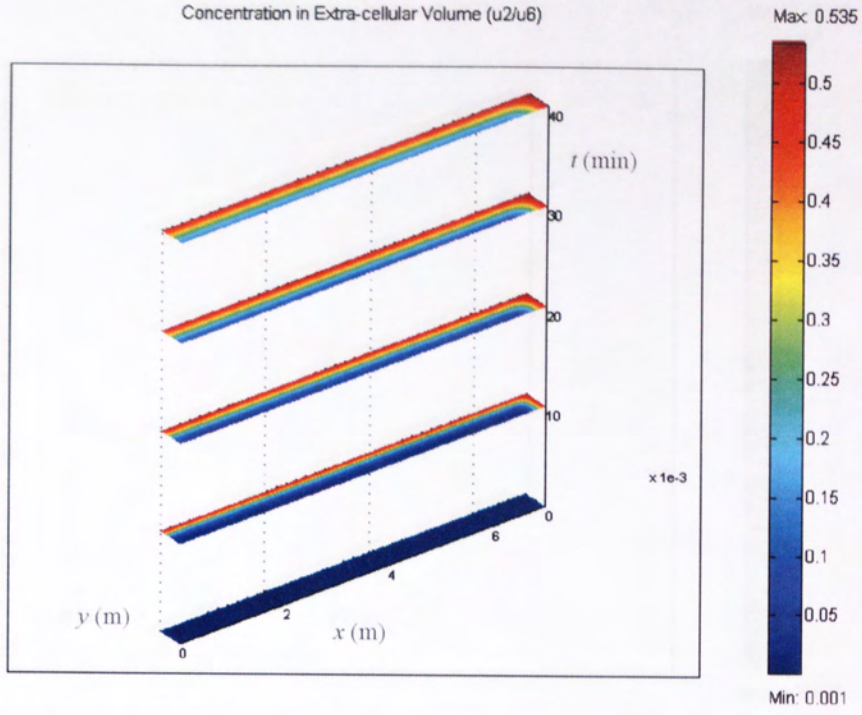

Figure 8.3 Distribution profiles of concentration in extra-cellular volume at different times (mins)

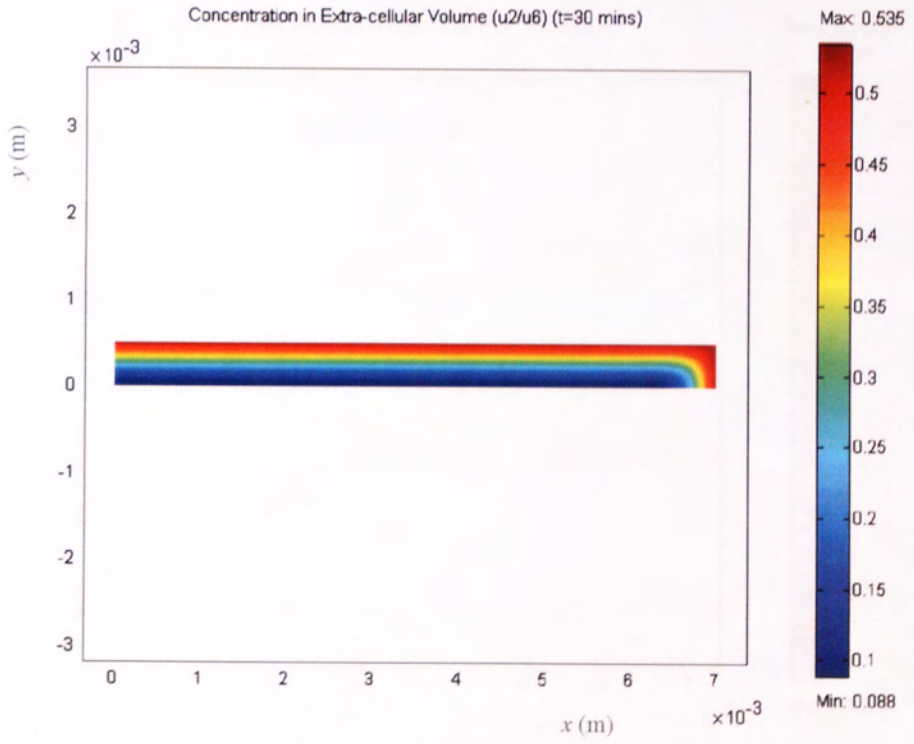

Figure 8.4 Distribution profiles of concentration in extra-cellular volume at time t=30 (mins)

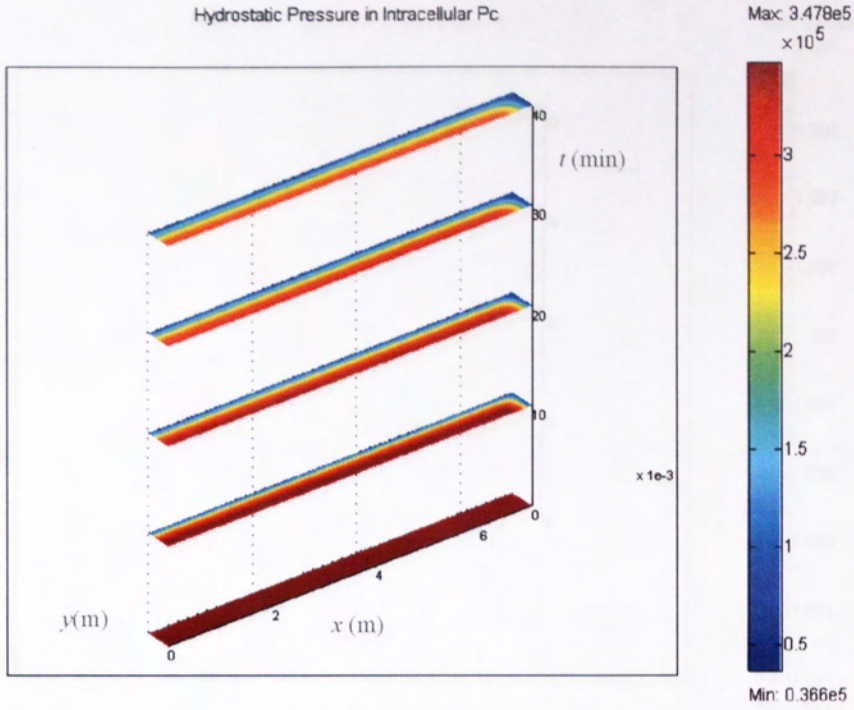

Figure 8.5 Distribution profiles of hydrostatic pressure in intracellular volume at different times (mins)

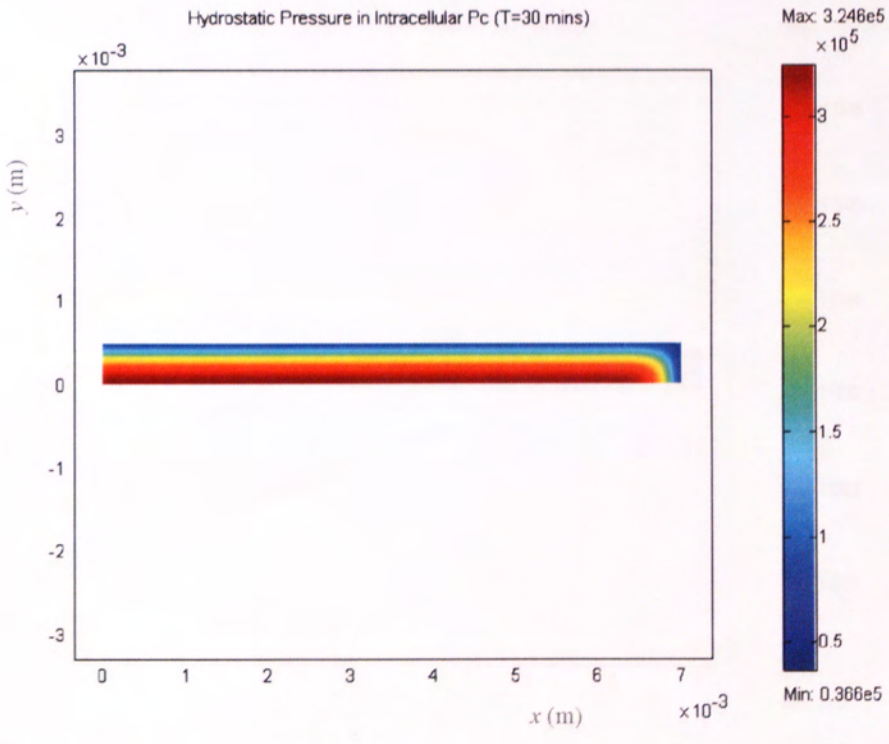

Figure 8.6 Distribution profiles of hydrostatic pressure in intracellular volume at time t=30 (mins)

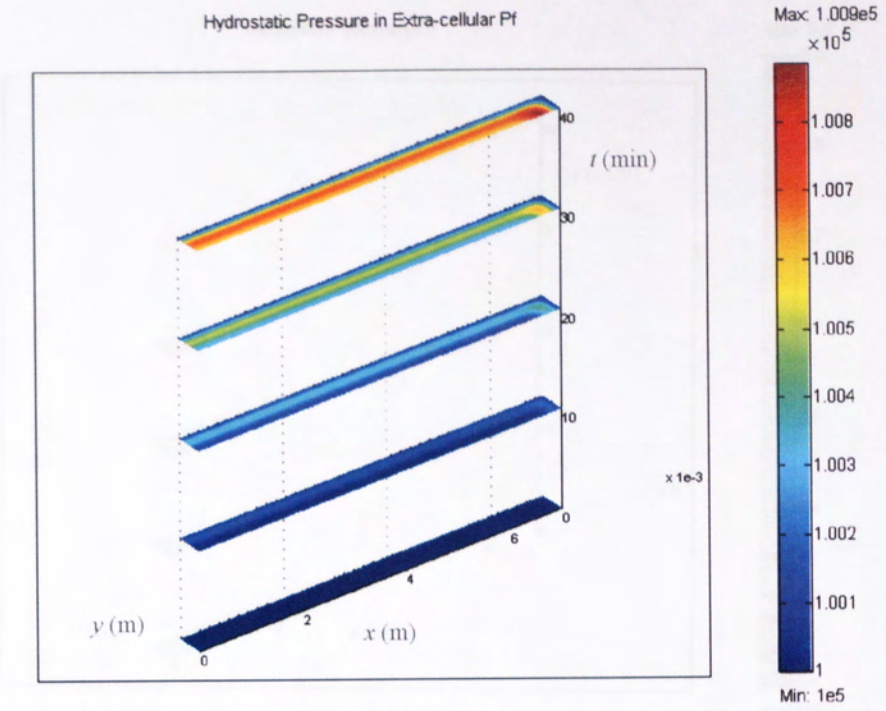

Figure 8.7 Distribution profiles of hydrostatic pressure in extra-cellular volume at different times (mins)

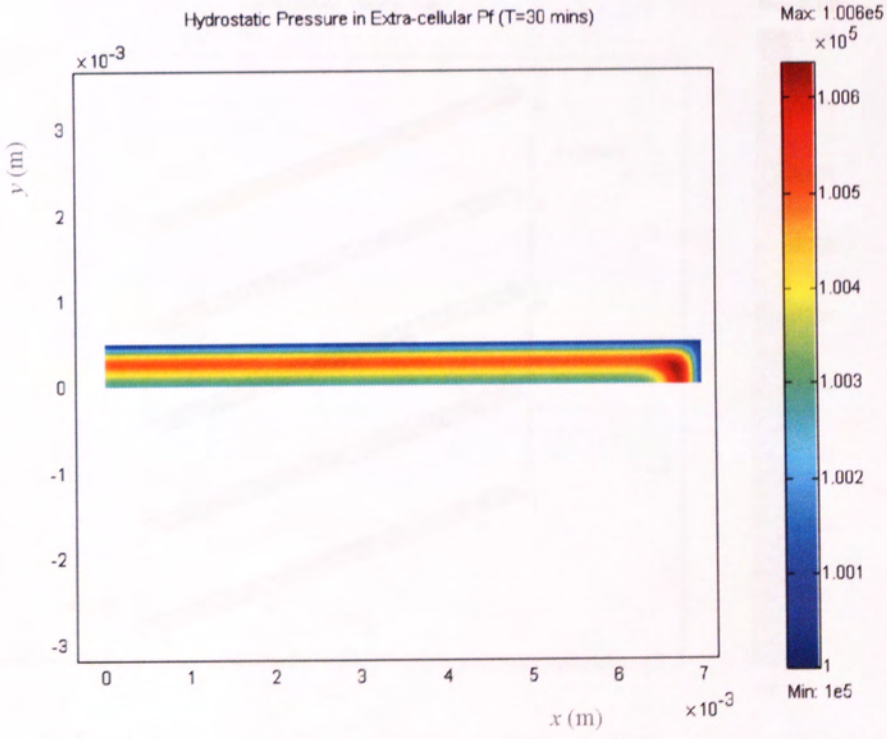

Figure 8.8 Distribution profiles of hydrostatic pressure in extra-cellular volume at time t=30 (mins)

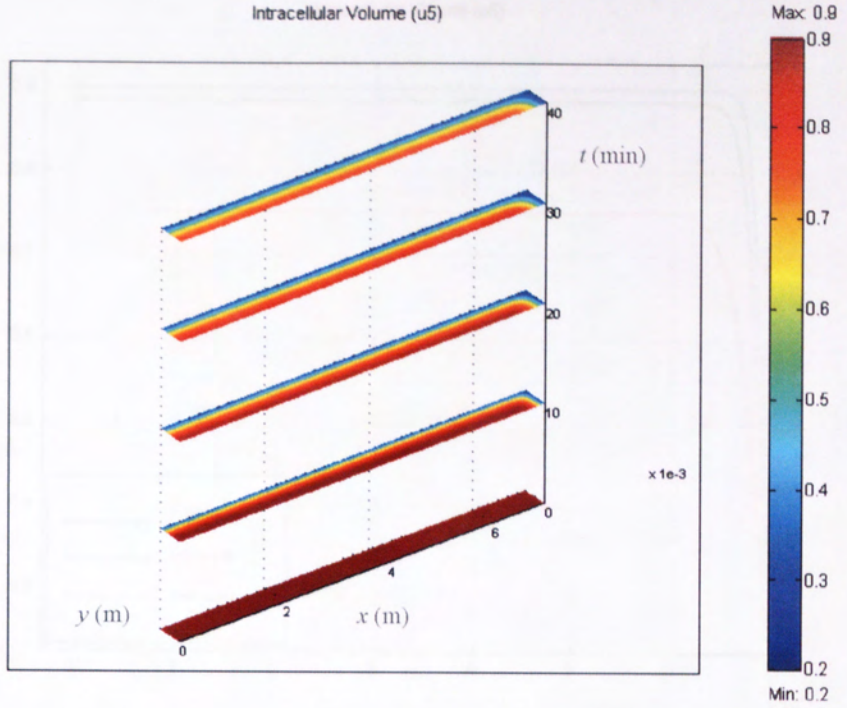

Figure 8.9 Evolution of the intracellular volume at different times (mins)

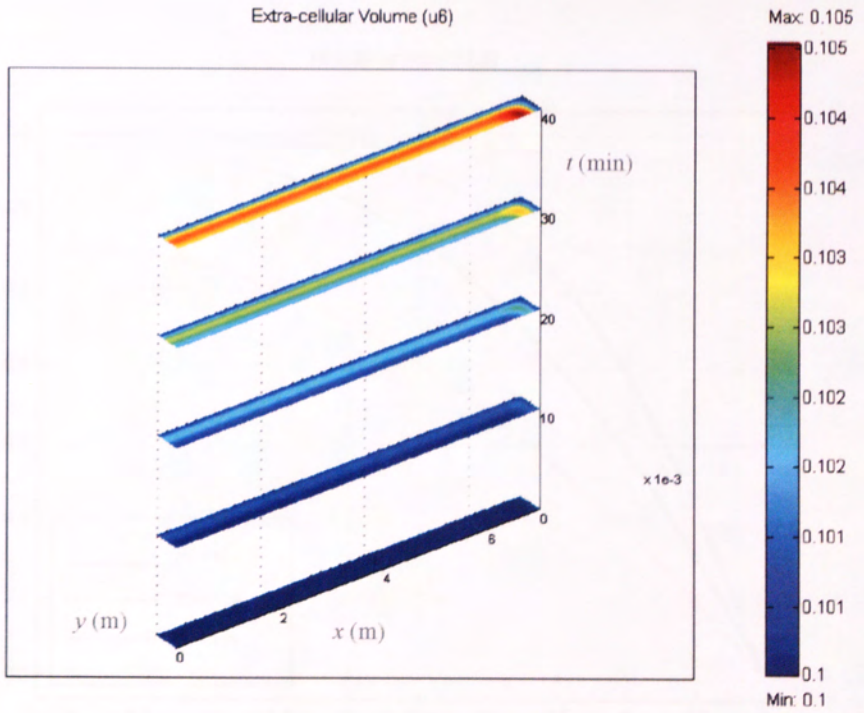

Figure 8.10 Evolution of the extra-cellular volume at different times (mins)

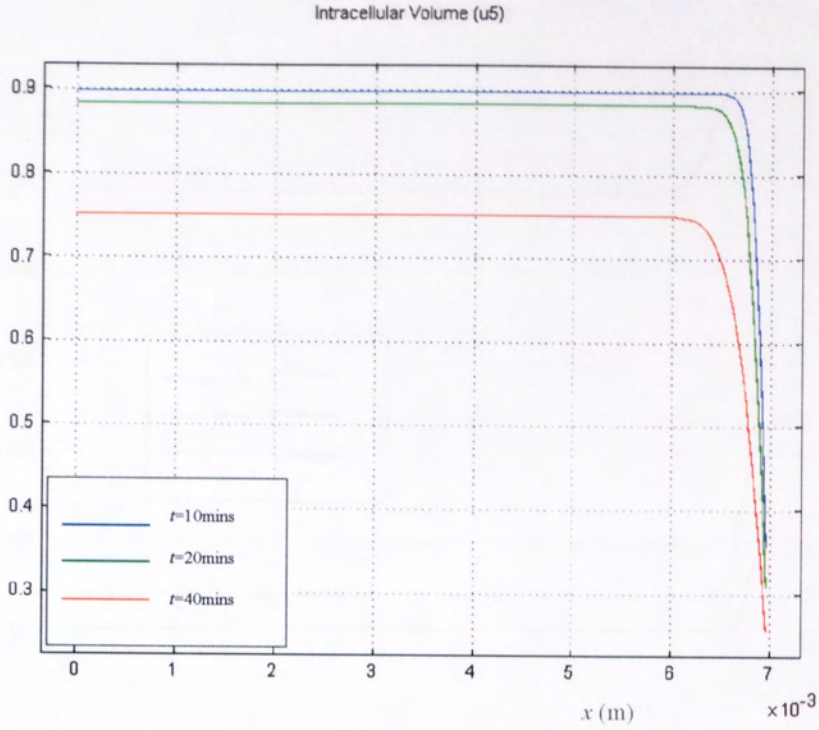

Figure 8.11 Evolution of the intracellular volume at one cross-section of x-direction at different times

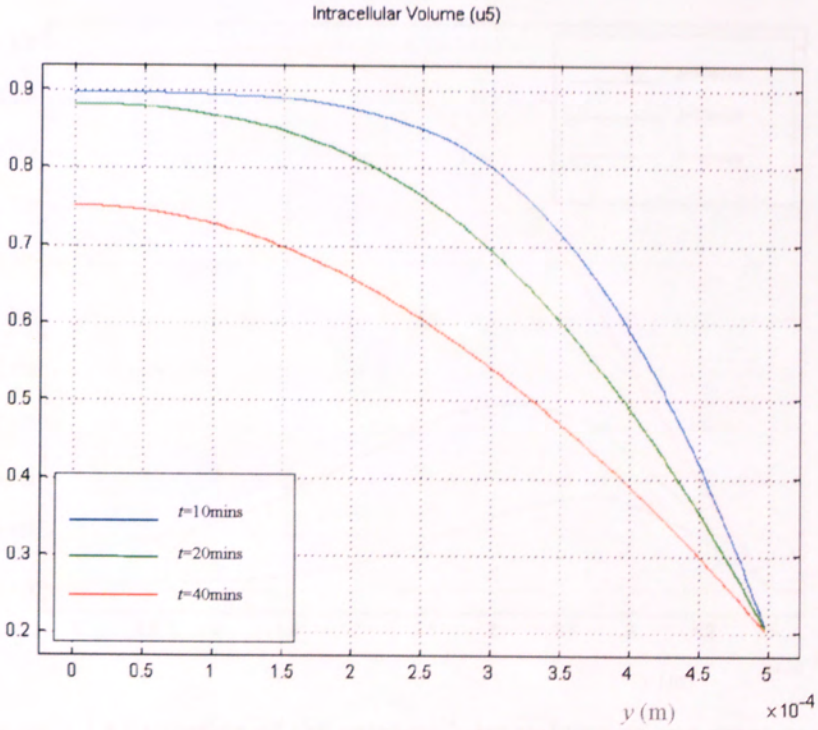

Figure 8.12 Evolution of the intracellular volume at one cross-section of y-direction at different times

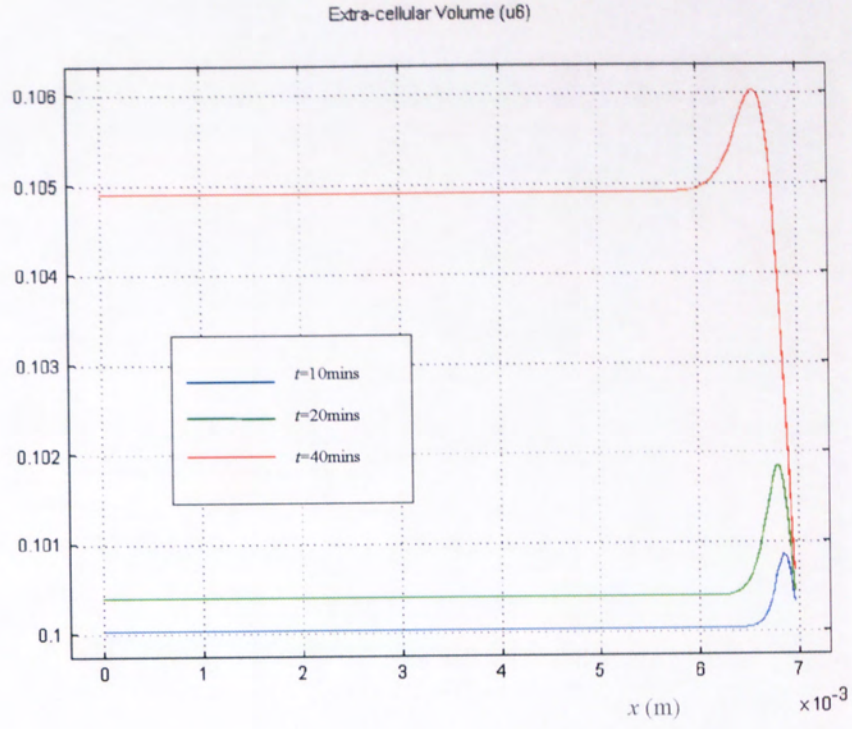

Figure 8.13 Evolution of the extra-cellular volume at one cross-section of x-direction at different times

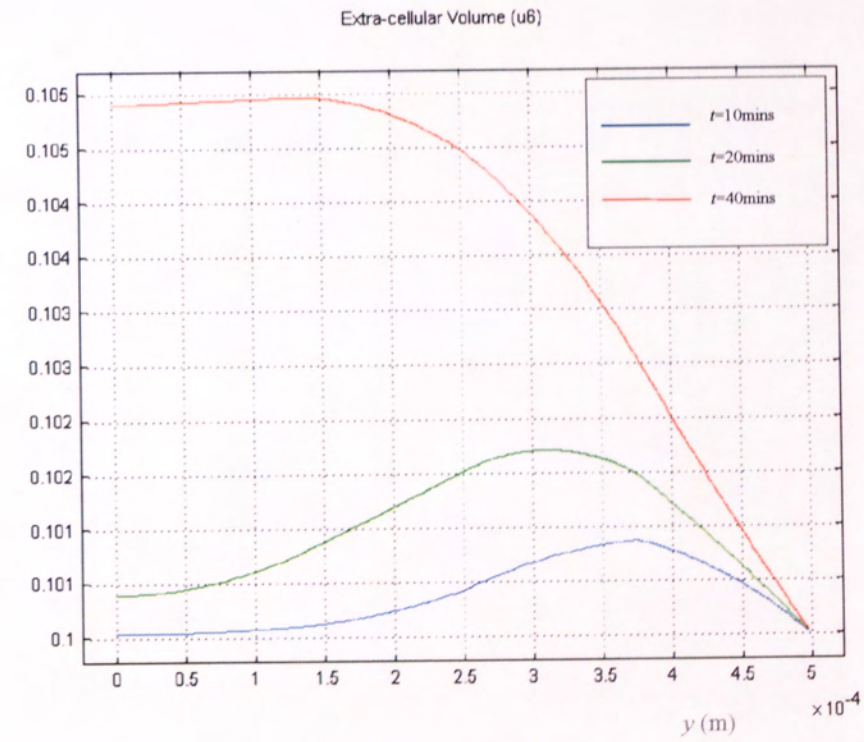

Figure 8.14 Evolution of the extra-cellular volume at one cross-section of y-direction at different times

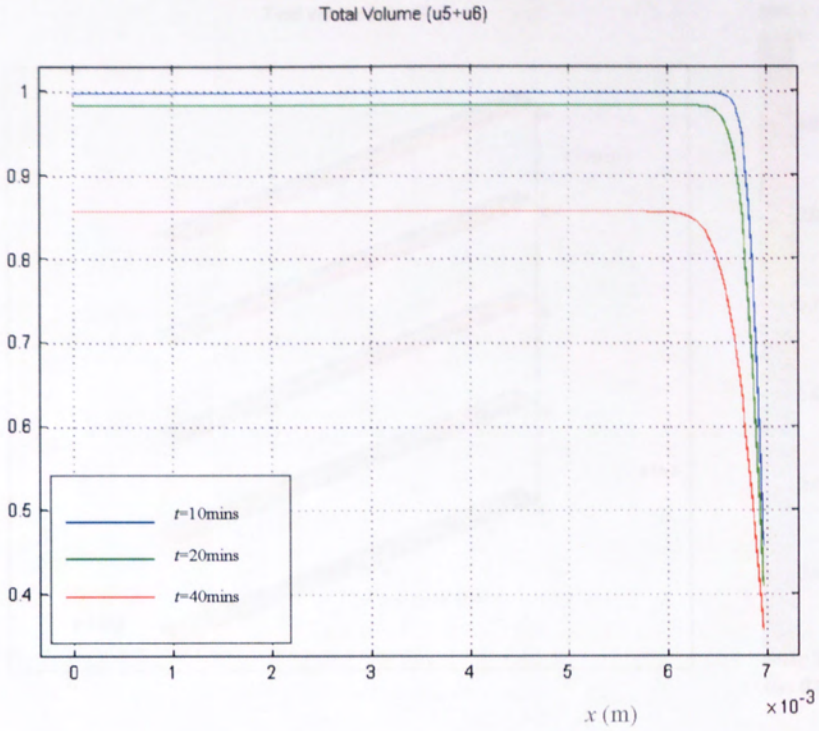

Figure 8.15 Evolution of the total volume at one cross-section of x-direction at different times

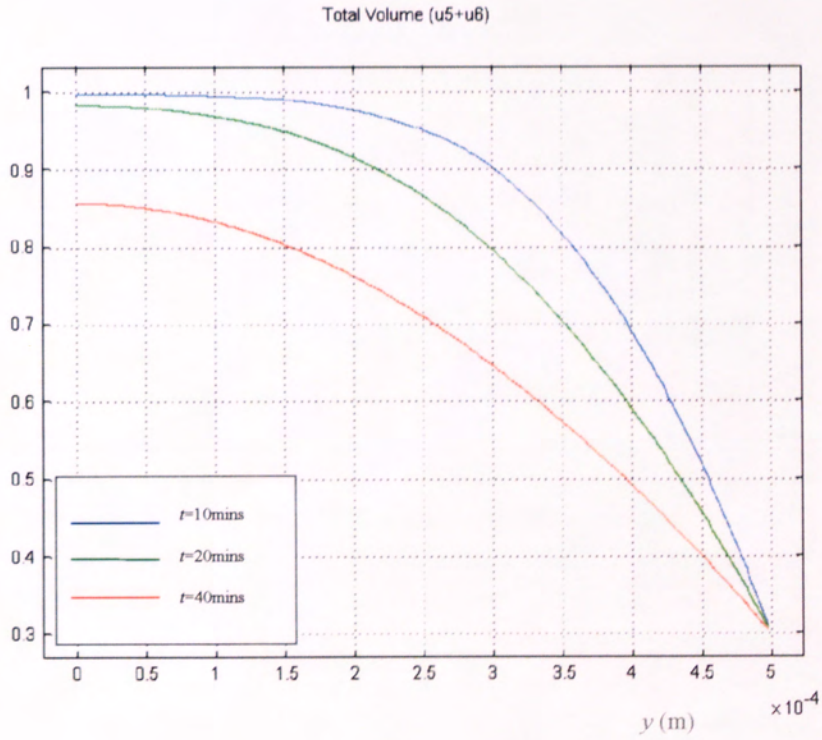

Figure 8.16 Evolution of the total volume at one cross-section in y-direction at different times

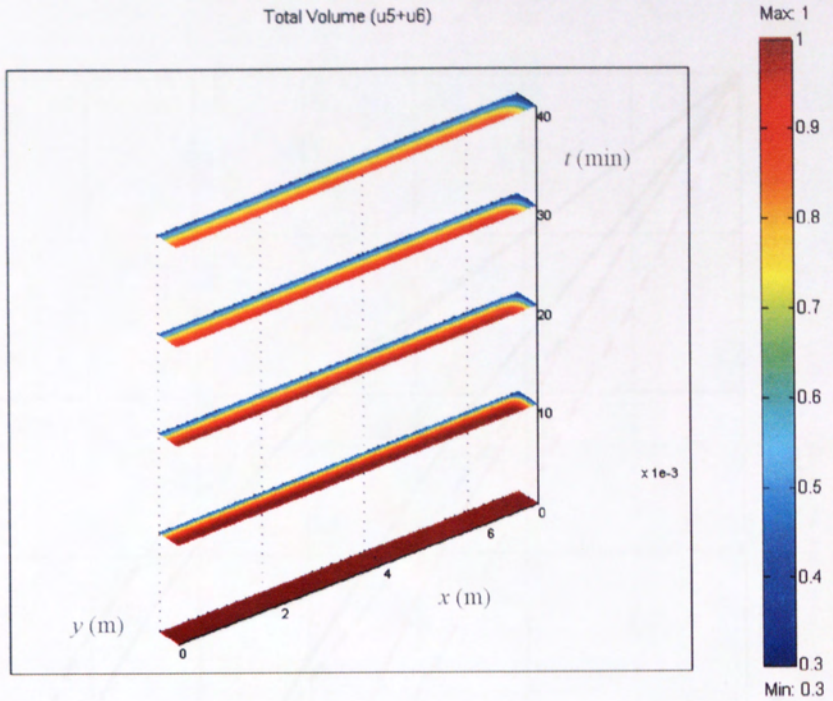

Figure 8.17 Evolution of the total volume at different times (mins)

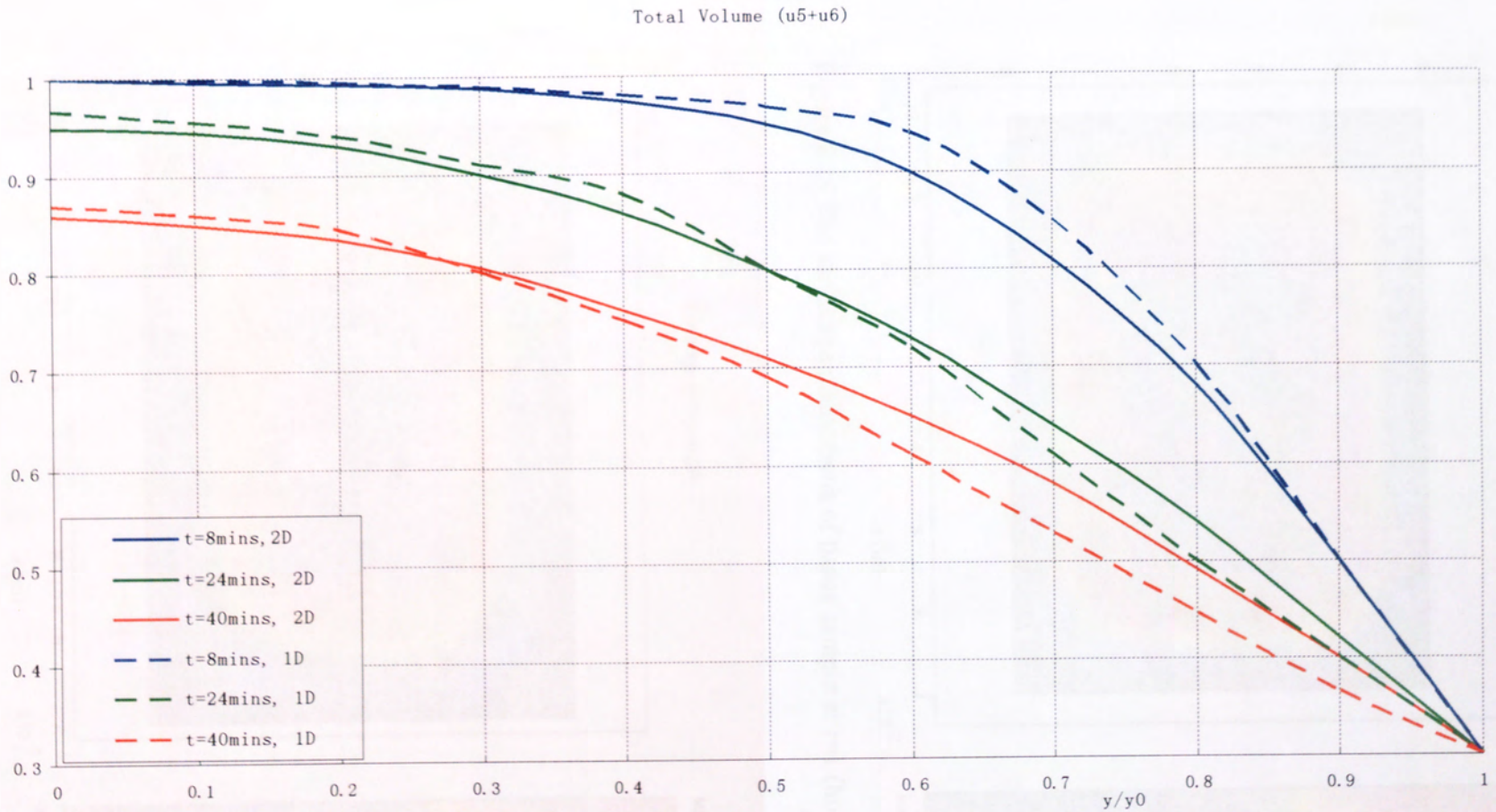

Figure 8.18 Comparison of the total volume of potato tissue at one cross-section in *y*-direction by 1D and 2D (thin slab) analyses

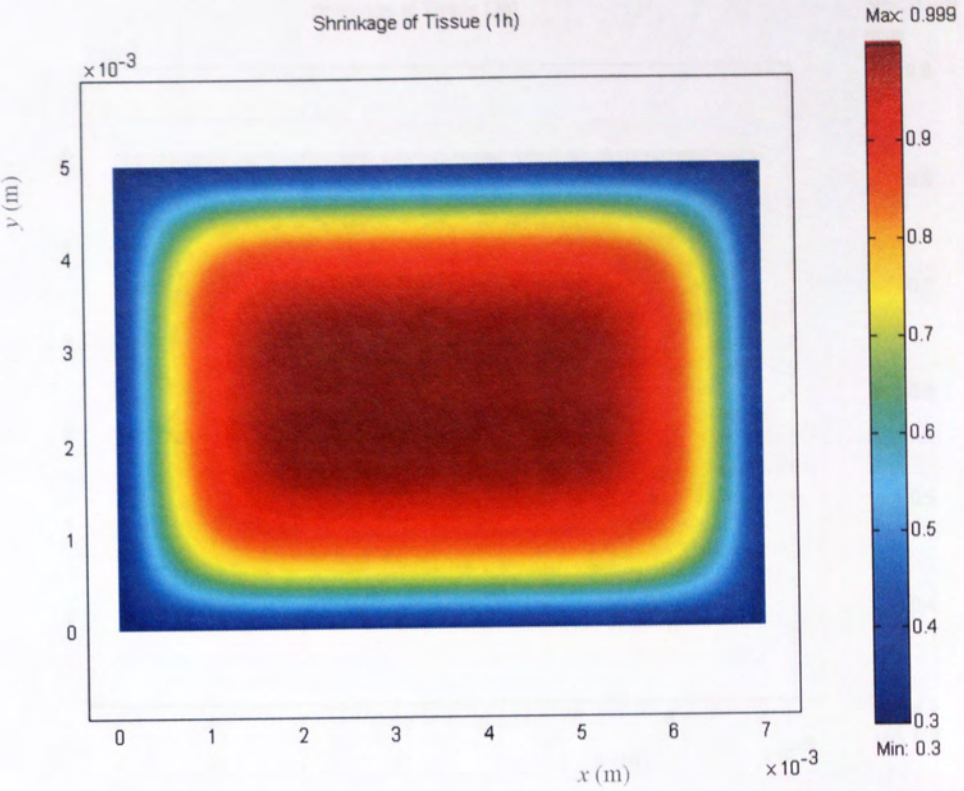

Figure 8.19 The shrinkage phenomena of tissue sample at t=1 (hour)

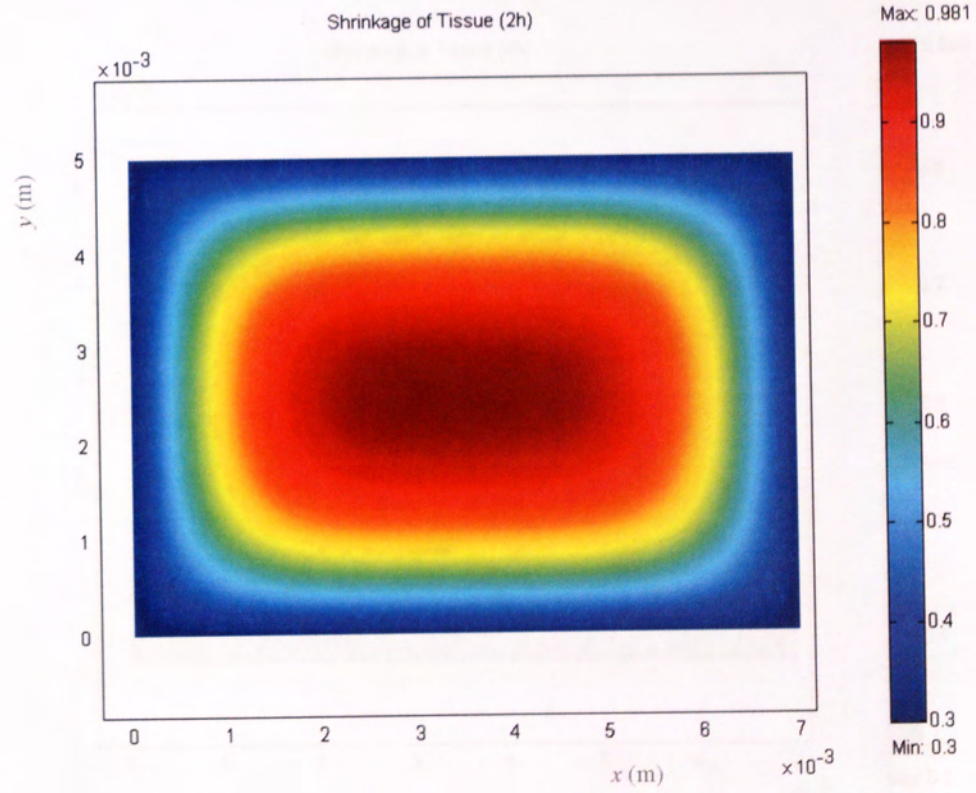

Figure 8.20 The shrinkage phenomena of tissue sample at t=2 (hours)

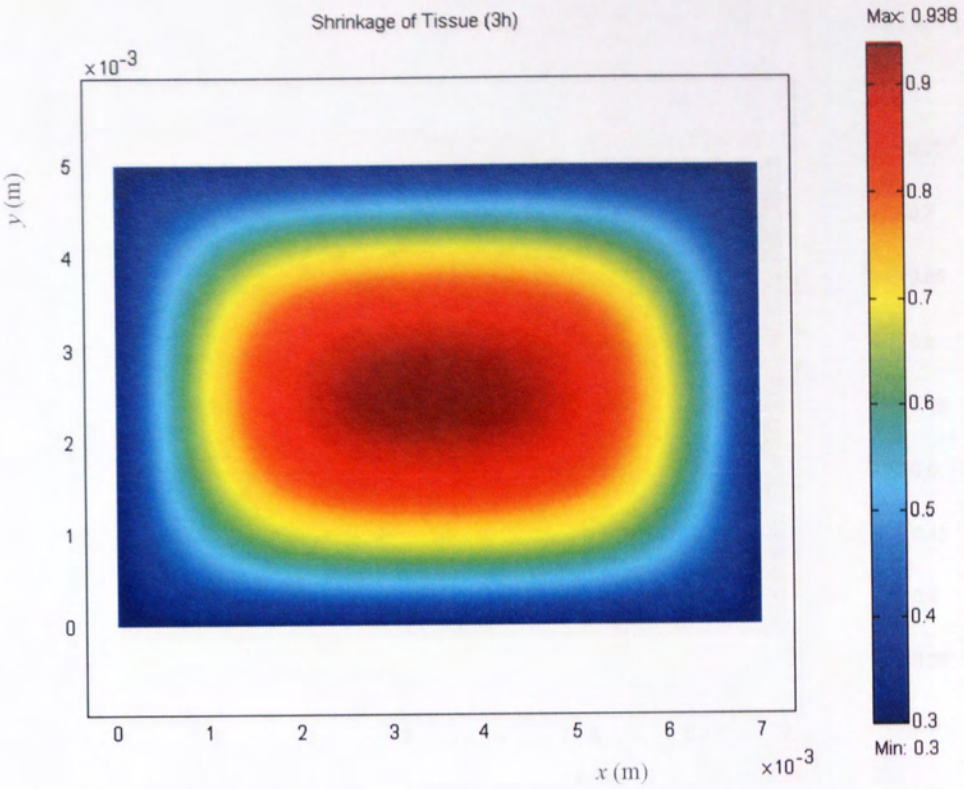

Figure 8.21 The shrinkage phenomena of tissue sample at t=3 (hours)

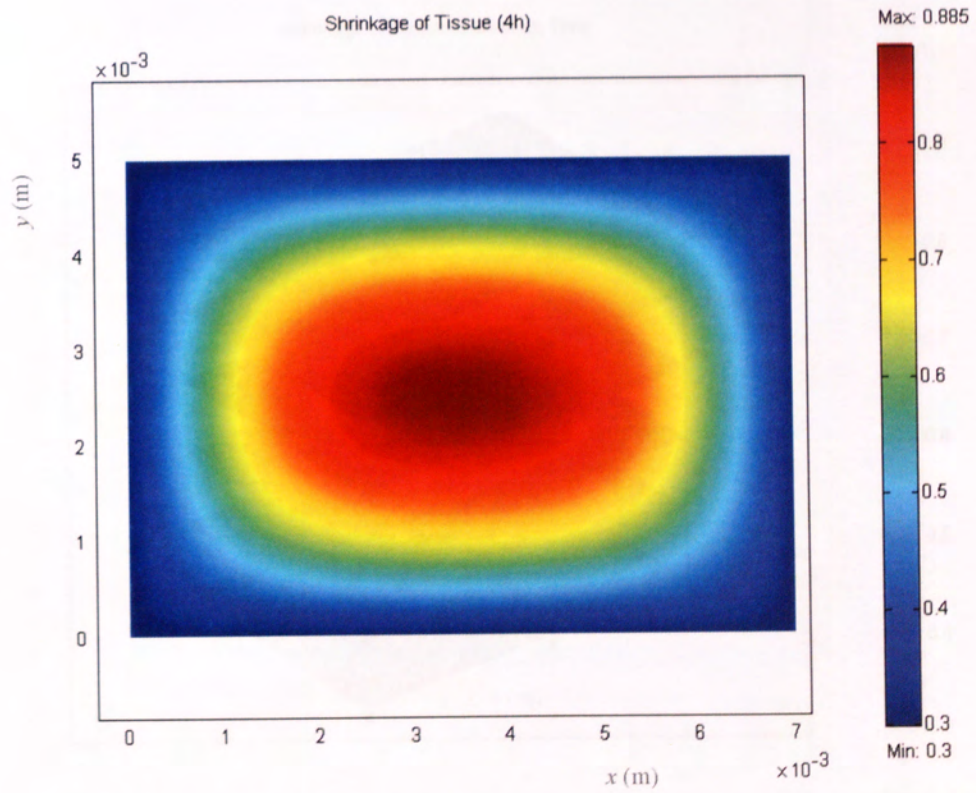

Figure 8.22 The shrinkage phenomena of tissue sample at t=4 (hours)

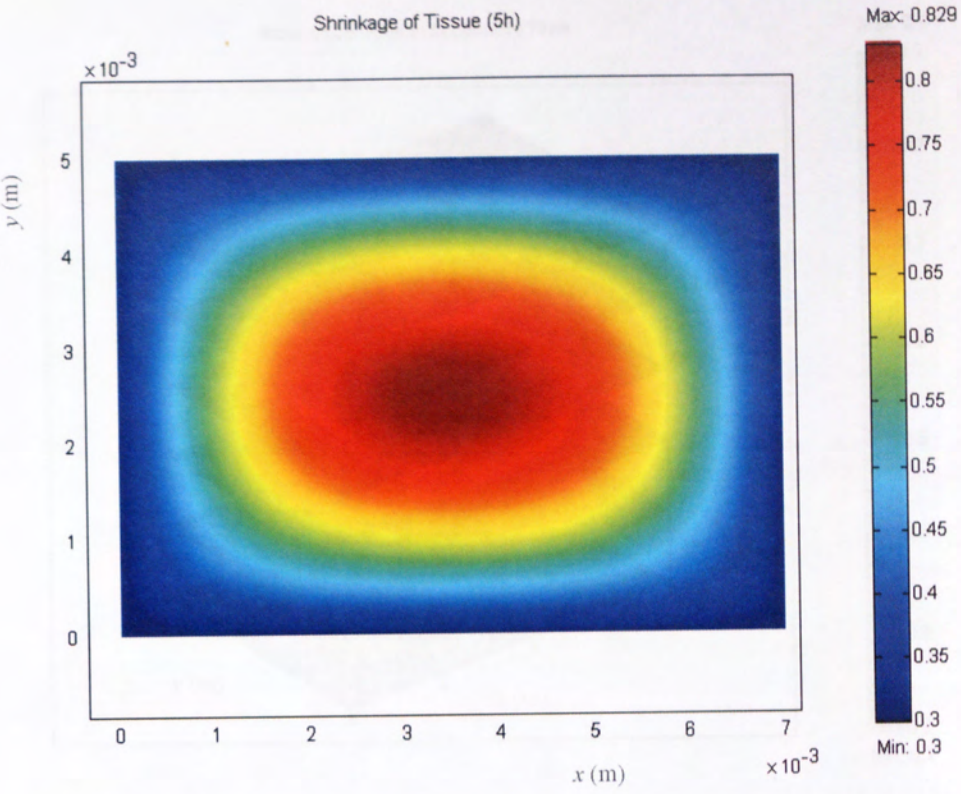

Figure 8.23 The shrinkage phenomena of tissue sample at t=5 (hours)

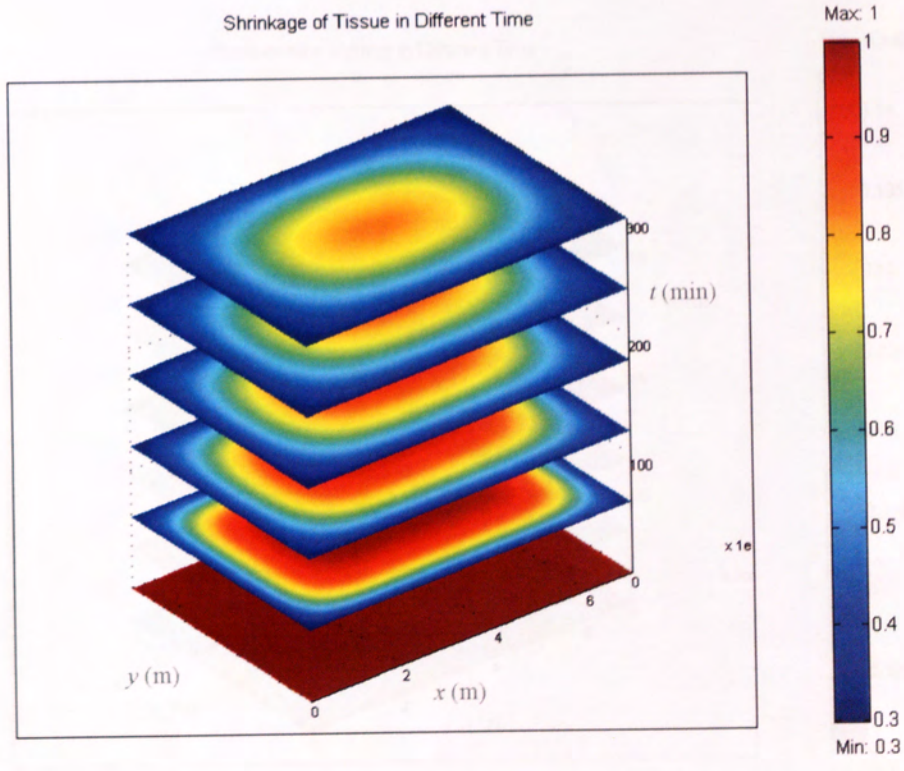

Figure 8.24 The shrinkage phenomena of tissue sample at different times (mins)

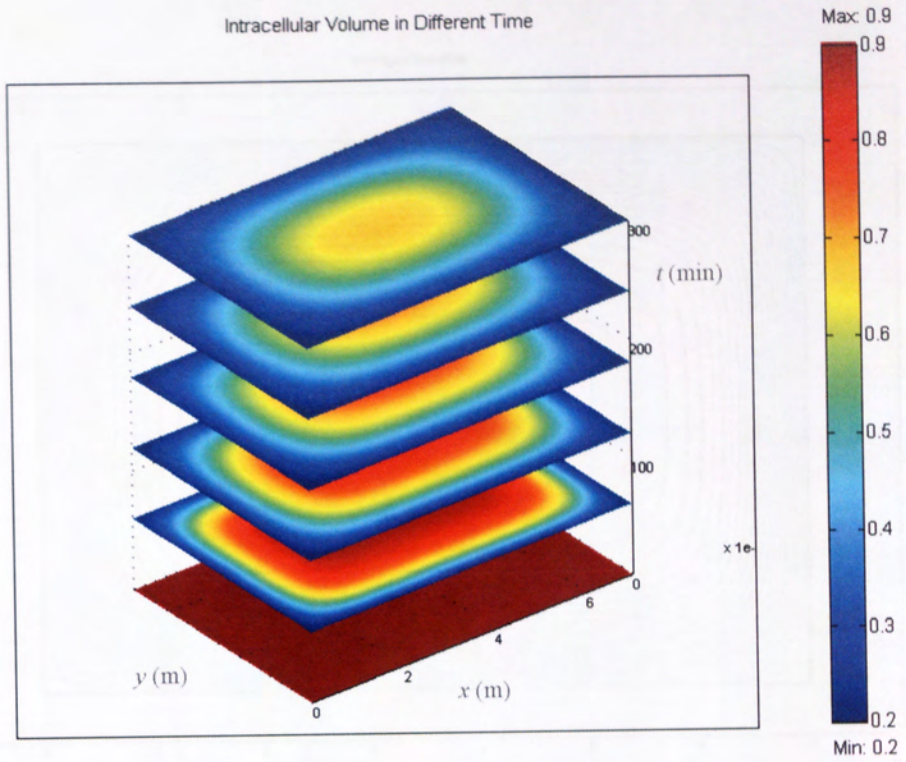

Figure 8.25 The change of intracellular volume at different times

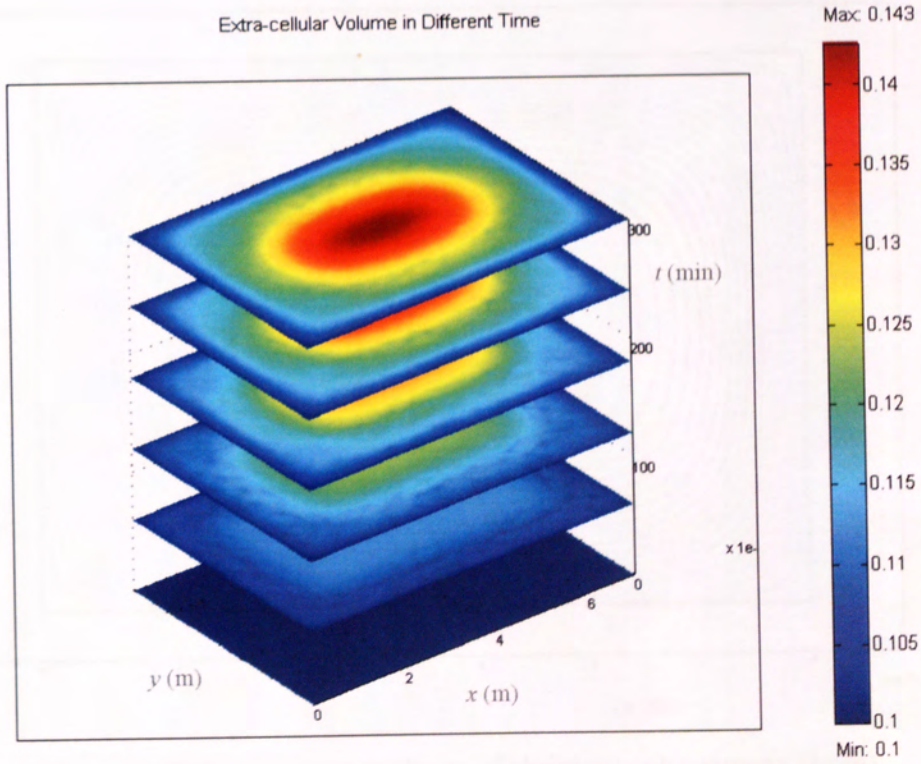

Figure 8.26 The change of extra-cellular volume at different times

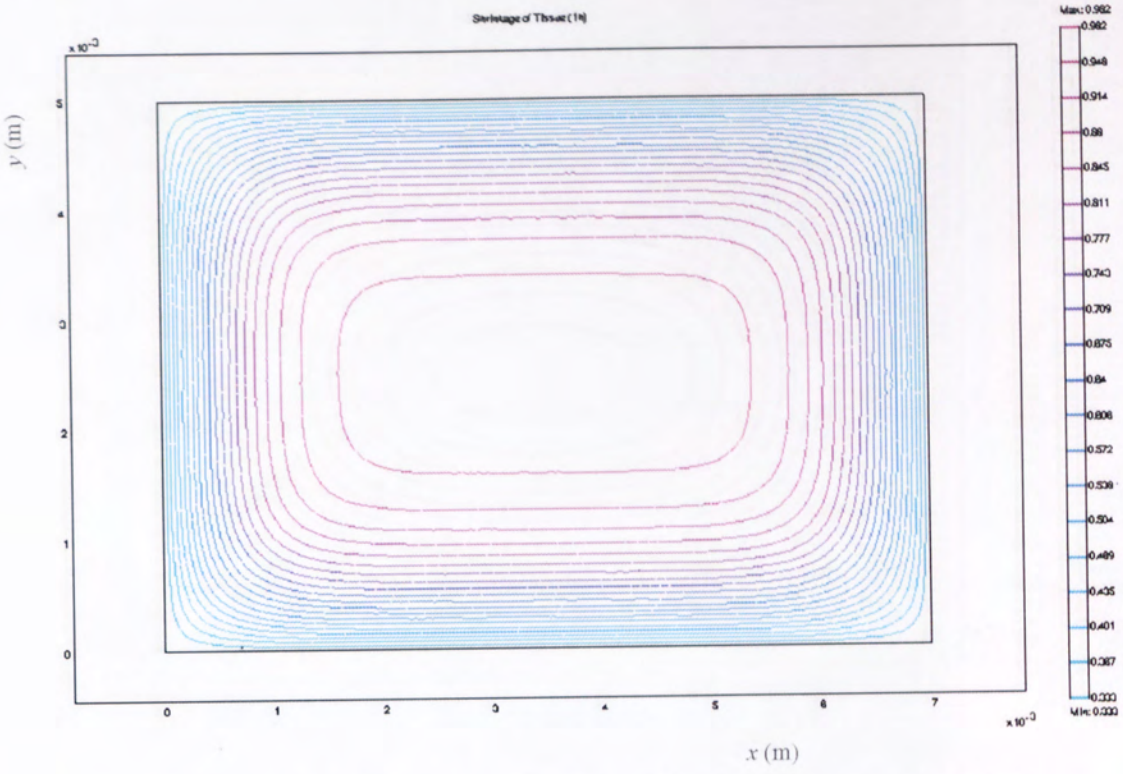

Figure 8.27 The contour analyses of shrinkage phenomena (t=1h)

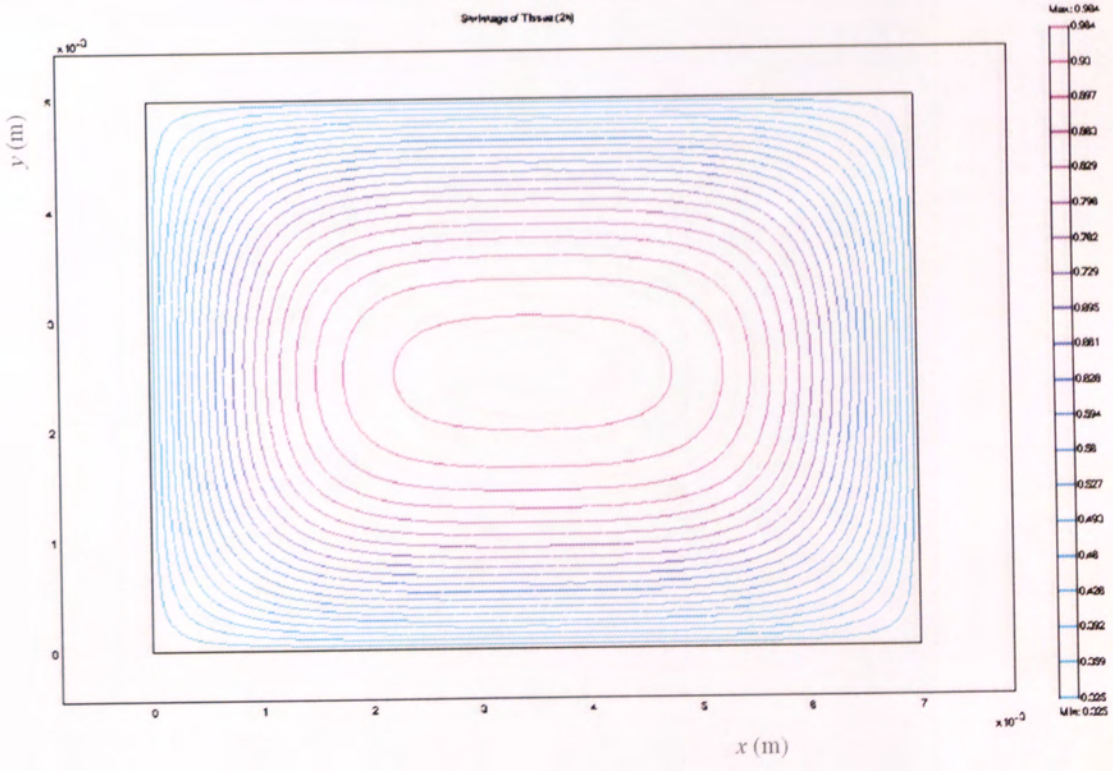

Figure 8.28 The contour analyses of shrinkage phenomena (t=2h)

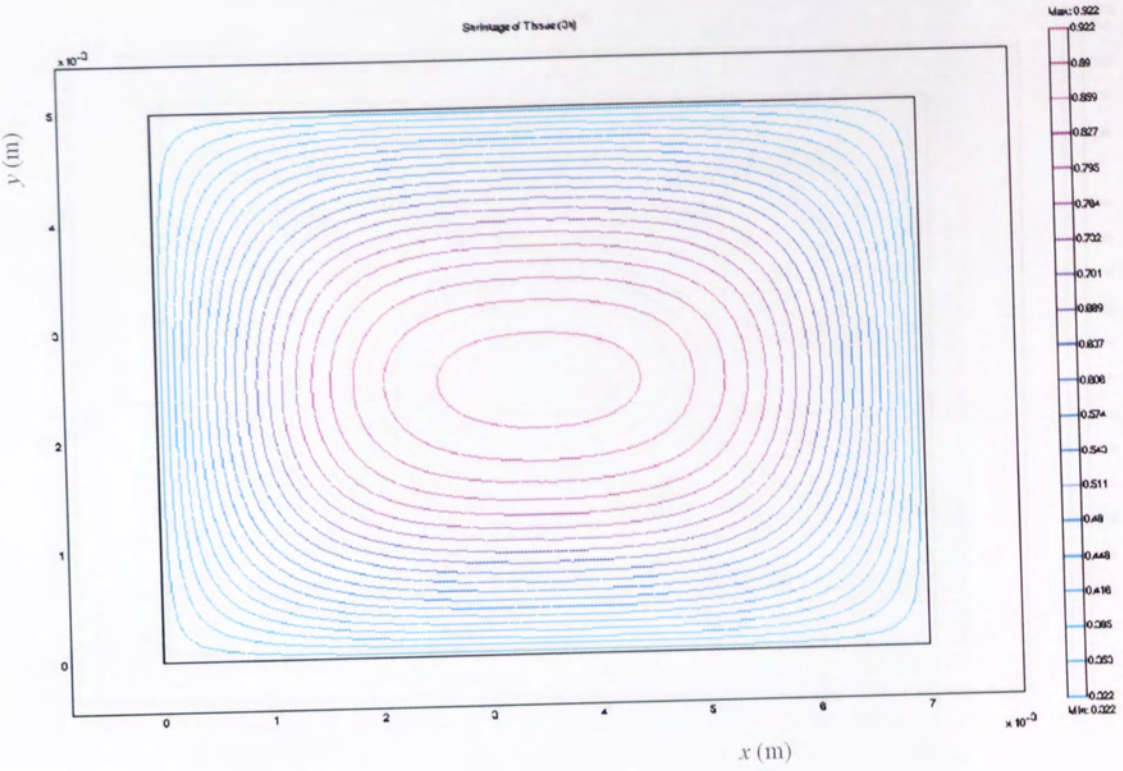

Figure 8.29 The contour analyses of shrinkage phenomena (t=3h)

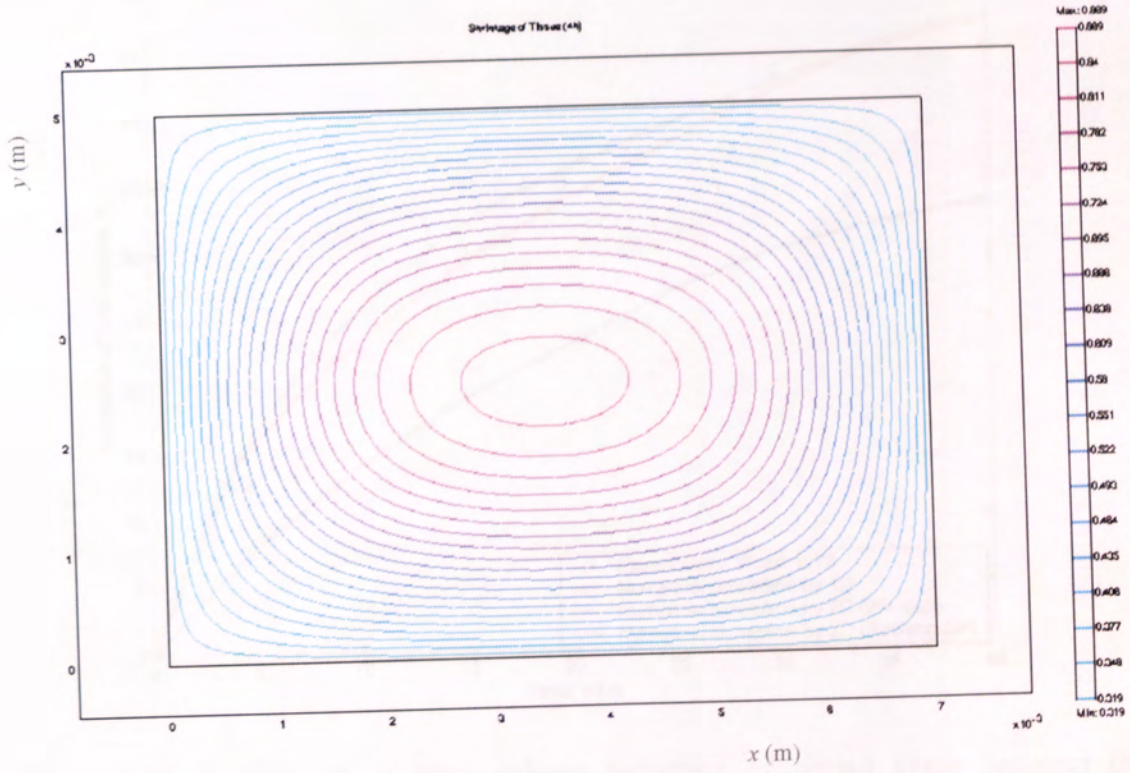

Figure 8.30 The contour analyses of shrinkage phenomena (t=4h)

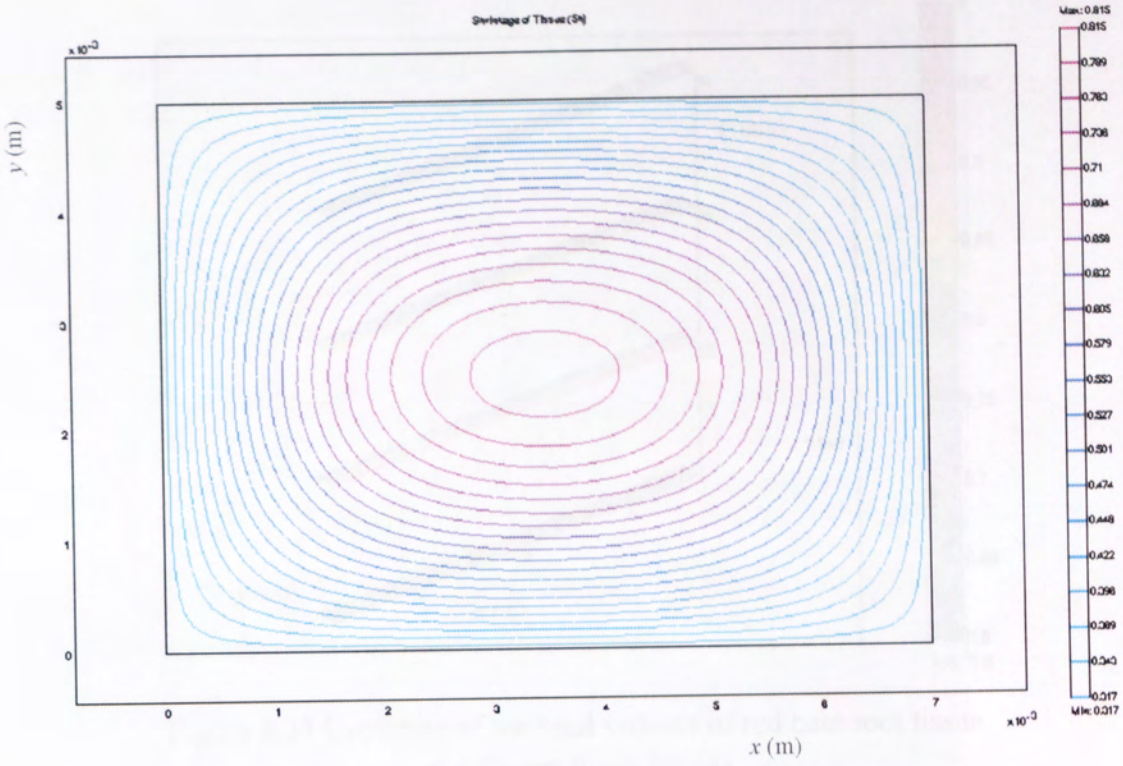

Figure 8.31 The contour analyses of shrinkage phenomena (t=10h)

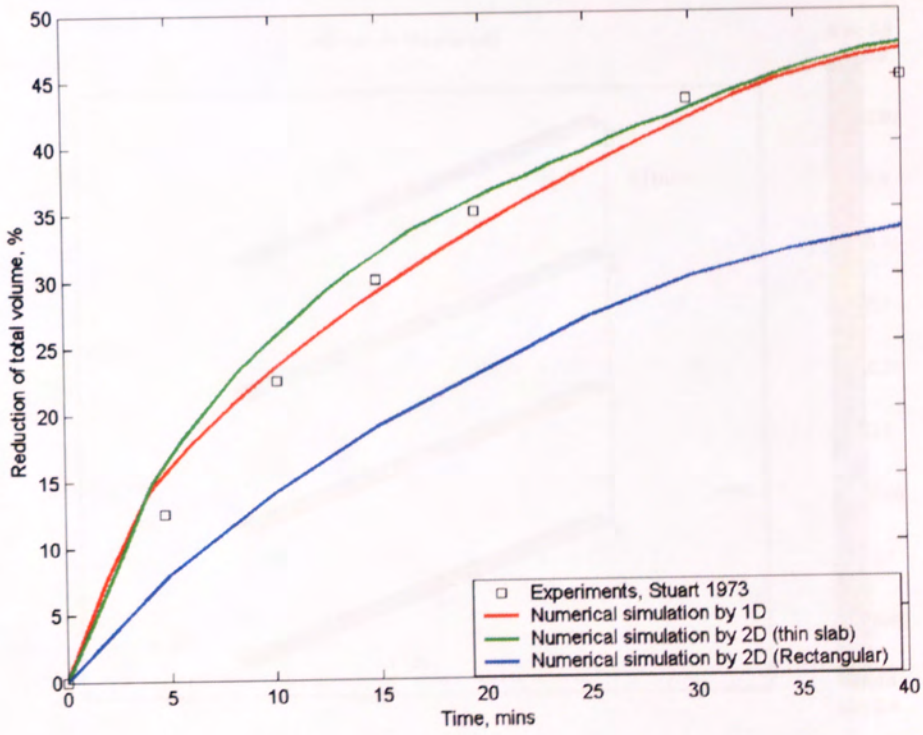

Figure 8.32 Comparison of total volume reduction of potato tissue between the simulations from the mathematical model 2 (1D, 2D thin slab, 2D rectangular) and the experimental results reported by Stuart (1973)

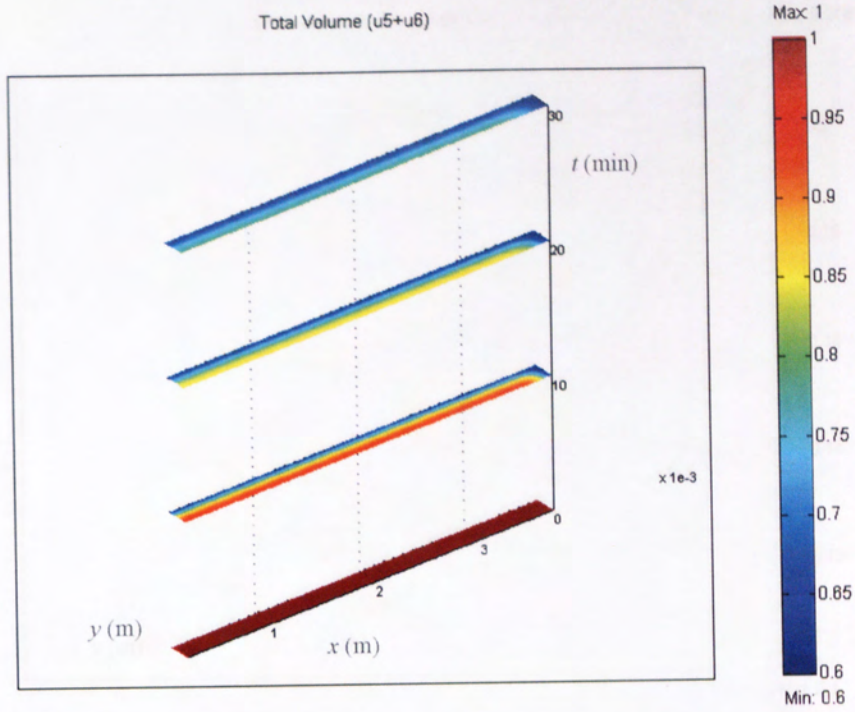

Figure 8.33 Evolution of the total volume of red beet root tissue at different times (mins)

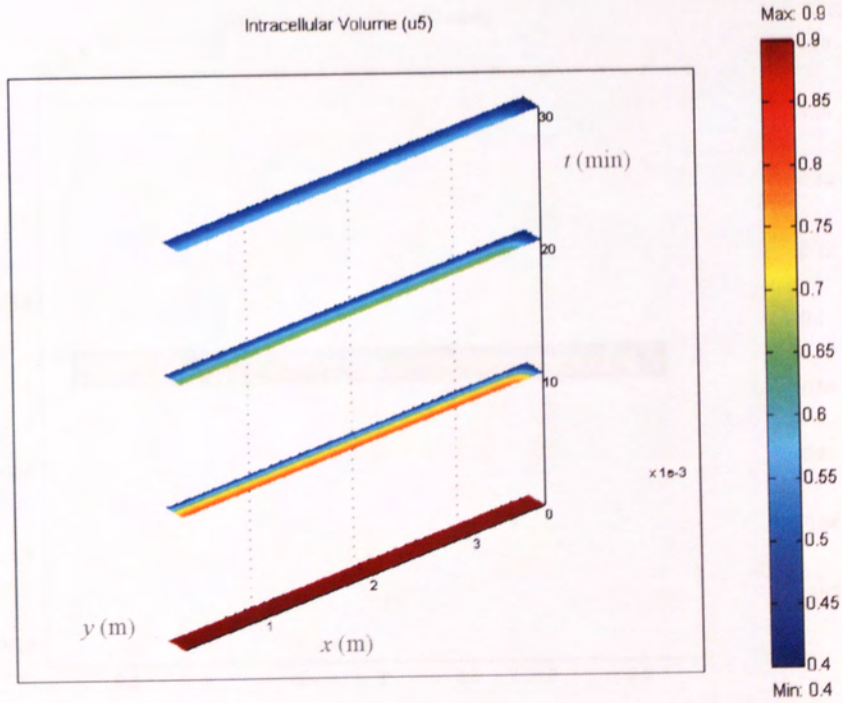

Figure 8.34 Evolution of the intracellular volume of red beet root tissue at different times (mins)

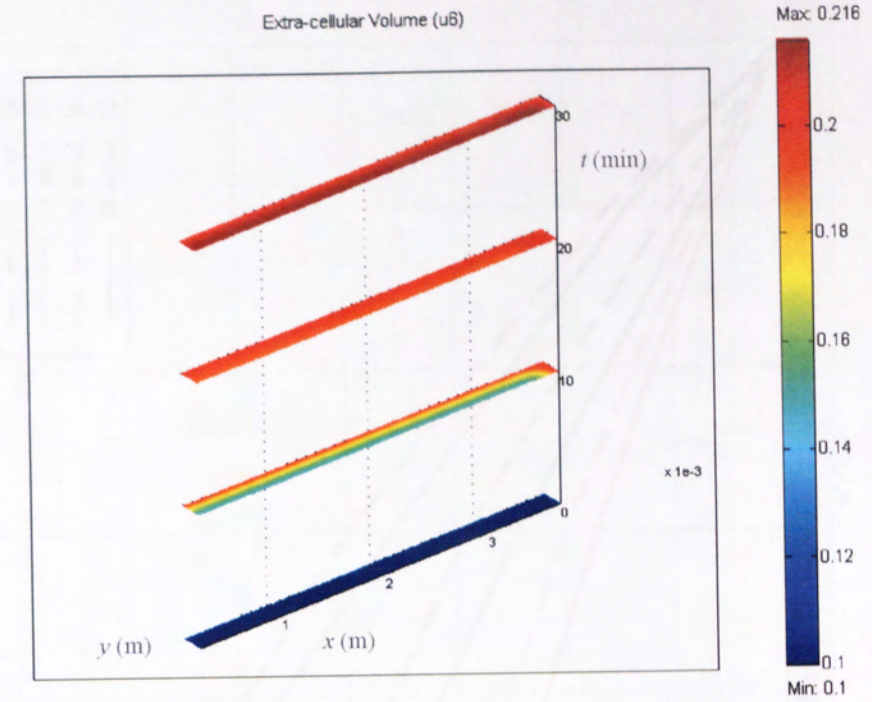

Figure 8.35 Evolution of the extra-cellular volume of red beet root tissue at different times (mins)

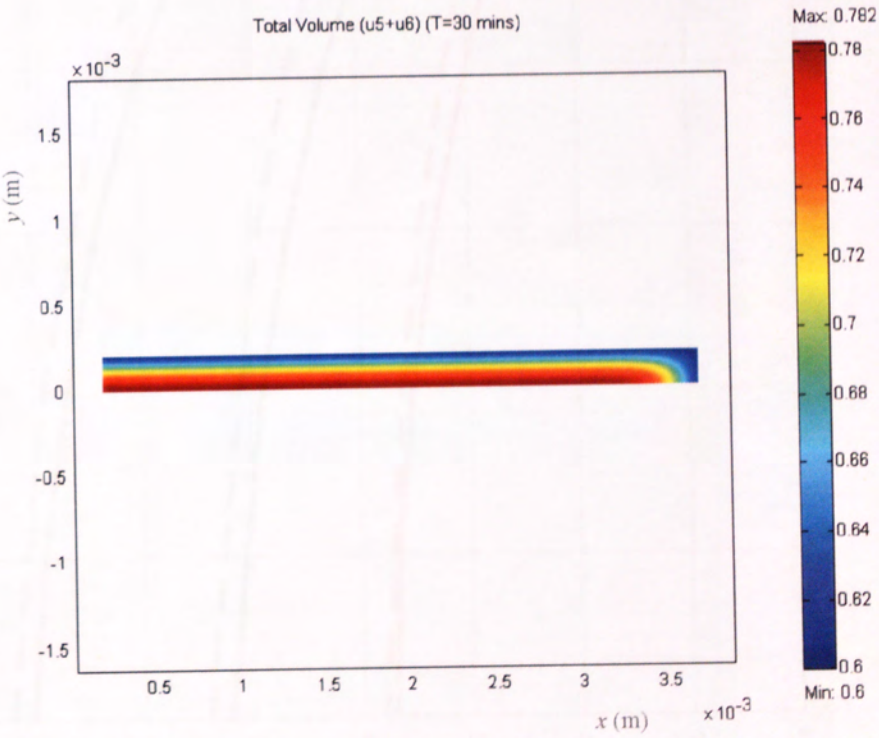

Figure 8.36 Distribution profiles of the total volume of red beet root tissue at time t=30 (mins)

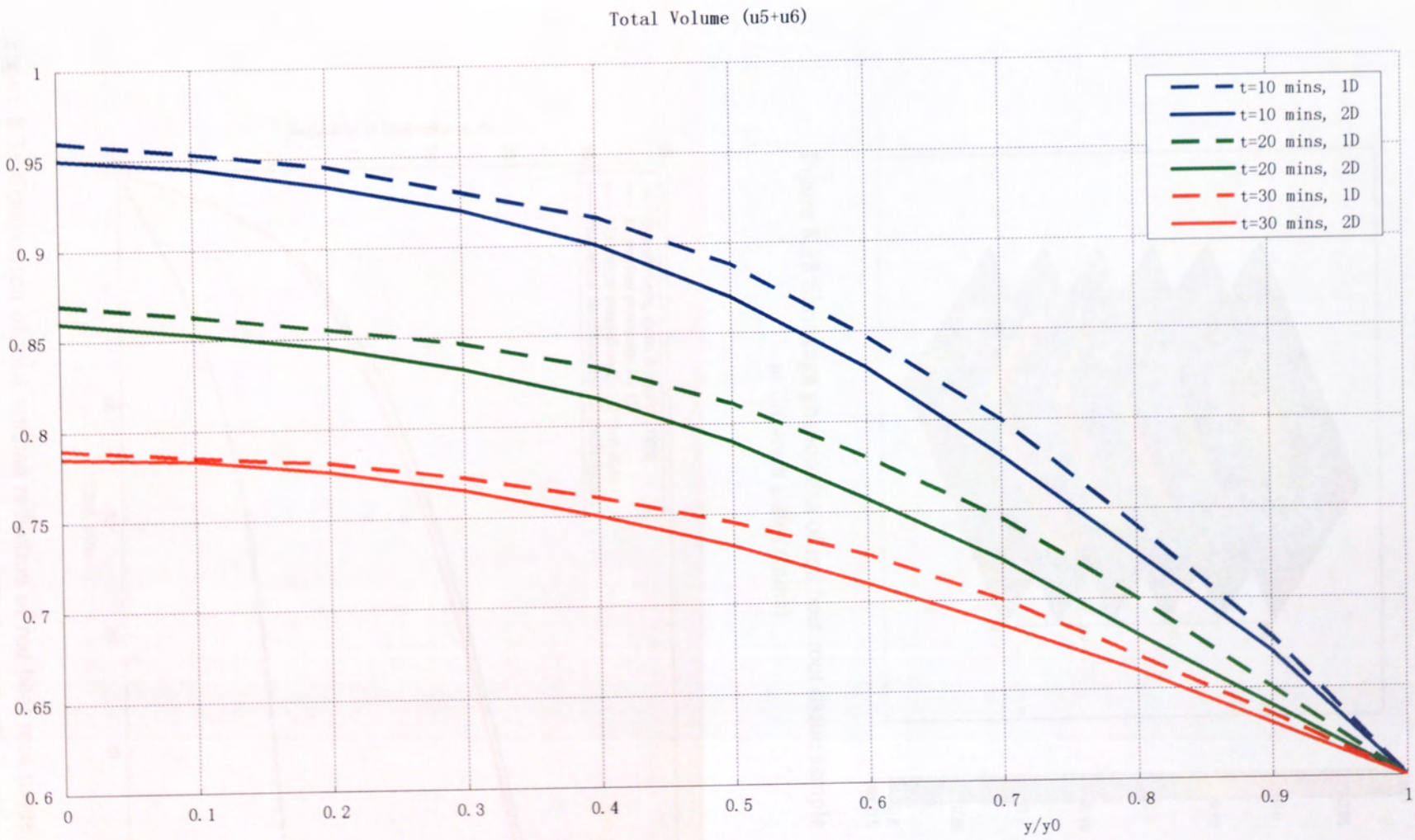

Figure 8.37 Comparison of the total volume of red beet root tissue at one cross-section in *y*-direction by 1D and 2D (thin slab) analyses

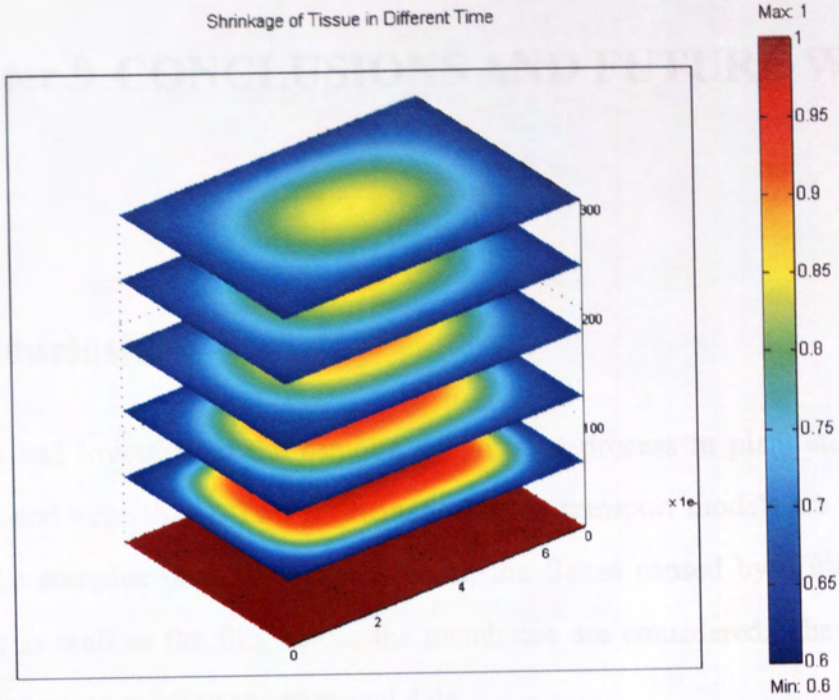

Figure 8.38 Shrinkage phenomena of red beet root tissue sample at different times (mins)

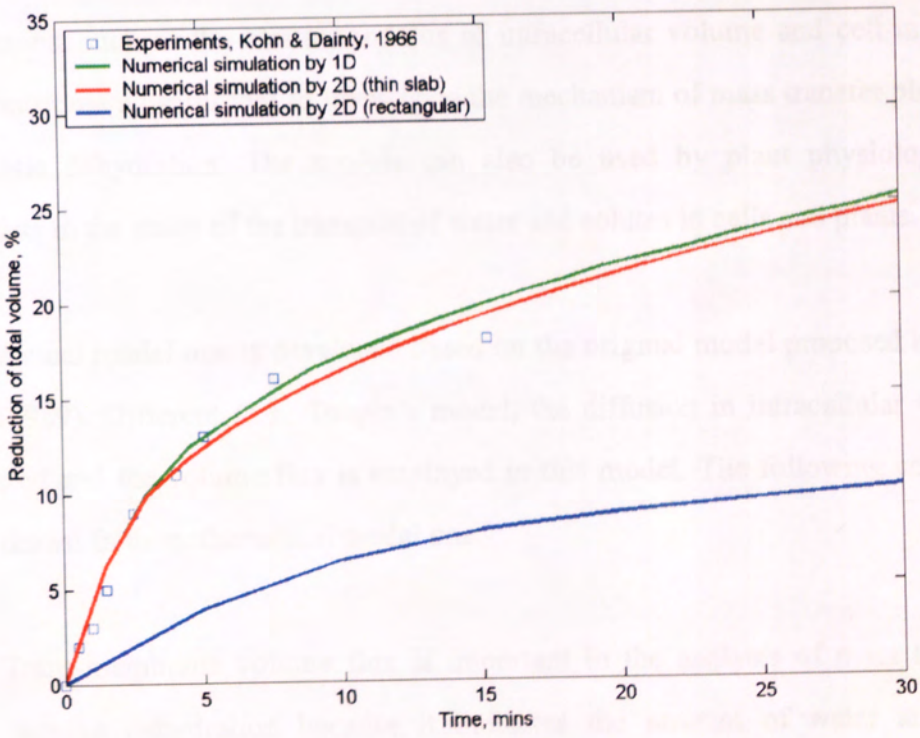

Figure 8.39 Comparison of total volume reduction of red beet root tissue between the simulations from the mathematical model 2 (1D, 2D thin slab, 2D rectangular) and the experimental results reported by Kohn & Dainty (1966)

Chapter 9 CONCLUSIONS AND FUTURE WORK

9.1 Conclusions

This thesis had investigated the osmotic dehydration process in plant storage tissues (like fruits and vegetables). Two mathematical mass transport models are presented to simulate the complex process. In each model, the fluxes caused by diffusion and by convection as well as the flux across the membrane are considered. The results have been verified using existing experimental data.

Both of the mathematical models are reasonable and successful to simulate the osmotic dehydration process although each of them employs some parameters from experiential assumptions, such as the elastic modulus of intracellular volume and cell membrane. They contribute a useful tool to investigate the mechanism of mass transfer phenomena in osmotic dehydration. The models can also be used by plant physiologists and cytologists in the study of the transport of water and solutes in cells and plants.

Mathematical model one is developed based on the original model proposed by Toupin *et al.*, (1989). Different from Toupin's model, the diffusion in intracellular volume is considered and the volume flux is employed in this model. The following conclusions can be drawn from mathematical model one:

- Trans-membrane volume flux is important in the analysis of mass transfer in osmotic dehydration because it indicates the amount of water and solutes removed from the intra-cellular volume.

- Bulk flow plays an important role in osmotic dehydration. The influence of the

bulk flow is consequently considerable, and indicates that attempting to interpret osmotically driven processes on the basis of pure diffusion would lead to serious underestimation of the time.

- Solute concentration of osmotic solution, diffusion coefficient can affect the overall behaviour of the osmotic dehydration significantly; more or less, the membrane conductivity coefficient, diffusibility of cell wall, elastic modulus of cell wall and critical cell volume all influence the progress of osmotic dehydration.

Mathematical model two is originally developed by Li, (2005). However, the turgor pressure is added by the author. Also, the original model is extended to two-dimension, which generalizes the osmotic dehydration process and gives us an intuitionistic expression of this process. It avoids the conceptual and abstract properties to understand the osmotic dehydration process. Besides the conclusions drawn from model one, the study of model two has reached to the following conclusions:

- The assumption that plant tissue can be considered as the porous medium is reasonable. The employment of Darcy's law to express the relation between the bulk velocities and hydrostatic pressures also appears suitable.

- The modification of the equations of hydrostatic pressures and volumes is successful, although it needs further verification by experimental data.

- The ratio of permeability to dynamic viscosity can affect the results of osmotic dehydration significantly. More or less, the membrane constants can influence the progress of osmotic dehydration process.

- When the size of the plant tissue samples in one direction is much bigger than the ones in other directions, the results obtained from one-dimensional analyses

and two-dimensional analyses are almost identical, which is expected. However, for the common geometrical tissue structure, the one-dimensional analyses are inaccurate and it must be treated as the multi-dimensional problems

- The results obtained from two-dimensional analyses can demonstrate the osmotic dehydration process more intuitionistic. The results in cross-sections of x-direction and y-direction can be visible to demonstrate how the plant tissue is shrunk.

9.2 Suggestions for Future Work

The osmotic dehydration in plant tissue is a very complex process. It is hard to build one model to solve all the problems in this area. The future work should concentrate on the following:

- based on mathematical model two, revise the pressure equations in intracellular and extra-cellular volume;

- do more research about the turgor pressure and revise the express of turgor pressure in plant tissue;

- explore other more general models;

- do some experiments to obtain more useful data, such as the hydrostatic pressures, the elastic modulus of cell wall, the membrane permeability, the dynamic viscosity of the plant tissue etc., to verify the presented or new built models.

REFERENCES

[1] Ade-Omowaye, B. I. O., Rastogi, N. K., Angersbach, A. and Knorr, D., (2002). Osmotic dehydration of bell peppers: Influence of high intensity electric field pulses and elevated temperature treatment. *Journal of Food Engineering*, **54**, 35-43.

[2] Agnelli, M. E., Marani, C. M. and Mascheroni, R. H., (2004). Modelling of heat and mass transfer during (osmo) dehydrofreezing of fruits. *Journal of Food Engineering* (in press).

[3] Azuara, E., Beristain, C. I. and Gutiérrez, G. F., (2002). Osmotic dehydration of apples by immersion in concentrated sucrose/maltodextrin solutions. *Journal of Food Processing Preservation*, **26**, 295-306.

[4] Azuara, E., Cortes, R., Garcia, H. S. and Beristain, C. I., (1992). Kinetic model for osmotic dehydration and its relationship with Fick's second law. *International Journal of Food Science and Technology*, **27**, 239–242.

[5] Azuara, E., Garcia, H. S. and Beristain, C. I., (1996). Effect of centrifugal force on osmotic dehydration of potatoes and apples. *Food Research International*, **29**, 195-199.

[6] Barat, J. M., Fito, P. and Chiralt A., (2001). Modelling of simultaneous mass transfer and structural changes in fruit tissues. *Journal of Food Engineering*, **49**, 77-85.

[7] Beristain, C. I., Azuara, E., Cortes, R. and Garcia, H. S., 1990. Mass transfer during osmotic dehydration of pineapple rings. *International Journal of Food Science and Technology*, **25**, 576–582.

[8] Biran, A. and Breiner, M. *MATLAB for Engineers*. Addison-wesley publishing company, 1995.

[9] Biswal, R. N., Bozorgmehr, K., Tompkins, F. D. and Liu, X., (1991). Osmotic concentration of green beans prior to freezing. *Journal of Food Science*, **56**, 1008–1012.

[10] Biswal, R. N. and Maguer, M. L., (1989). Mass transfer in plant material in contact with aqueous solutions of ethanol and sodium chloride equilibrium data. *Journal of Food Process Engingeering*, **11**, 159–176.

[11] Bolin, H. R., Huxsoll, C. C., Jackson, R. and Ng, K. C., (1983). Effect of osmosis agents and concentration on fruit quality. *Journal of Food Science*, **48**, 202–205.

[12] Burton, W. G. and Spragg, W. T., (1955). A note on the intercellular space of the potato tuber. *New Phytology*, **49**, 8-10.

[13] Conway, J. M., Castaigne, F., Picard, G. and Voxan, X., (1983). Mass transfer considerations in the osmotic dehydration of apples. *Canadian Institute of Food Science and Technology*, **16**, 25-29.

[14] Crank, J. *The mathematics of Diffusion*. Clarendon Press, Oxford, UK, 2nd Edn. 1979.

[15] Crapiste, G. H. and Rotstein, E., (1982). Prediction of sorptional equilibrium data for starch-containing foodstuffs. *Journal of Food Science*, **47**, 1501-1507.

[16] Cussler, E. L. *Diffusion –Mass transfer in fluid systems*, 2nd Edn. Cambridge University Press, 1997.

[17] Dainty. J., (1963a). Water relations of plant cells. *Advanced Botanical*. Research I, 279-326.

[18] Dainty, J., (1976). *Water relations of plant cells. In Transport in plants II.* Part A. Cells, edited by U. Luttge & M.G. Pitman. Springer-Verlag, Berlin, Heidelberg, New York, pp. 12-35.

[19] Davis, R. M., (1962). Tissue air space in the potato: its estimation and relation to dry matter and specific gravity. *American Potato Journal*, **39**, 298-305.

[20] Dixon, G. M. and Jen, J. J., (1977). Change of suger and acid in osmovac dried appli slices. *Journal of Food Science*, **42**, 1126-1131.

[21] Djelveh, G., Gros, J. -B. and Emam-Djomeh, Z., (2001). Osmotic dehydration of foods in a multicomponet solution. Part II. Water loss and solute uptake in Agar gels and meat. *Lebensmittel-Wissenschaft und-Technologie,* **34**, 319-323.

[22] Dornenburg, H. & Knorr, D., (1993). Cellular permeabilization of cultured plant tissue by high electric field pulse and ultra high pressure for recovery of secondary metabolites. *Food Biotechnology*, **7**, 35-48.

[23] Dullien, F. A. L. *Porous media – Fluid transport and pore structure.* Academic press, New York, London, Toronto, Sydney, San Francisco, 1979.

[24] Farr, D., (1990). High pressure technology in food industry. *Trends in Food Science and Technology*, **1**, 14-16.

[25] FEMLAB 3.0. *FEMLAB Quick Start; FEMLAB Modelling Guild; FEMLAB User's Guild.* COMSOL AB, 2004.

[26] Ferrier, J. M. & Dainty, J., (1978). The external force method for measuring hydraulic conductivity and elastic coefficients in higher plant cells: application to multilayer tissue sections and further theoretical developments. *Can. Journal of Botany*, 56, 22-26.

[27] Fito, P., Chiralt, A., Barat, J. M., Spiess, W. E. L. and Behsnilian, D. *Osmotic Dehydration & Vacuum Impregnation*. Lancaster, Basel, 2001.

[28] Gekas, V., (2001). Mass transfer modelling. *Journal of Food Engineering*, **49**, 97-102.

[29] Giangiacomo, R., Torreggiani, D. and Abbo, E., Osmotic dehydration of fruit. Part I: sugar exchange between fruit and extracting syrup. *Journal of Food Processing and Preservation*, **11**, 183–195.

[30] Greenkorn, R. A. *Flow phenomena in porous media*. Fundamentals and Applications in Petroleum, Water, and Food Production. New York, Basel, 1983.

[31] Hawkes, J. and Flink, J. M., (1978). Osmotic concentration of fruit slices prior to osmotic dehydration. *Journal of Food Processing*, **2**, 265–284.

[32] Hayden, R. I., Moyse, C. A., Calder, F. W., Crawford, D. P. and Fensom, D. S., (1969). Electrical impedance studies on potato alfalfa tissue. *Journal of Experimental Botanical*, **20**, 177-200.

[33] House, C. R. (1973). *Water Transport in Cells and Tissues*. London; published 1974 by Edward Arnold Ltd.

[34] Islam, M. N. and Flink, J. N., (1982). Dehydration of potato II. Osmotic concentration and its effect on air drying behaviour. *Journal of Food Technology*, **17**, 387-403.

[35] Isse, M. G. and Schubert, H., (1991). Osmotic dehydration of mango: mass transfer between mango and syrup. 4th World Congress of Chemical Engineering, Karlsruhe, Germany.

[36] Kaymak-Ertekin, F. and Cakaloz, T., (1996). Osmotic dehydration of Peas: I. Influence of process variables on mass transfer. *Journal of Food Processing and Preservation*, **20**, 87-104.

[37] Kaymak-Ertekin, F. and Sultanoglu, M. (2000). Modelling of mass transfer during osmotic dehydration of apples. *Journal of Food Engineering*, **46**, 243-250.

[38] Kedem, O. and Katchalsky, A., (1958). Thermodynamic analysis of the permeability of biological membranes to non-electrolytes. *Biochimica et Biophysica Acta*, **27**, 229-246.

[39] Kohn, P. G. and Dainty, J., (1966). The measurement of permeability to water in disks of storage tissue. *Journal of Experimental Botanical*, **17**, 809-821.

[40] Kowalska, H. and Lenart, A., (2001). Mass exchange during osmotic pre-treatment of vegetables. *Journal of Food Engineering*, **49**, 137-140.

[41] Lenart, A. and Flink, J. M., (1984). Osmotic dehydration of potatoes. II. Criteria for the end point of the osmotic process. *Journal of Food Technology*, **19**, 45–63.

[42] Lenart, A. and Lewicki, P. P., (1988). Osmotic preconcentration of carrot tissue followed by convection drying. *Preconcentration and drying of food materials*, 307-308.

[43] Lenart, A. and Lewicki, P. P., (1990). Osmotic dehydration of carrots at high temperature. In Spiess, W. E. L. and Schubert, H., *Engineering and food preservation processes and related techniques*, **2**, 731–740.

[44] Lerici, C. L., Pinnavaia, G., Dalla Rosa, M. and Bartolucci, L., (1985). Osmotic dehydration of fruit: influence of osmotic agents on drying behaviour and product quality. *Journal of Food Science*, **50**, 1217-1219.

[45] Lewicki, P. P., (1989). Measurement of Water Activity of Saturated Salt Solutions with the Vapour Pressure Manometer. *Journal of Food Engineering*, **10**, 39-55.

[46] Li, L. Y., (2004). Transport of multi-component ionic solutions in membrane systems. *Philosophical Magazine Letters*, **84**, No. 9, 593-599.

[47] Li, L. Y., (2005). Numerical simulation of mass transfer during the osmotic dehydration of biological tissues. *Computational Materials Science*, **35**, No. 3.

[48] Li, L. Y. and Page, C. L., (2000). Finite element modelling of chloride removal from concrete by an electrochemical method. *Corrosion Science*, **42**, 2145-2165.

[49] Li, L. Y., Purkiss, J. A. and Tenchive, R., (2002). An engineering model for coupled heat and mass transfer analysis in heated concrete. *Proceedings of the Institute of Mechanical Engineers*, **216,** (Part C) 1-12.

[50] Li, L. Y., Tighe, B. J. and Rubberti, J. W., (2004). Mathematical modelling of corneal swelling. *Biomechanics and modelling in mechanobiology*, **3**, (2) 99-114.

[51] Lüttge, U. and Pitman, M. G., (1976). *Transport in Plants II. Part A Cells.* Springer-Verlag Birlin Heidelberg New York.

[52] Lüttge, U. and Pitman, M. G., (1976). *Transport in Plants II. Part B Tissues and Organss.* Springer-Verlag Birlin Heidelberg New York.

[53] Magee, T. R. A., Hassaballah, A. A. and Murphy, W. R., (1983). Internal mass transfer during osmotic dehydration of apple slices in sugar solutions. *International Journal of Food Science and Technology*, **1**, 177–178.

[54] Marcotte, M., (1988). *Mass transport phenomena in osmotic processes: experimental measurements and theoretical considerations*. M. Sc thesis. Department of Food Science, University of Alberta, Edmonton, Canada.

[55] Marcotte, M. and Le Maguer, M., (1991). Mass transfer in cellular tissues. Part II: Computer simulations vs experimental data. *Journal of Food Engineering*, **17**, 177–199.

[56] Marcotte, M., Toupin, C. J. and Le Maguer, M., (1991). Mass transfer in cellular tissues. Part I: the mathematical model. *Journal of Food Engineering*, **13**, 199–200.

[57] Matusek, A. and Merész, P., (2002). Modelling of sugar transfer during osmotic dehydration of carrots. *Periodica Polytechnica Ser. Chem. Eng.*, **46**, 83-92.

[58] Mauro, M. A., Tavares, D. Q. and Menegalli, F. C., (2002). Behavior of plant tissue in osmotic solutions. *Journal of Food Engineering*, **56**, 1-15.

[59] Mavroudis, N. E., Gekas, V. and Sjöholm, I., (1998). Osmotic dehydration of apples – effects of agitation and raw material characteristics. *Journal of Food Engineering* **35**, 191–209.

[60] Mavroudis, N., Gekas, V. and Sjöholm, I., (1998). Osmotic Dehydration of Apple. Shrinkage Phenomena and the Significance of Initial Structure on Mass Transfer Rates. *Journal of Food Engineering*, **38**, 101-123.

[61] Medina-Vivanco, M., Sobral, P. J. do A. and Hubinger, M. D., (2002). Osmotic dehydration of tilapia fillets in limited volume of ternary solutions. *Chemical Engineering Journal*, **3966**, 1-7.

[62] Mizrahi, S., Eichler, S. and Ramon, O., (2001). Osmotic dehydration phenomena in gel systems. *Journal of Food Engineering*, **49**, 87-96.

[63] Moreira, R. & Sereno, A. M., (2003). Evaluation of mass transfer coefficients and volumetric shrinkage during osmotic dehydration of apple using sucrose solutions in static and non-static conditions. *Journal of Food Engineering,* **57**, 25-31.

[64] Mujica-Paz, H., Valdex-Fragoso, A., Lopez-Malo, A., Palou, E. and Welti-Chanes, J., (2003). Impregnation properties of some fruits at vacuum pressure. *Journal of Food Engineering*, **56**, 307-314.

[65] Nilsson, S. B., Herts, C. H. and Falk, S., (1958). On the relation between tugor pressure and tissue rigidity. II Theoretical calculations on model systems. *Physiologia Plantarum*, **11**, 818-837.

[66] Nobel, P. S., (1983). *Biophysical plant physiology and ecology*. W. H. Freeman, San Francisco.

[67] Ponting, J. D., (1973). Osmotic dehydration of fruits-recent modifications and applications. *Process Biochemistry*, **8**, 18-20.

[68] Ponting, J. D., Walters, G. G., Forrey, R. R., Jackson, R. and Stanley, W.L., (1966). Osmotic dehydration of fruits. *Food Technology*, **20**, 125–128.

[69] Poole, R. J., (1976). Transport in cells of storage tissues. *Transportation in plants II. Part A. Cells*, ed. U. Luttge & M. G. Pitman. Springer-Verlag, New York, pp. 229-48.

[70] Rahman, M. S. and Lamb, J., (1990). Osmotic dehydration of pineapple. *Journal of Food Science and Technology*, **7**, 150-152.

[71] Rastogi, N. K. and Niranjan, K., (1998). Enhanced mass transfer during osmotic dehydration of high pressure treated pineapple. *Journal of Food Science*, **63**, 508-511.

[72] Rastogi, N. K., Angersbach, A. and Knorr, D., (2000a). Synergistic effect of high hydrostatic pressure pre-treatment and osmotic stress on mass transfer during osmotic dehydration. *Journal of Food Engineering*, **45**, 25-31.

[73] Rastogi, N. K., Eshtiaghi, M. N. and Knorr, D. (1999). Accelerated mass transfer during osmotic dehydration of high intensity electrical field pulse pre-treated carrots. *Journal of Food Science*, **64**, 1020-1023.

[74] Rastogi, N. K. and Raghavarao, K. S. M. S. (1995). Kinetics of osmotic dehydration of coconut. *Journal of Food Process Engineering*, **18**, 187–197.

[75] Rastogi, N. K. and Raghavarao, K. S. M. S., (1997a). Water and solute diffusion coefficients of carrot as a function of temperature and concentration. *Journal of Food Engineering*, **34**, 429–440.

[76] Rastogi, N. K. and Raghavarao, K. S. M. S., (1997b). Mass transfer during osmotic dehydration of carrot: Comparison of different methods for the estimation of effective diffusion coefficients. In The *Proceedings of 7th International Congress on Engineering and Food (ICEF)* (Vol. **2**, G 73–76), Brighton, UK.

[77] Rastogi, N. K., Raghavarao, K. S. M. S. and Niranjan, K., (1997). Mass Transfer during Osmotic Dehydration of Banana: Fickian Diffusion in Cylindrical Configuration. *Journal of Food Engineering*, **31**, 423-432.

[78] Rastogi, N. K., Raghavarao, K. S. M. S., Niranjan, K. and Knor, D., (2002). Recent developments in osmotic dehydration: method to enhance mass transfer. *Trends in Food Science & Technology*, **13**, 48-59.

[79] Rastogi, N. K., Subramanian, R. and Raghavarao, K. S. M. S., (1994). Application of high pressure technology in food industry. *Indian Food Industry*, **13**, 30-34.

[80] Raoult-Wack, A. L., (1994). Recent advances in the osmotic dehydration of foods. *Trends in Food Science & Technology*, **5**, 255-260.

[81] Reeve, R. M., Timm, H. and Weaver, M. L., (1973). Cell wall thickness during growth of domestic and foreign potato cultivars. *American Potato Journal*, **50**, 204-11.

[82] RILEM. *Transfers of water in porous media*. Paris, 1965.

[83] Sacchetti, G., Gianotti, A. and Rosa, M. D., (2001). Sucrose-salt combined effects on mass transfer kinetics and product acceptability. Study on apple osmotic treatments. *Journal of Food Engineering*, **49**, 163-173.

[84] Sajnin, C., Gerschenson, L. N. and Rojas, A. M., (1999). Turgor pressure in vegetable tissues: comparison of the performance of incipient plasmolysis technology and polyethylenglycol. *Food Research International*, **32**, 531-537.

[85] Scheidegger, A. E. *The physics of flow through porous media*. Third Edition. University of Toronto Press, 1974.

[86] Schijndel, A. W. M., (2003). Modeling and solving building physics problems with Femlab. *Building and Environment*, **38**, 319-327.

[87] Sereno, A. M., Moreira, R., and Martinez, E., (2001). Mass transfer coefficients during osmotic dehydration of apple in single and combined aqueous solutions of sugar and salt. *Journal of Food Engineering*, **47**, 43-49.

[88] Sherwood, T. K., (1974). A review of the development of mass transfer theory. *Chemical Engineering Education*, **3**, 204-213.

[89] Shi, X. Q. and Maupoey, F. P., (1994). Mass transfer in vacuum osmotic dehydration of fruits: a mathematical model approach. *Lebensmittel-Wissenschaft und-Technologie*, **27**, 67-72.

[90] Shi, X. Q., Fito, P. and Chiralt, A., (1995). Influence of vacuum treatment on mass transfer during osmotic dehydration of fruits. *Food Research International*, **28**, 445-454.

[91] Simal, S., Benedito, J., Sanchez, E. S., & Rossello, C., (1998). Use of ultrasound to increase mass transport rates during osmotic dehydration. *Journal of Food Engineering*, **36**, 323-336.

[92] Spiazzi, E. and Mascheroni, R., (1997). Mass Transfer Model for Osmotic Dehydration of Fruits and Vegetables – I. Development of the Simulation Model. *Journal of Food Engineering*, **34**, 387-410.

[93] Sterling, C., (1966). Anatomy and histology of the tuber with respect to processed quality. *Proc. Plant Sci. Symp.*, **11**, 25.

[94] Stuart, D. M. (1973). Reduction of water permeability in potato tuber slices by cyanide, ammonia, 2, 4-dinitrophenol and oligomycin and its reversal by adenosine 5'-triphophate and cytidine 5'-triphophate. *Plant Physiol.*, **51**, 485-8.

[95] Telis, V. R. N., Murari, R. C. B. D. L. and Yamashita, F., (2004). Diffusion coefficients during osmotic dehydration of tomatoes in ternary solutions, *Journal of Food Engineering,* **61**, 253-259.

[96] Tenchev, R. T., Li, L. Y., Purkiss, J. A. and Khalafallah, B. H., (2001). Finite element analysis of coupled heat and mass transfer in concrete when it is in a fire. *Magazine of Concrete Research*, **53**, 117-125.

[97] Thain, J. F. *Principles of Osmotic Phenomena*. London: The Royal Institute of Chemistry, 1967.

[98] Torreggiani, D., (1993). Osmotic dehydration in fruits and vegetable processing. *Food Research International*, **26**, 59–68.

[99] Toupin, C. J., Marcotte, M. and Le Maguer, M., (1989). Osmotically-Induced Mass Transfer in Plant Storage Tissues: A Mathematical Model. Part I. *Journal of Food Engineering*, **10**, 13-38.

[100] Toupin, C. J. and Le Maguer, M., (1989). Osmotically-Induced Mass Transfer in Plant Storage Tissues: A Mathematical Model. Part II. *Journal of Food Engineering*, **10**, 97-121.

[101] Treybal, R. E. *Mass transfer operations*. 3rd Edn. McGraw-Hill Book Company, 1980.

[102] Vankan, W. J., Huyghe, J. M., Drost, M. R., Janssen, J. D. and Huson, A., (1997). A finite element mixture model for hierarchical porous media. *Int. J. Numer. Meth. Eng.*, **40**, 193-210.

[103] Walker, N. A. and Pitman, M. G., (1976). Measurement of Fluxes across Membranes. *Transportation in plants II. Part A. Cells*, ed. U. Lüttge & M. G. Pitman. Springer-Verlag, New York, pp. 93-126.

[104] Welti-Chanes, J., Velez-Ruiz, J. F. and Barbosa-Canovas, G. V. *Transport Phenomena in Food Processing*. Boca Raton, London, New York, Washington, D. C., 2003.

[105] Welty, J. R., Wicks, C. E. and Wilson, R. E. *Momentum, Heat and Mass Transfer*, 3rd Edn, John, Wiley & Sons, New York, 1984.

[106] Wijmans, J. G. and Baker, R. W., (1995). The solution-diffusion model: a review. *Journal of Membrane Science*, **107**, 1-21.

[107] Wu, N. and Pitts, M. J., (1999). Development and validation of a finite element model of an apple fruit cell. *Postharvest Biology and Technology*, **16**, 1-8.

[108] Yao, Z., (1994). Modelling and simulation of mass transfer in osmotic dehydration processes. Ph.D. thesis, Food Science Department, University of Guelph, Canada.

[109] Yao, Z. and Le Maguer, M., (1996). Mathematical Modelling and Simulation of Mass Transfer in Osmotic Dehydration Processes. Part I: Conceptual and Mathematical Models. *Journal of Food Engineering*, **29**, 349-360.

[110] Yao, Z. and Le Maguer, M., (1997). Mathematical Modelling and Simulation of Mass Transfer in Osmotic Dehydration Processes. Part II: Simulation and Model Verification. *Journal of Food Engineering*, **32**, 21-32.

[111] Yao, Z. and Le Maguer, M., (1997). Mathematical Modelling and Simulation of Mass Transfer in Osmotic Dehydration Processes. Part III: Parametric Study. *Journal of Food Engineering*, **32**, 33-46.

[112] Yao, Z. and Le Maguer, M., (1997). Analysis of Mass Transfer in Osmotic Dehydration Based on Profiles of Concentration, Shrinkage, Transmembrane Flux and Bulk Velocity in the Domain of time and space. *Journal of Food Process Engineering*, **20**, 401-414.

APPENDIX A

Chemical Potential of A Species in A Solution

It is well known that the chemical potential of a species in a mixed solution can be expressed by

$$\mu_j = \mu_j^* + RT \ln a_j + \overline{V}_j P + z_j FE + m_j gh \tag{A.1}$$

where μ_j in J/mole is the total chemical potential of the species s, μ_j^* in J/mole is the potential of the species in reference level since the chemical potential is a relative quantity. $\overline{V}_j$ in m^3/mole is the partial molar volume of the species, P in N/m^2 is the hydrostatic pressure, R=8.314 J/(mole-K) is the universal gas constant, T in K is the absolute temperature, a_j is the activity of the species, z_j is the charge number of the species, F=96458 C/mole is the Faraday constant, E in V is the electrical potential, g is in N/s^2 is the gravitational acceleration. The gravitational term $m_j gh$ expressing the amount of work required to raise an object of mass m_j per mole to a vertical height h.

If we ignore the gravitational term and the considered solutes are non-electrolytes, then the Eq. (A.1) can be simplified to:

$$\mu_j = \mu_j^* + RT \ln a_j + \overline{V}_j P \tag{A.2}$$

The activity of a species is usually related to its mole fraction or its concentration ratio in the solution by means of an activity coefficient, that is:

$$a_j = \frac{\gamma_j N_j}{N_w + \sum N_k} = \frac{\gamma_j C_j}{C_w + \sum C_k} \tag{A.3}$$

where γ_j is the activity coefficient of the species, N_s in mole is the mole number of the species in the solution, N_w in mole is the mole number of the solvent in the solution, C_s in mole/m^3 is the concentration of the species in the solution, C_w in mole/m^3 is the concentration of the solvent in the solution. The summation in Eq. (A.3) is applied to all the species involved in the solution except for the solvent.

For an ideal solution γ_s=1 and therefore Eq. (A.2) can be rewritten as:

$$\mu_j = \mu_j^* + RT \ln\left[\frac{C_j}{C_w + \sum C_k}\right] + \overline{V}_j P \tag{A.4}$$

Since it contains an unknown constant, the actual value of the chemical potential is not determinable. But for most applications of chemical potential, we are interested in the difference in the chemical potential between particular locations, so only relative values of the chemical potential are important anyway. Therefore, μ_j^* is cancelled out when the chemical potential in one location is subtracted from that in another to obtain the chemical potential difference between the two locations. Note that for any solution the concentrations of species and solvent satisfy:

$$C_w \overline{V}_w + \sum C_k \overline{V}_k = 1 \tag{A.5}$$

Hence, any change in the concentration of one particular species will result in the changes of the concentrations of other species and solvent. The differentiation of Eq. (A.5) leads to:

$$\Delta\mu_j = \overline{V}_j \Delta P + RT\left[\frac{\Delta C_j}{C_j} - \frac{\Delta C_w + \sum \Delta C_k}{C_w + \sum C_k}\right] \tag{A.6}$$

Using Eq. (A.5) and noting that

$$\Delta C_w = -\frac{\sum \Delta C_k \overline{V}_k}{\overline{V}_w} \tag{A.7}$$

so Eq. (A.6) can be rewritten as:

$$\Delta\mu_j = \overline{V}_j \Delta P + RT\left[\frac{\Delta C_j}{C_j} - \frac{\sum (\overline{V}_w - \overline{V}_k)\Delta C_k}{1 + \sum (\overline{V}_w - \overline{V}_k) C_k}\right] \tag{A.8}$$

Similarly to the solute, the potential of the solvent in a solution can be expressed by

$$\mu_w = \mu_w^* + RT \ln\left[\frac{C_w}{C_w + \sum C_k}\right] + \overline{V}_w P \tag{A.9}$$

Note that the electrical term is not included for the solvent. This is because the solvent (water) carries no net charge (z_w=0). The differentiation of Eq. (A.9) leads to:

$$\begin{aligned}\Delta\mu_w &= \overline{V}_w\Delta P + RT\left[\frac{\Delta C_w}{C_w} - \frac{\sum(\overline{V}_w - \overline{V}_k)\Delta C_k}{1+\sum(\overline{V}_w - \overline{V}_k)C_k}\right] \\ &= \overline{V}_w\Delta P - RT\left[\frac{\sum\overline{V}_k\Delta C_k}{1-\sum\overline{V}_k C_k} + \frac{\sum(\overline{V}_w - \overline{V}_k)\Delta C_k}{1+\sum(\overline{V}_w - \overline{V}_k)C_k}\right]\end{aligned} \tag{A.10}$$

Eqs. (A.8) and (A.10) are the expressions for the chemical potential gradients of species and solvent which can be applied to any ideal solution. If the solution is a dilute solution, that is $\overline{V}_w C_w \approx 1$, and $\sum\overline{V}_j C_j << 1$, Eqs. (A.8) and (A.10) can be simplified into:

$$\Delta\mu_j = \overline{V}_j\Delta P + RT\frac{\Delta C_j}{C_j} \tag{A.11}$$

$$\begin{aligned}\Delta\mu_w &= \overline{V}_w\Delta P - RT\left[\sum\overline{V}_k\Delta C_k + \sum(\overline{V}_w - \overline{V}_k)\Delta C_k\right] \\ &= \overline{V}_w\Delta P - RT\overline{V}_w\sum\Delta C_j\end{aligned} \tag{A.12}$$

which are well-known equations appeared in literatures.

APPENDIX B

B.1 The PDE Terms

The dependent variables are called u_1 and u_2, and the equation system solved is

$$d_a \frac{\partial u}{\partial t} - \nabla \cdot (c\nabla u + au - \gamma) + \beta \cdot \nabla u + \alpha u = f \tag{B.1}$$

where $u = (u_1, u_2)$. The coefficients and equation terms are now generations (vectors and matrices) of the corresponding scalars for the 1-variable coefficient form PDE described earlier.

The mass term is defined as

$$d_a \frac{\partial u}{\partial t} = \begin{bmatrix} d_{a11} & d_{a12} \\ d_{a21} & d_{a22} \end{bmatrix} \begin{bmatrix} \frac{\partial u_1}{\partial t} \\ \frac{\partial u_2}{\partial t} \end{bmatrix} = \begin{bmatrix} d_{a11}\frac{\partial u_1}{\partial t} & d_{a12}\frac{\partial u_2}{\partial t} \\ d_{a21}\frac{\partial u_1}{\partial t} & d_{a22}\frac{\partial u_2}{\partial t} \end{bmatrix} \tag{B.2}$$

The components of this term are not available as variables.

The diffusive flux is defined as

$$c\nabla u = \begin{bmatrix} c_{11} & c_{12} \\ c_{21} & c_{22} \end{bmatrix} \nabla \begin{bmatrix} u_1 \\ u_2 \end{bmatrix} = \begin{bmatrix} c_{11} & c_{12} \\ c_{21} & c_{22} \end{bmatrix} \begin{bmatrix} \nabla u_1 \\ \nabla u_2 \end{bmatrix} = \begin{bmatrix} c_{11}\nabla u_1 + c_{12}\nabla u_2 \\ c_{21}\nabla u_1 + c_{22}\nabla u_2 \end{bmatrix} =$$
$$\begin{bmatrix} c_{11}\begin{bmatrix} \frac{\partial u_1}{\partial x} \\ \frac{\partial u_1}{\partial y} \end{bmatrix} + c_{12}\begin{bmatrix} \frac{\partial u_2}{\partial x} \\ \frac{\partial u_2}{\partial y} \end{bmatrix} \\ c_{21}\begin{bmatrix} \frac{\partial u_1}{\partial x} \\ \frac{\partial u_1}{\partial y} \end{bmatrix} + c_{22}\begin{bmatrix} \frac{\partial u_2}{\partial x} \\ \frac{\partial u_2}{\partial y} \end{bmatrix} \end{bmatrix} = \begin{bmatrix} \begin{bmatrix} c_{11}\frac{\partial u_1}{\partial x} + c_{12}\frac{\partial u_2}{\partial x} \\ c_{11}\frac{\partial u_1}{\partial y} + c_{12}\frac{\partial u_2}{\partial y} \end{bmatrix} \\ \begin{bmatrix} c_{21}\frac{\partial u_1}{\partial x} + c_{22}\frac{\partial u_2}{\partial x} \\ c_{21}\frac{\partial u_1}{\partial y} + c_{22}\frac{\partial u_2}{\partial y} \end{bmatrix} \end{bmatrix} = \begin{bmatrix} \begin{bmatrix} cu_{1x} \\ cu_{1y} \end{bmatrix} \\ \begin{bmatrix} cu_{2x} \\ cu_{2y} \end{bmatrix} \end{bmatrix} \tag{B.3}$$

where ∇u_1 and ∇u_2 are considered to be column vectors. The variable names for the diffusive flux components are ***cu1x***, ***cu1y***, ***cu2x***, and ***cu2y***. The flux matrix of flux

tensor is presented here as a column vector. It can also be presented in Matrix form as

$$c\nabla u = \begin{bmatrix} cu_{1x} & cu_{1y} \\ cu_{2x} & cu_{2y} \end{bmatrix} \tag{B.4}$$

For anisotropic materials, each of the components c_{11}, c_{12}, c_{21}, and c_{22} can be matrices as described above for the 1-variable coefficient form *PDE*. In this case, the diffusive flux reads

$$c\nabla u = \begin{bmatrix} c_{11} & c_{12} \\ c_{21} & c_{22} \end{bmatrix} \begin{bmatrix} \nabla u_1 \\ \nabla u_2 \end{bmatrix} = \begin{bmatrix} \begin{bmatrix} c_{1111} & c_{1112} \\ c_{1121} & c_{1122} \end{bmatrix} & \begin{bmatrix} c_{1211} & c_{1212} \\ c_{1221} & c_{1222} \end{bmatrix} \\ \begin{bmatrix} c_{2111} & c_{2112} \\ c_{2121} & c_{2122} \end{bmatrix} & \begin{bmatrix} c_{2211} & c_{2212} \\ c_{2221} & c_{2222} \end{bmatrix} \end{bmatrix} \begin{bmatrix} \nabla u_1 \\ \nabla u_2 \end{bmatrix} = \tag{B.5}$$

$$\begin{bmatrix} \begin{bmatrix} c_{1111} & c_{1112} \\ c_{1121} & c_{1122} \end{bmatrix} \nabla u_1 + \begin{bmatrix} c_{1211} & c_{1212} \\ c_{1221} & c_{1222} \end{bmatrix} \nabla u_2 \\ \begin{bmatrix} c_{2111} & c_{2112} \\ c_{2121} & c_{2122} \end{bmatrix} \nabla u_1 + \begin{bmatrix} c_{2211} & c_{2212} \\ c_{2221} & c_{2222} \end{bmatrix} \nabla u_2 \end{bmatrix}$$

The variable names are the same as for the isotropic diffusive flux.

The conservative convective flux is defined as

$$\alpha u = \alpha \begin{bmatrix} u_1 \\ u_2 \end{bmatrix} = \begin{bmatrix} \alpha_{11} & \alpha_{12} \\ \alpha_{21} & \alpha_{22} \end{bmatrix} \begin{bmatrix} u_1 \\ u_2 \end{bmatrix} = \begin{bmatrix} \begin{bmatrix} \alpha_{111} \\ \alpha_{112} \end{bmatrix} & \begin{bmatrix} \alpha_{121} \\ \alpha_{122} \end{bmatrix} \\ \begin{bmatrix} \alpha_{211} \\ \alpha_{212} \end{bmatrix} & \begin{bmatrix} \alpha_{221} \\ \alpha_{222} \end{bmatrix} \end{bmatrix} \begin{bmatrix} u_1 \\ u_2 \end{bmatrix} = \begin{bmatrix} \begin{bmatrix} \alpha_{111} \\ \alpha_{112} \end{bmatrix} u_1 + \begin{bmatrix} \alpha_{121} \\ \alpha_{122} \end{bmatrix} u_2 \\ \begin{bmatrix} \alpha_{211} \\ \alpha_{212} \end{bmatrix} u_1 + \begin{bmatrix} \alpha_{221} \\ \alpha_{222} \end{bmatrix} u_2 \end{bmatrix} \tag{B.6}$$

The variable names for these components are ***alu1x***, ***alu1y***, ***alu2x*** and ***alu2y***. Here the third index, k, of α_{ijk} corresponds to the space coordinate suffixes x and y.

The conservative flux source is defined as

$$\gamma = \begin{bmatrix} \begin{bmatrix} \gamma_{11} \\ \gamma_{12} \end{bmatrix} \\ \begin{bmatrix} \gamma_{21} \\ \gamma_{22} \end{bmatrix} \end{bmatrix} \tag{B.7}$$

The variables names for these components are ***ga1x***, ***ga1y***, ***ga2x***, and ***ga2y***. Here the second index, j, of γ_{ij} denotes the space coordinate suffixes for x and y.

For the flux terms the divergence operator works on each row separately. To illustrate this, consider the divergence of the conservative flux source

$$\nabla \cdot \gamma = \nabla \cdot \begin{bmatrix} \begin{bmatrix} \gamma_{11} \\ \gamma_{12} \end{bmatrix} \\ \begin{bmatrix} \gamma_{21} \\ \gamma_{22} \end{bmatrix} \end{bmatrix} = \begin{bmatrix} \nabla \cdot \begin{bmatrix} \gamma_{11} \\ \gamma_{12} \end{bmatrix} \\ \nabla \cdot \begin{bmatrix} \gamma_{21} \\ \gamma_{22} \end{bmatrix} \end{bmatrix} \tag{B.8}$$

The convection term is defined as

$$\beta \cdot \nabla u = \begin{bmatrix} \beta_{11} & \beta_{12} \\ \beta_{21} & \beta_{22} \end{bmatrix} \cdot \begin{bmatrix} \nabla u_1 \\ \nabla u_2 \end{bmatrix} = \begin{bmatrix} \begin{bmatrix} \beta_{111} \\ \beta_{112} \end{bmatrix} & \begin{bmatrix} \beta_{121} \\ \beta_{122} \end{bmatrix} \\ \begin{bmatrix} \beta_{211} \\ \beta_{212} \end{bmatrix} & \begin{bmatrix} \beta_{221} \\ \beta_{222} \end{bmatrix} \end{bmatrix} \cdot \begin{bmatrix} \nabla u_1 \\ \nabla u_2 \end{bmatrix} = \begin{bmatrix} \begin{bmatrix} \beta_{111} \\ \beta_{112} \end{bmatrix} \cdot \nabla u_1 + \begin{bmatrix} \beta_{121} \\ \beta_{122} \end{bmatrix} \cdot \nabla u_2 \\ \begin{bmatrix} \beta_{211} \\ \beta_{212} \end{bmatrix} \cdot \nabla u_1 + \begin{bmatrix} \beta_{221} \\ \beta_{222} \end{bmatrix} \cdot \nabla u_2 \end{bmatrix} \tag{B.9}$$

The variable names for these components are ***beu1*** and ***beu2***.

The absorption term is defined as

$$au = \begin{bmatrix} a_{11} & a_{12} \\ a_{21} & a_{22} \end{bmatrix} \begin{bmatrix} u_1 \\ u_2 \end{bmatrix} = \begin{bmatrix} a_{11}u_1 + a_{12}u_2 \\ a_{21}u_1 + a_{22}u_2 \end{bmatrix} \tag{B.10}$$

The variable names for these components are ***au1*** and ***au2***.

The source term is defined as

$$f = \begin{bmatrix} f_1 \\ f_2 \end{bmatrix} \tag{B.11}$$

The variable names for these components are ***f1*** and ***f2***.

B.2 The Boundary Condition Terms

The Dirichlet boundary condition, in expanded form, reads

$$\begin{bmatrix} h_{11} & h_{12} \\ h_{21} & h_{22} \end{bmatrix} \begin{bmatrix} u_1 \\ u_2 \end{bmatrix} = \begin{bmatrix} r_1 \\ r_2 \end{bmatrix} \tag{B.12}$$

The components of this equation are not available as variables.

If the Dirichlet condition is chosen, the generalized Neumann boundary condition can also be got, which reads

$$n \cdot (c\nabla u + \alpha u - \gamma) + qu = g - h^T \mu \tag{B.13}$$

The normal vector $n=(n_x, n_y)$ operates on the flux vector in the same way as the divergence operator as explained earlier. If h has full rank, for instance as in the default identity matrix, only the constrains from the Dirichlet condition are active.

If the Neumann condition is chosen, the only boundary condition is

$$n \cdot (c\nabla u + \alpha u - \gamma) + qu = g \tag{B.14}$$

The normal component of the diffusive flux is defined as

$$n \cdot c\nabla u = n \cdot \begin{bmatrix} c_{11} & c_{12} \\ c_{21} & c_{22} \end{bmatrix} \begin{bmatrix} \nabla u_1 \\ \nabla u_2 \end{bmatrix} = \begin{bmatrix} n \cdot (c_{11}\nabla u_1 + c_{12}\nabla u_2) \\ n \cdot (c_{21}\nabla u_1 + c_{22}\nabla u_2) \end{bmatrix} \tag{B.15}$$

The variable names for these components are ***ncu1*** and ***ncu2***.

The normal component of the conservative convective flux is defined as

$$n \cdot \alpha u = n \cdot \begin{bmatrix} \begin{bmatrix} \alpha_{111} \\ \alpha_{112} \end{bmatrix} u_1 + \begin{bmatrix} \alpha_{121} \\ \alpha_{122} \end{bmatrix} u_2 \\ \begin{bmatrix} \alpha_{211} \\ \alpha_{212} \end{bmatrix} u_1 + \begin{bmatrix} \alpha_{221} \\ \alpha_{222} \end{bmatrix} u_2 \end{bmatrix} = \begin{bmatrix} (n_x, n_y) \cdot \left(\begin{bmatrix} \alpha_{111} \\ \alpha_{112} \end{bmatrix} u_1 + \begin{bmatrix} \alpha_{121} \\ \alpha_{122} \end{bmatrix} u_2 \right) \\ (n_x, n_y) \cdot \left(\begin{bmatrix} \alpha_{211} \\ \alpha_{212} \end{bmatrix} u_1 + \begin{bmatrix} \alpha_{221} \\ \alpha_{222} \end{bmatrix} u_2 \right) \end{bmatrix} \quad \text{(B.16)}$$

The variable names for these components are ***nalu1*** and ***nalu2***.

The normal component of the conservative flux source is defined as

$$n \cdot \gamma = (n_x, n_y) \cdot \begin{bmatrix} \begin{bmatrix} \gamma_{11} \\ \gamma_{12} \end{bmatrix} \\ \begin{bmatrix} \gamma_{21} \\ \gamma_{22} \end{bmatrix} \end{bmatrix} = \cdot \begin{bmatrix} (n_x, n_y) \cdot \begin{bmatrix} \gamma_{11} \\ \gamma_{12} \end{bmatrix} \\ (n_x, n_y) \cdot \begin{bmatrix} \gamma_{21} \\ \gamma_{22} \end{bmatrix} \end{bmatrix} \quad \text{(B.17)}$$

The variable names for these components are ***ngau1*** and ***ngau2***.

The boundary absorption term is defined as

$$qu = \begin{bmatrix} q_{11} & q_{12} \\ q_{21} & q_{22} \end{bmatrix} \begin{bmatrix} u_1 \\ u_2 \end{bmatrix} = \begin{bmatrix} q_{11}u_1 + q_{12}u_2 \\ q_{21}u_1 + q_{22}u_2 \end{bmatrix} \quad \text{(B.18)}$$

The variable names for these components are ***qu1*** and ***qu2***.

The boundary source term is defined as

$$g = \begin{bmatrix} g_1 \\ g_2 \end{bmatrix} \quad \text{(B.19)}$$

The variable names for these components are ***g1*** and ***g2***.